DEVELOPMENT OF ADAPTIVE PVD COATED ADVANCED COMPOSITE (CERMET) TOOLS FOR HIGH-SPEED DRY MACHINING OF STAINLESS STEEL

DEVELOPMENT OF ADAPTIVE PVD COATED ADVANCED COMPOSITE

(CERMET) TOOLS FOR HIGH-SPEED DRY MACHINING OF STAINLESS STEEL

By

UTTKARSH PATEL, B. Eng., M.Tech

(McMaster University, Canada)

A Thesis

Submitted to the School of Graduate Studies

in Partial Fulfilment of the Requirements

for the Degree

Doctor of Philosophy

McMaster University

© Copyright by Uttkarsh Patel, August 2021

DOCTOR OF PHILOSOPHY (2021)   McMaster University

(Mechanical Engineering)   Hamilton, Ontario

TITLE: Development of Adaptive PVD Coated Advanced
                    Composite (Cermet) Tools For High-Speed Dry Machining
                    of Stainless Steel

AUTHOR: Uttkarsh Patel, B. Eng., M.Tech.

SUPERVISOR: Dr. Stephen Veldhuis

                    Department of Mechanical Engineering

                    McMaster University

SUPERVISORY   Dr. Eu-Gene Ng

COMMITTEE: Department of Mechanical Engineering

                    McMaster University

                    Dr. Igor Zhitomirsky

                    Department of Materials Science and Engineering

                    McMaster University

NUMBER OF PAGES: xxiii, 176

Dedicated to

My Mother, Father, Sister, Brother and to

my beloved Wife

Acknowledgements

Completing my doctoral thesis has been a long journey, spans four years with many learning experiences, challenges, and memories. This research would not have been possible without the guidance and assistance of many individuals who contributed and extended their valuable assistance, inspiration, motivation, love in preparing and completing this study. This is an occasion, and I am privileged to express my gratitude to all of them.

First and foremost, I would like to thank the Almighty God for giving me good health, peace of mind, and patience to complete this study

My utmost gratitude goes to my research supervisor, Dr. Stephen Veldhuis, for allowing me to join his team, who has supported me in doing my thesis with his unending patience, understanding, motivation, enthusiasm, immense knowledge, robust planning and management. His guidance helped me through my time of research and writing of this thesis. I would like to express my heartfelt thanks to him for supporting me during the four years of study while away far from my family. I could not have imagined having a better adviser than him who considered me like a family member and provided constant support.

I am thankful to the committee members Dr. Eu-Gene Ng from the Department of Mechanical Engineering and Dr. Igor Zhitomirsky from the Department of Materials Science and Engineering for their useful suggestions and critical evaluation of the progress of my thesis.

Lay Abstract

Cutting is the process of removing unwanted material from the bulk material to obtain the desired shape. Each metal material has unique mechanical properties that lead to various machining challenges. The cutting process is done with the help of a cutting tool that wears out during the process, and a coating layer is often used to protect the tool. Stainless steel 304 is a widely used material that is difficult to machine. This study includes a systematic approach to understanding the wear mechanisms of tools and existing commercial coatings during the dry machining of stainless steel 304. An in-house coating was developed and deposited on the selected cutting tool to protect it, reduce tool wear and extend its working life. The research results will help reduce machining costs by reducing tool and coolant costs and meet the current industry demand for dry high-speed machining. It will also reduce environmental impact by reducing waste and hazardous chemicals and addressing occupational health and safety concerns.

Abstract

Stainless steel is a metal material widely used in many industries because of its high tensile strength, toughness, and corrosion resistance. Machining stainless steel is challenging due to its high work hardening tendency, low thermal conductivity, and ductility of the material resulting in built-up edge formation. Machining stainless steel at lower cutting speeds must be performed with coolant, which adds to the cost of the process and increases concerns for the environment and the operator's health and safety. Industries such as the aerospace and die-mold industries demand high-speed machining to realize productivity targets. Therefore, a cermet tool material was selected for the present study because of its high temperature resistance, high bending strength, and fracture toughness.

The study focused on investigating wear mechanisms and developing a coating on a cermet tool for dry high-speed machining stainless steel to increase tool life. The wear mechanisms of tools were investigated at a fixed cutting interval in relation to the tool's composition and microstructure. Scanning Electron Microscope (SEM) was used to study the microstructure and identify elements on the tool. X-ray diffraction (XRD) was used to identify the phases and concentrations of key elements on the tool. The new advanced in-house coating was developed with Super Fine Cathode (SFC) technology on a Kobelco AIP-20 Physical Vapour Deposition (PVD) coater. The micromechanical properties of the commercial coating and in-house coatings were investigated with the help of nanoindentation and scratch tests. Atomic Force

Microscopy (AFM) and SEM were used to investigate the coating microstructure and surface topography. An Alicona variable focus 3D microscope was used to investigate wear volume and wear behaviour.

It was discovered that various secondary carbides used by manufacturers to manufacture cermet tools change the microstructure, which affects the machining performance of the cermet tool material. Microchipping at the depth of cut (DOC) causes catastrophic notch wear. It was found that the developed in-house coatings were able to delay the initial wear (microchipping), which improved the tool's life by 318%. This research contributes to meeting the manufacturing industry's challenging demand for dry-high speed machining with reduced manufacturing costs.

Table of Contents

List of Figures

List of Tables

Abbreviations

BUE	Built up edge
AFM	Atomic Force Microscope
BEC	Backscattered electron composition
CVD	Chemical vapor deposition
DOC	Depth Of Cut
E	Elastic modulus
EDS	Energy-Dispersive X-ray Spectrometry
H	Hardness
PVD	Physical vapor deposition
SEI	Secondary Electron Imaging
SEM	Scanning electron microscopy
SFC	Super fine cathode
SS	Stainless Steel
XPS	X-Ray Photoelectron Spectroscopy
XRD	X-Ray diffraction

Chapter 1 : Introduction

1.1 Background

Research and development are unceasing processes in manufacturing. Advanced materials are continuously being developed to meet modern industrial requirements. For example, the aerospace industry requires materials that are strong and lightweight. The introduction of these new advanced materials requires novel machining processes to produce the intended shapes.

Stainless steel 304 represents 72% of the metals market (Kulkarni, Sargade and More, 2018). It is widely used for manufacturing machine parts, chemical and food processing equipment due to its high corrosion resistance (Groover, 2007). It is well-known for the physical properties of high ductility, tensile strength, fracture toughness, low thermal conductivity, and high work hardening (Modern Metal Cutting: A Practical Handbook, 1994; Abou-El-Hossein and Yahya, 2005; Philip Selvaraj and Chandramohan, 2010). However, the machinability of this material remains a challenge.

Machinability is influenced by such properties as the strength of a material, work hardening tendency, low thermal conductivity, and stickiness (severe adhesion or galling) (Korkut et al., 2004; Philip Selvaraj and Chandramohan, 2010). The stickiness of stainless steel can result in a high built-up edge tendency, which contributes to poor surface finish and high tool wear rates (O'Sullivan and Cotterell, 2002). When machining this material, cutting force fluctuation can occur due to the variation in built-up edge formation which is much

more apparent when machining Stainless steel 304 than when machining unalloyed steel (Modern Metal Cutting: A Practical Handbook, 1994). Work hardening also contributes to the poor machinability of austenitic stainless steel like AISI 304 (Jiang, Roos and Liu, 1997).

Manufacturers are always looking for cost effective ways to increase the productivity of stainless-steel machining. To reduce the overall time and cost of producing a part, new tools need to be developed that can function at increased cutting speeds, have enhanced chip control, and provide better cut quality. However, high cutting speeds present further machining challenges, such as high cutting temperatures that increase wear rates and lower tool life. Based on past testing performed at the MMRI improved cutting tool performance and tool life can be provided by adaptive PVD coatings, which have been observed to enhance lubricity during machining (Biksa et al., 2010), while maintaining a good compressive residual stress state within the tool (Jindal et al., 1999). However, almost all stainless-steel tools fail to deliver the desired level of performance under dry cutting conditions.

Moreover, various tool materials such as diamond tools, high-speed steel (HSS) tools, cemented carbide tools and ceramic tools fail to provide adequate performance, as well. This is especially the case for AISI 304 due to its machining limitations in terms of chemical affinity, hot hardness, adhesion wear, notching, and poor tensile strength. Composite materials made of ceramic and metal, or cermet, are being developed as alternatives to achieve a high wear resistance combined with strength.

The current research investigates the performance of a cermet tool during the high-speed dry machining of 304 stainless steel. A comprehensive comparative study of the microstructure and mechanical properties of different cermet tool materials is presented in this work. The possibility of further improving the performance of these new materials is explored by the application of an advanced adaptive PVD coating.

1.1.1 Stainless Steel 304

Stainless steel 304 comprises at least 18% chromium which increases hardness without changing the ductility of the steel. Chromium further develops grain refinement in the steel, which increases the hardness of the steel. Additionally, it also enriches the high-temperature strength of the steel. Stainless steel 304 contains at least 8% nickel, which further develops toughness, particularly at low temperatures, and diminishes corrosion and limits scratches. Nickel additionally bestows some heat resistance properties to stainless steel 304 (whose thermal conductivity is 3 times lower than steel and 5 times lower than iron), making machining exceptionally challenging because of the high temperatures present in the cutting zone. During machining, 80% of the heat generated is transferred to the tool, raising the cutting tool temperature up to 1000˚C. High temperature accelerates tool wear through diffusion and oxidation (Bapat et al., 2015). Moreover, AISI 304's high strain hardening rate advances the adhesion of stainless steel to the tool's cutting edge, which causes unstable chips and built-up edge (BUE) formation (Korkut et al., 2004).

1.1.2 Machining Challenges of Stainless Steel 304

1.1.2.1 Built-up Edge Problem

Built-up edge (BUE) is the aggregation of workpiece material welded to the tool's rake face. The material adheres to the rake face of the tool due to high pressure and friction between the tool and the workpiece. When a critical amount of material becomes deposited at the rake face of the tool, the welded material (BUE) itself contributes to the cutting process. Thus, the BUE effectively changes the geometry of the tool, which also affects the dimensional accuracy and surface finish of the final workpiece. If the balance of forces around the build-up edge varies, a portion of the BUE will detach along with the chips. Over time, this may lead to flank wear, since the BUE can also carry away a part of the tool material with it.

In 2004, Tekiner and Yeşilyurt (Tekiner and Yeşilyurt, 2004) conducted turning experiments on AISI 304 with varying cutting speeds, feed rates, and depths of cut, using a WC P10 cemented carbide tool. They reported that although increasing the feed rate intensifies the BUE, the latter decreases as the cutting speed increases.

1.1.2.2 Work Hardening

A part of the frictional heat generated between the cutting tool and the workpiece during machining is transferred to the workpiece, resulting in a structural change of the material, and the hardening of the workpiece surface. The work-hardened surface produces abrasive chips, which are responsible for the tool's abrasion and subsequent notch wear. Another reason for notch wear may be corrosion or other chemical processes occurring on the

surface of the tool (Stephenson and Agapiou, 2016). Selvaraj et al. (Philip Selvaraj et al., 2014) observed that tool wear was caused by diffusion, thermal softening, and notch wear at higher cutting speeds.

1.1.2.3 Thermal Conductivity

During machining, heat is generated from the plastic deformation of the workpiece material in the primary shear deformation zone. The sheared material forms chips that flow on the tool rake face. To overcome the friction between the chip-tool interface, chips undergo further plastic deformation in the secondary shear deformation zone, which increases the temperature at the tool-chip interface. Since stainless steel has low thermal conductivity, only a small amount of heat is passed to the workpiece. The remainder, about 80% of the heat generated, is conducted to the tool. It raises the temperature of the tool up to 1000˚C. At such high temperatures, diffusion and oxidation occur and cause rapid tool wear and reduce tool performance and life (Bapat et al., 2015).

1.1.2.4 Plastic Deformation

Ductile materials are often difficult to machine because they plastically deform beyond their yield point and produce continuous chips which tend to stick to the tool. These high-temperature continuous chips aggressively bond to the cutting tool during cutting. When the chip splits away, it may carry a portion of the tool with it, resulting in rapid tool chipping and wear (Sushil, Amit and Rohit, 2017). Long continuous chips lead to chip nesting and tangles on the cutting tool during machining which can damage the cutting tool or workpiece.

1.1.3 High-Speed Machining

Steel (including stainless steel), aluminum and titanium are widely used in the aerospace and die/mold industries. These industries demand precise and high-speed machining. Each of the mentioned materials has its own unique properties. Therefore, the parameters associated with high-speed machining are diversely characterized for each. High-speed machining generally keeps the feed rate at the same or lower level, but the surface cutting speed or RPM is substantially increased. The focus is on taking advantage of the thermal softening effect that takes place at the higher temperatures associated with higher speeds and the tendency of the heat to exit the cutting zone with the chip. High-speed machining is highly desirable because of the higher potential production rates and the general reduction of BUE at higher speeds (D. G. Flam, R. Kamanduri, 1984; Tekiner and Yeşilyurt, 2004), which results in the improvement of the surface finish and quality. Adopting high-speed machining, however, introduces new challenges. As the cutting speed increases, the magnitudes of all the stress components also increase (M'saoubi et al., no date; Outeiro, Umbrello and M'Saoubi, 2006).

1.1.4 Wet Machining

Cemented carbide tools are the most commonly used tools for machining metal materials. During the machining process, the temperature at the tool-chip interface rises to more than 500 °C with an increase in cutting speed of more than 140 m/min. At such high temperatures, the WC/Co or WC/TiC/Co elements diffuse into the stainless steel from carbide tools and also from the stainless steel into the tool material. As a result, the tool suffers from rapid wear on the rake face, which weakens the cutting edge. In addition, the

highly reported wear methods while machining stainless steel with carbide tools are adhesive and abrasive wear (Jianxin et al., 2011). Xavior et al. (Xavior and Adithan, 2009) researched the effect of various cutting fluids on tool wear and surface roughness, especially during the turning of AISI 304 with carbide cutting tools. The results show that the cutting speed and feed rate have a greater effect on tool wear than the cutting fluid. Mahdavinejad et al. 2011 (Mahdavinejad and Saeedy, 2011) optimized the cutting parameters using the design of experiments (DOE) and analysis of variance (ANOVA) method for dry and water-miscible cutting fluid. During machining, they determined that the cutting speed had the greatest influence on the tool life. They also reported a significant improvement in tool life compared to dry machining. Ahmed et al. 2017 (Ahmed et al., 2017) studied the effect of BUE formed during wet machining of stainless steel 304 using uncoated carbide cutting tools (WC-Co) during the steady stage zone of the tool life curve. They observed an increase in surface roughness with an increase in BUE and a decrease in tensile residual stress. Hossein and Yahya (Abou-El-Hossein and Yahya, 2005) reported notch wear to be the dominant tool failure mode while performing AISI 304 milling using carbide inserts with coolant. Dhananchezian et al. (Dhananchezian, Kumar and Sornakumar, 2011) reported a reduction in surface roughness with the help of cryogenic (liquid nitrogen) turning.

1.1.5 Dry High-Speed Machining

Recently, green or dry manufacturing has gained interest in the manufacturing industry as a way to reduce the environmental impact and address occupational health and safety concerns. The major benefits of dry machining include decreased water and atmospheric

pollution, no liquid residue on the part that requires cleaning, and no subsequent disposal cost of the liquids and cleaning chemicals. The use of liquid coolants and lubricants may also trigger skin irritation and airway damage from inhalation. In general, dry machining lowers machining costs by as much as 16-20% (Sreejith and Ngoi, 2000; Sharma, Tiwari and Dixit, 2016). However, the adverse effects of the dry machining condition include an increase in friction and adhesion between the tool and the chip, which increases the temperature in the cutting zone, resulting in a higher wear rate and a shorter tool life (Zhang, Li and Wang, 2012).

Outeiro and M'Saoubi (M'Saoubi et al., 1999; Outeiro, Umbrello and M'Saoubi, 2006) reported that during dry turning of AISI 304 and 315L, as cutting speeds increased, the tensile superficial stresses in the hoop and axial directions increased.

Tekiner and Yeşilyurt (Tekiner and Yeşilyurt, 2004) researched the most suitable cutting conditions for machining stainless steel 304 using acoustic emission at multiple cutting speeds, feed rates, and cut depths using a WC P10 cemented carbide tool. They found a decrease in BUE with increasing speed and feed rate. Ciftci (Ciftci, 2006) also reported similar results at high cutting speed with low surface roughness. The CVD coating used in the study reduced the coefficient of friction of the multi-layer coated cemented carbide insert. Korkut et al. In 2004 (Korkut et al., 2004) used a multilayer (TiC, TiCN, Al_2O_3, TiN) coating for cemented carbide tools at various cutting speeds, 120,150, and 180 m/min. They found a decrease in surface roughness with increasing cutting speed.

Many researchers have used different cutting tools, different conditions and different coatings deposited by various methods to improve the machinability of 304 stainless steel.

Achieving an acceptable surface quality is never easy in machining. A large volume of research has focused on improving surface roughness by optimizing machining parameters and operating conditions. Xavior et al. (Xavior and Adithan, 2009) used different cutting fluids to study tool wear and surface roughness of AISI 304. Selvaraj and Chandramohan (Philip Selvaraj and Chandramohan, 2010) minimized the surface roughness during dry machining of AISI 304 by finding optimal process parameters using the Taguchi method. However, achieving low surface roughness under dry machining still presents a challenge.

1.1.6 Various Cutting Tool Materials

To machine various alloys, High-Speed Steel (HSS) was historically one of the most commonly used tool materials. However, the catastrophic failure of the tool above a relatively low cutting speed (45 m/min) limits its widespread use. In these cases, the chips became red hot. According to Jiang et al. the HSS tool failed due to fatigue during machining steel, and the tool life with HSS was shorter than that associated with the use of a cement carbide tool (Jiang et al., 1996). Due to their excellent properties, such as high hardness and high dimension stability during machining, diamond tools are used to machine many nonferrous materials. Diamond tools such as natural diamond (ND), synthetic single crystal diamond, polycrystalline diamond (PCD), and cubic boron nitride (CBN) are available for machining various metals. However, diamond tools cannot be used for

machining stainless steel due to its high affinity for carbon. In addition, diamond tools are the most expensive cutting tool materials available (Liu, Wan and Ai, 2004; Grzesik, 2017).

Dogra et al. (Dogra et al., 2010) reported ploughing issues during hard turning with CBN cutting tools. They also reported poor surface quality after machining. Ceramic tools are excellent for non-ferrous metal machining due to their low affinity and chemical stability. They have many other advantages, such as extreme abrasion and crater wear resistance, high-temperature hardness and high compressive strength (Whitney, 1994). However, due to their limited tensile strength, fracture toughness and thermal shock resistance, the use of ceramic cutting tools is limited for machining steel alloys (Low, 2014).

1.1.7 Dry High-Speed Finish Turning by Cermet Tools

Cermet is a composite material made of ceramic particles joined together by a metal binder. Cermet's material properties, such as high-temperature resistance, bending strength, and fracture toughness, make them well suited for high-speed machining. In addition, they also possess higher thermal shock resistance compared to oxide-based ceramics and can undergo plastic deformation like a metal (Gruss, 1987). Compared to WC (Tungsten carbide), the diffusion wear and thermal expansion coefficients are lower in cermet (Stephenson and Agapiou, 2016). In summary, cermet tools are used in the industry for machining stainless steel due to their superior performance compared to coated carbide tooling.

1.1.8 Cermet Tool Microstructure

Cermet tools are mainly produced with a core-rim structure, with titanium carbon-nitride (C, N) as the hard phase (core), with nickel or cobalt as a binder (matrix), and a rim as a core surrounding phase (Figure 1.1). Sometimes the rim consists of two parts, the outer and inner rim. Contemporary cermet contains sintered TiC and TiN particles with a refractory metallic binder. Ni as a binder increases the bending strength of cermet but decreases the hardness. However, the use of a Co binder will result in high toughness and resistance to oxidation (Peng, Miao and Peng, 2013). Materials such as molybdenum (Mo) have also been introduced. The atomic radius of Mo is significantly more than Ni. The solid solubility of Ti will decrease in Ni, resulting in a stable carbonitride. Mo promotes the formation of a TiCN grain and suppresses crystallization (Conforto, Mari and Cutard, 2004).
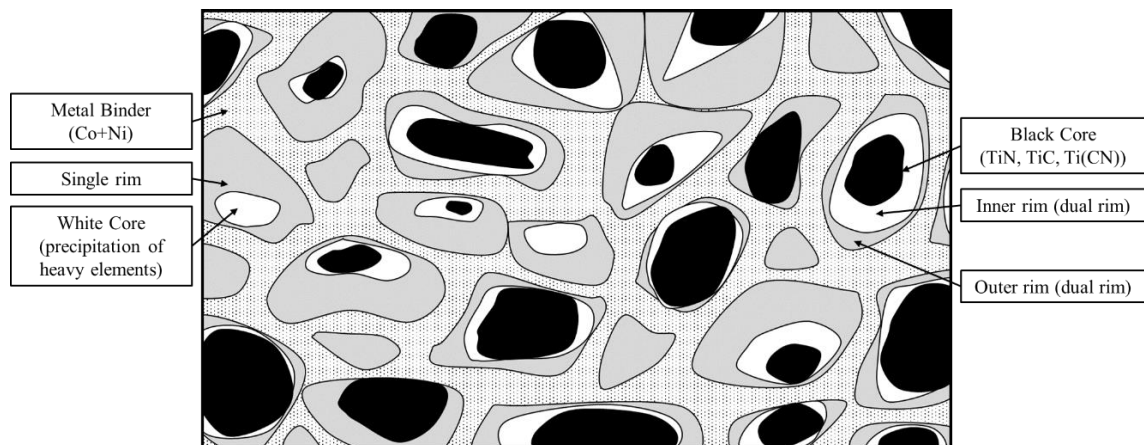
Figure 1.1 *Schematic representation of an SEM image of a Ti(C,N)-based cermet tools.*

Stronger chemical bonds can be established between the binder phase and the hard phase by improving the wettability with the help of secondary carbides like WC, VC, NbC, Cr_3C_2, TaC, Mo_2C (Peng, Miao and Peng, 2013). WC (10 to 20 wt.%) improves the wettability, which improves the carbonitride grain formation and facilitates the formation of the core-rim structure. As a result, the fracture toughness, bending strength and hardness of the cermet increases (Jun et al., 2009). The addition of Mo_2C in cermet can also enhance the wettability of the hard phases and can also dissolve in the binder phase, which encourages the formation of larger TiCN cores. In this way, the use of secondary carbides increases the hardness and the strength of the cermet (Xiong et al., 2007). By adding about 5 wt% of NbC, the sintering temperature can be reduced. Due to the consistent solid arrangement of NbC and TaC in the hard phase, the volume fractions will increase (lower porosity) in the internal rim. Consequently, the hot-hardness and plastic deformation of the cermet will increase (Wang et al., 2009). Due to the lower solubility of Cr_3C_2 and VC, it can dissolve in the hard phase, and part of them can dissolve in the binder phase. As a result, rim plasticity and bending strength increase. Moreover, it also inhibits the core growth, which can result in higher hardness (Ying et al., 2011; Wan et al., 2012).

TiC provides beneficial properties to cermet, such as chemical stability, oxidation resistance, and hot hardness and diminishes the tendency of the work-hardened material to adhere to the tool. TiN also enhances the material's resistance to fracture and thermal shock (Stephenson and Agapiou, 2016).

Cermet tools last approximately 20% to 100% longer than coated carbide tools when used appropriately. Cermet shows good workability with iron and steel and produces a

continuous chip during machining. Cermet has a high ability to perform at high cutting speed with long tool life. It also produces a high-quality surface finish without any use of cutting fluid (Rufe, 2013; Stephenson and Agapiou, 2016).

1.1.9 Wear Mechanisms in Cermet Tools

Different types of wear such as abrasion, adhesion, diffusion, notching and micro-chipping, as well as failure modes such as catastrophic cracking were reported in the literature to be present in cermet tools. Abrasion wear occurs when hard particles from the workpiece produced by chips flowing over the tool during the machining process abrade the soft components of the tool. Zhang et al. 2017 reported this to occur in the Ti(C, N)/Al_2O_3 cermet tool during turning of 40Cr (AISI 5140) hardened steel. They also reported micro-chipping near the tool nose due to thermal stress and cutting force, which caused internal crack growth and eventual micro-chipping (Zhang et al., 2017). Manoj Kumar et al. (Manoj Kumar, Kumar and Basu, 2007) studied crater wear and the wear mechanisms associated with the use of a TiCN-Ni based cermet with WC addition for machining boiler steel under different cutting parameters. The high temperature and pressure at the tool edge during machining promoted diffusion, which was chemically activated in this process due to a tribo-chemical reaction. Diffusion in this case promoted crater wear. Zou et al. (Zou et al., 2014) also reported the crater wear in Ti(C_7N_3)-based cermet with WC and TaC particles due to adhesive wear during machining of martensitic stainless steel (17-4PH) at a cutting speed of 350 m/min.

Table 1.1 *wear/failure summary of different cermet tools with various steels.*

Authors	Tool Material	Workpiece Material	Machining Parameters			Type of failure/wear ■flank ◆notch ▫crater ○diffusion ✳chipping ☼cracks ✚fracture •abrasive ✿adhesive
			Cutting speed (mm/min)	Feed (mm/r)	DOC (mm)	
(Zou *et al.*, 2014)	Ti(C$_7$N$_3$)	17-4PH martensitic stainless steel	350	0.1	0.3	▫ ◆ •✿
(Zou *et al.*, 2015)	Ti(C$_7$N$_3$)/ WC/TaC	321 austenitic stainless steel 17-4PH martensitic stainless steel	300 350 400	01. 0.15 0.2	0.25 0.30 0.35	■ ▫ ◆ •✿☼✚
(Ghani, Choudhury and Masjuki, 2004)	TiC/TiN	AISI H13	Milling 224 280 355	Milling 0.1 0.16 0.25	Milling 0.3 0.5 0.8	✳ ◆ ○☼✚
(Xing *et al.*, 2014)	Ti(C,N) based	quenched steel Hardness 61–62 HRC	60 80 100	0.1	0.2 0.5	✳•✿○
(Li *et al.*, 2015)	Ti(C,N) based	Heat-treated stainless steel 3Cr13Cu -44 HRC	Milling 60 80 120 160 200 240	Milling 0.1	Milling 1	✳ ◆ ☼
(Khan and Hajjaj, 2006)	Ti(C,N) based	Autenitic stainless steel (SUS 304)	300 400 500 700	0.05 0.1 0.2 0.4	0.1 0.2 0.3 0.5	▫ ☼✚
(Ji *et al.*, 2018)	Ti(C,N)- TiB2	17-4 PH stainless steel	150 200 250 300	0.1	0.3	✳•
(Zhang *et al.*, 2017)	Ti(C, N)/ Al$_2$O$_3$	40Cr (AISI 5140) 50±2HRC	120 180 240	0.1 0.125 0.15	0.1 0.2 0.3	✳☼

Notch wear was caused by the interaction of the machined surface with the cutting tool. Zou et al. (Zou et al., 2015) used the Ti(C_7N_3)/WC/TaC cermet cutting tool for the high-speed turning of 17-4 PH martensitic and 321 austenitic stainless steel at a cutting speed of 300 ~ 400m/min under a wet coolant condition. A work-hardened layer resulted in a high cutting zone temperature. The extreme conditions in this region caused chipping and localized rapid tool wear. A similar problem was observed in other studies (Zou et al., 2014). Li et al. (Li et al., 2015) reported boundary wear to be present on milling inserts during the milling of 3Cr13Cu at a cutting speed of 120m/min along with mechanical fatigue cracks.

Zhang et al. (Zhang et al., 2017) observed cracks forming in the tool material. Cracks formed under high applied loads would degrade the bonding between the hard, wear-resistant particles and accelerate tool failure. Zou et al. (Zou et al., 2015) also reported that high temperatures in the cutting zone promoted the formation of cracks. Cracks are highly undesirable as they can cause the sudden failure of the tool due to a lack of support for the cutting edge. The summary of the wear/failure mechanism of different cermet tools with various steel materials is shown below in Table 1.1.

1.1.10 PVD Coating

The first commercial PVD coating was developed around 1980 on carbide inserts for high-speed steel drills, and later, for the milling process was TiN (Wolfe, Petrosky and Quinto, 1986). Other binaries and ternary compounds of Ti, Al, and Cr were added to coatings over time (Yamamoto et al., 2003; Kalss et al., 2006). A new realm of the manufactured

functional coating was opened in the mid-1990s with the advancement of nanostructured coating that can be designed at the atomic level.

Currently, most of the tools used in the machining industry are coated tools. The primary purpose of the coating is to improve the wear resistance of the cutting tool. To accomplish this, the coating must maintain excellent adhesion to the cutting tool material even at elevated temperatures and under extreme loads. The three most common materials that meet these criteria are titanium nitride TiN, titanium carbide TiC and aluminum oxide Al_2O_3 (Prengel, Pfouts and Santhanam, 1998; Klocke and Krieg, 1999). TiC is harder and provides high levels of abrasion resistance (Srivastava and Das, 2010), TiN is suitable for a wide range of materials and prevents the formation of a built-up edge (Kümmel et al., 2013), and Al_2O_3 is an excellent thermal insulator and provides high-temperature stability (Marshall et al., 1998; Limarga, Widjaja and Yip, 2005). A major drawback of these PVD coatings is a lack of high-temperature lubricity. Consequently, the adhesive wear mechanism is not adequately diminished by these coatings (Childs, 2000) since their application requires withstanding high temperatures. The application of a TiCN coating does not significantly reduce tool wear due to the similarity of the coating material to that of cermet as reported by Rahman (M.Rahman, K.H.W.Seah, T.N. Goh, 1996). Yang et al. in 2017 (Yang et al., 2017) investigated TiAlN's coating performance on a Ti(C,N) based cermet. Although the coating was found to have better adhesion to the cermet tool, its use promotes adhesive wear on the flank side of the tool and poor resistance to oxidation wear. Tijun et al. in 2017 (Li et al., 2017) reported that after applying a TiAlCrN coating, cutting performance was reduced with the addition of WC by up to 10% in the cermet tool due to

the increased hardness and transverse rupture strength of the tool deteriorating the adhesion strength of the coating.

1.1.11 Industrial Literature and Machining Parameters Selection

Figure 1.2 represents a summary of the industrial and academic literature for machining parameters. Based on the range of cutting speeds used in the literature, a machining condition has been carefully selected for the present study for dry high-speed machining, given the range of cutting inserts according to the manufacturer.
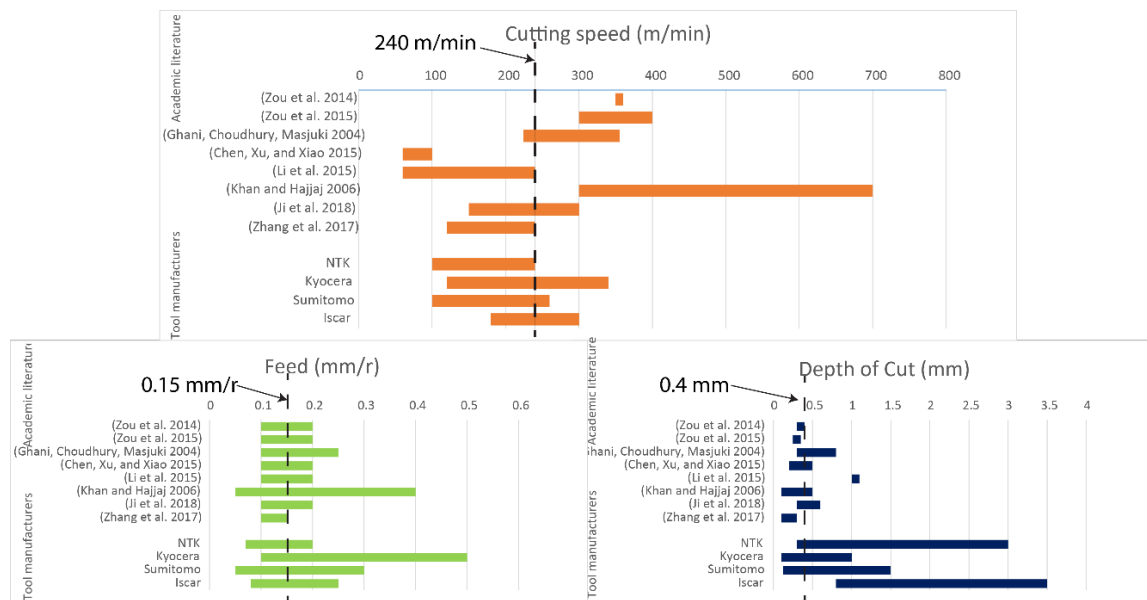
Figure 1.2 *Machining parameters selection based on research and industrial literature*

1.2 Research Gaps

Based on the literature review for machining stainless steel 304 and considering the challenges associated with it, a cermet tool can be a potential tool material choice. However, when it comes to high-speed machining without coolant, no adequate solutions are reported in the literature. Cemented carbide tools are still being used for machining

stainless steel alloys due to the limited availability of alternative tools and the difficulty associated with depositing a wear-resistant coating on cermet tools. Cemented carbide tools do not show significant improvement in performance to reduce the BUE problem, exhibit excessive abrasion and suffer from a high amount of diffusion wear. Cemented carbide tools also have limitations in terms of cutting speed for machining stainless steel. The literature shows that cermet tools perform better than cemented carbide tools and are a promising alternative for machining stainless steel if they are used with appropriate conditions.

1.3 Motivation and Research Objectives

Stainless steel 304 comprises 72% of the market for stainless steel, but has severe machinability issues and poor tool life. Developing a way to improve tool life during machining of AISI 304 will be beneficial to many industries. Service benefits of dry high-speed machining such as cost-effectiveness, reduced instrument clean up, wet scrap handling and cost, operator's health and safety, and environmental perspective prompt us to consider this challenging machining situation in the current research. The increasing demand for high-speed machining by manufacturers and the die/mold and aerospace industries motivates this research. To meet this demand and develop a cutting tool for such a challenging application, extensive studies are needed on the wear mechanisms and failure modes of cermet tools and existing commercial and conventional PVD coatings. Current research aims to increase the life of cermet cutting tools by mitigating or delaying tool wear

with the help of a newly developed advanced PVD coating for cermet cutting tools to be performed under dry high-speed machining conditions.

Based on the gaps in the literature, the proposed research objectives for this thesis are:

1. Study the tool wear mechanisms of commercial cermet tools of the same design with varying compositions for high-speed dry finish turning of AISI 304. (Phase-I)

2. Investigate the role of different commercial PVD coatings in enhancing the cermet tool performance. (Phase-II)

3. With the knowledge gained, design and develop new adaptive PVD coating(s) for high-speed dry finish turning of AISI 304 using cermet tools. (Phase-III)

1.4 Thesis Outline

The current thesis is divided into three phases of the study. Each phase of the study aims to address an objective. The complete study of each phase is included as a chapter in the thesis, as a published journal article or has been submitted for publication at the time this thesis was prepared. The last chapter of the thesis summarizes and gives the overall conclusion of the entire study.

Chapter 1 provides general background about stainless steel, its demand, properties, machining challenges, and various cutting tools. Brief literature on cermet cutting tools, wear mechanisms, and coatings. The end of this chapter provides a research objective based on literature review, gaps, and research motivation.

Chapter 2 presents the effect of cermet tool constituents and compositions on the tool's microstructure, wear mechanism, and machining performance. A progressive wear study was conducted with the help of a SEM. A comprehensive explanation of how the individual elements and compositions presented in the tool can alter the microstructure and affect the wear mechanism and tool performance is provided. The present chapter addresses the first objective of the research and is presented as a published article.

U.S. Patel, S.K. Rawal, A.F.M. Arif, S.C. Veldhuis, Influence of secondary carbides on microstructure, wear mechanism, and tool performance for different cermet grades during high-speed dry finish turning of AISI 304 stainless steel, Wear. 452–453 (2020) 203285. https://doi.org/10.1016/j.wear.2020.203285.

Chapter 3 contains the methodology and dataset of the research work completed in the previous Chapter 2. This chapter provides a detailed description of the methodology and approach used to perform all experimental work and all published data to the data repository for research review and conducts further studies. This chapter is presented as an article published in the journal Data in Brief.

U. Patel, S. Rawal, A.F.M. Arif, S. Veldhuis, Dataset and methodology on identification and correlation of secondary carbides with microstructure, wear mechanism, and tool performance for different CERMET grades during high-speed dry finish turning of AISI 304 stainless steel, Data in Brief. (2020) 105753.

https://doi.org/https://doi.org/10.1016/j.dib.2020.105753.

Chapter 4 studies consist of research work focused on the second objective of this research. This research phase aims to investigate the performance of various commercial coatings on cermet tools based on micromechanical properties, tool performance and surface roughness. Performance compared to similar composition coatings prepared in-house on our Kobelco coater. Investigate wear mechanisms with progressive wear studies and use findings from the causes of tool coating failure to develop an advanced in-house coating for Objective 3. The research work with this chapter is written below as a journal paper submitted for review.

U. Patel, S. Rawal, B Bose, A.F.M. Arif, S. Veldhuis, Performance Evaluations of Ti-based PVD coatings deposited on cermet tools for high-speed dry finish turning of AISI 304 stainless steel, Submitted to the "Wear" journal, July 2021.

Chapter 5 focuses on developing various in-house coatings to mitigate or delay coating failure and enhance cutting tool performance based on knowledge gains, with objectives 1 and 2. Various coating combinations with Ti, Al, Cr, Si, Y, and Ta were developed, optimized, and evaluated specifically to perform high-speed machining of stainless steel 304 with cermet tools. Detailed comprehensive analysis and explanation of the developed coating are provided in this chapter. This chapter covers the third objective of the research and is being prepared for publishing in the journal Wear.

U. Patel, B Bose, S. Rawal, A.F.M. Arif, S. Veldhuis, Development of PVD coatings to improve the machining performance of CERMET tools for high-speed dry finish turning

of AISI 304 stainless steel, Submitted to the "International Journal of Refractory Metals and Hard Materials" journal, September 2021.

Chapter 6 consists of combined general findings from previous chapters/objectives to the current thesis research work. This chapter also provides research contributions and suggestions for future research directions.

1.5   Note to the Reader

This thesis consists of a series of journal papers. A reader should note that chapters 2 to 5 are journal publications either published or under review. Although each chapter focuses on individual research objectives, some overlap or duplication may be found during reading. Similarities may be present particularly in the introduction and experimental work sections. A section describing the experimental work may be repeated since the test facilities and equipment used are the same for all experiments. However, readers are encouraged to read through all the material in each chapter as it contains valuable information for each study.

1.6   References

Abou-El-Hossein, K. A. and Yahya, Z. (2005) 'High-speed end-milling of AISI 304 stainless steels using new geometrically developed carbide inserts', in Journal of Materials Processing Technology, pp. 596–602. doi: 10.1016/j.jmatprotec.2005.02.129.

Ahmed, Y. S. et al. (2017) 'Effect of built-up edge formation during stable state of wear in AISI 304 stainless steel on machining performance and surface integrity of the machined part', Materials, 10(11), pp. 1–15. doi: 10.3390/ma10111230.

Bapat, P. S. et al. (2015) 'A Numerical Model to Obtain Temperature Distribution During Hard Turning of AISI 52100 Steel', Materials Today: Proceedings, 2(4–5), pp. 1907–1914. doi: 10.1016/j.matpr.2015.07.150.

Biksa, A. et al. (2010) 'Wear behavior of adaptive nano-multilayered AlTiN/MexN PVD coatings during machining of aerospace alloys', Tribology International, 43(8), pp. 1491–1499. doi: 10.1016/j.triboint.2010.02.008.

Childs, T. (2000) 'Metal Machining Theory and Applications', Materials Technology, p. 416.

Ciftci, I. (2006) 'Machining of austenitic stainless steels using CVD multi-layer coated cemented carbide tools', Tribology International, 39(6), pp. 565–569. doi: 10.1016/j.triboint.2005.05.005.

Conforto, E., Mari, D. and Cutard, T. (2004) 'The role of molybdenum in the hard-phase grains of (Ti, Mo)(C, N)-Co cermets', Philosophical Magazine, 84(17), pp. 1717–1733. doi: 10.1080/14786430310001659516.

D. G. Flam, R. Kamanduri, M. L. (1984) 'HIGH-SPEED MACHINING OF METALSl', Ann. Rev. Mater. Sci., 14, pp. 231–278.

Dhananchezian, M., Kumar, M. P. and Sornakumar, T. (2011) 'Cryogenic Turning of AISI 304 Stainless Steel with Modified Tungsten Carbide Tool Inserts', Materials and Manufacturing Processes, 26(5), pp. 781–785. doi: 10.1080/10426911003720821.

Dogra, M. et al. (2010) 'Tool wear, chip formation and workpiece surface issues in CBN hard turning: A review', International Journal of Precision Engineering and Manufacturing, 11(2), pp. 341–358. doi: 10.1007/s12541-010-0040-1.

Ghani, J. A., Choudhury, I. A. and Masjuki, H. H. (2004) 'Wear mechanism of TiN coated carbide and uncoated cermets tools at high cutting speed applications', Journal of Materials Processing Technology, 153–154(1–3), pp. 1067–1073. doi: 10.1016/j.jmatprotec.2004.04.352.

Groover, M. P. (2007) Fundamentals of Modern Manufacturing. Third Edit. John Wiley & Sons.

Gruss, W. W. (1987) Turning and milling of steel with cermet cutting tools. Scottsdale, AZ: Proceedings of ASM Tool Materials for High-Speed Machining Symposium.

Grzesik, W. (2017) 'Cutting Tool Materials', in Gifford, C. and Cain, H. (eds) Advanced Machining Processes of Metallic Materials. Second Edi. Joe Hayton, pp. 35–63. doi: 10.1016/B978-0-444-63711-6.00004-1.

Ji, W. et al. (2018) 'Design and fabrication of gradient cermet composite cutting tool, and its cutting performance', Journal of Alloys and Compounds, 732, pp. 25–31. doi: 10.1016/j.jallcom.2017.10.187.

Jiang, L. et al. (1996) 'Active wear and failure mechanisms of TiN-coated high speed steel and TiN-coated cemented carbide tools when machining powder metallurgically made stainless steels', Metallurgical and Materials Transactions A: Physical Metallurgy and Materials Science, 27(9), pp. 2796–2808. doi: 10.1007/BF02652372.

Jiang, L., Roos, A. and Liu, P. (1997) 'The influence of austenite grain size and its distribution on chip deformation and tool life during machining of AISI 304L', Metallurgical and Materials Transactions A: Physical Metallurgy and Materials Science, 28(11), pp. 2415–2422. doi: 10.1007/s11661-997-0198-z.

Jianxin, D. et al. (2011) 'Wear mechanisms of cemented carbide tools in dry cutting of precipitation hardening semi-austenitic stainless steels', Wear, 270(7–8), pp. 520–527. doi: 10.1016/j.wear.2011.01.006.

Jindal, P. C. et al. (1999) 'Performance of PVD TiN, TiCN, and TiAlN coated cemented carbide tools in turning', International Journal of Refractory Metals and Hard Materials, 17(1), pp. 163–170. doi: 10.1016/S0263-4368(99)00008-6.

Jun, W. et al. (2009) 'Effect of WC on the microstructure and mechanical properties in the Ti(C0.7N0.3)-xWC-Mo2C-(Co, Ni) system', International Journal of Refractory Metals and Hard Materials, 27(1), pp. 9–13. doi: 10.1016/j.ijrmhm.2008.01.010.

Kalss, W. et al. (2006) 'Modern coatings in high performance cutting applications', International Journal of Refractory Metals & Hard Materials, 24, pp. 399–404. doi: 10.1016/j.ijrmhm.2005.11.005.

Khan, A. A. and Hajjaj, S. S. (2006) 'Capabilities of Cermets Tools for High Speed Machining of Austentic Stainless Steel', 6, pp. 779–784.

Klocke, F. and Krieg, T. (1999) 'Coated tools for metal cutting-features and applications', CIRP Annals-Manufacturing Technology, 48(2), pp. 515–525. Available at: http://www.sciencedirect.com/science/article/pii/S0007850607632314.

Korkut, I. et al. (2004) 'Determination of optimum cutting parameters during machining of AISI 304 austenitic stainless steel', Materials and Design, 25(4), pp. 303–305. doi: 10.1016/j.matdes.2003.10.011.

Kulkarni, A., Sargade, V. and More, C. (2018) 'Machinability Investigation of AISI 304 Austenitic Stainless Steels using Multilayer AlTiN/TiAlN Coated Carbide Inserts', Procedia Manufacturing, 20, pp. 548–553. doi: 10.1016/j.promfg.2018.02.082.

Kümmel, J. et al. (2013) 'Surface layer states of worn uncoated and TiN-coated WC/Co-cemented carbide cutting tools after dry plain turning of carbon steel', Advances in Tribology, 2013. doi: 10.1155/2013/519686.

Li, P. et al. (2015) 'Study on serrated chip formation and tool wear of cermet tools for milling stainless steel 3Cr13Cu', International Journal of Advanced Manufacturing Technology, 77(1–4), pp. 461–467. doi: 10.1007/s00170-014-6476-1.

Li, T. et al. (2017) 'Structures and properties of TiAlCrN coatings deposited on Ti(C,N)-based cermets with various WC contents', International Journal of Refractory Metals and Hard Materials, 69(April), pp. 247–253. doi: 10.1016/j.ijrmhm.2017.08.020.

Limarga, A. M., Widjaja, S. and Yip, T. H. (2005) 'Mechanical properties and oxidation resistance of plasma-sprayed multilayered Al2O3/ZrO2thermal barrier coatings', Surface and Coatings Technology, 197(1), pp. 93–102. doi: 10.1016/j.surfcoat.2005.02.087.

Liu, Z. Q., Wan, Y. and Ai, X. (2004) 'Recent Developments in Tool Materials for High Speed Machining', Materials Science Forum, 471–472, pp. 438–442. doi: 10.4028/www.scientific.net/MSF.471-472.438.

Low, I. M. (2014) Advances in ceramic matrix composites, Advances in Ceramic Matrix Composites. Cambridge, UK: Woodhead Publishing. doi: 10.1533/9780857098825.

M.Rahman, K.H.W.Seah, T.N. Goh, C. H. L. (1996) 'EFFECTIVENESS OF VARIOUS COATINGS ON CERMET CUTTING TOOLS', Journal of Materials Processing Technology, 58(4), pp. 368–373. doi: 10.1016/0924-0136(95)02209-0.

M'saoubi, R. et al. (no date) Residual stress analysis in orthogonal machining of standard and resulfurized AISI 316L steels. Available at: https://ac.els-cdn.com/S0924013699003593/1-s2.0-S0924013699003593-main.pdf?_tid=65c62d61-385b-4502-8a23-90ae0e52a25c&acdnat=1547826764_1df3bdd192e92092b48f42c2223832f9 (Accessed: 18 January 2019).

M'Saoubi, R. et al. (1999) 'Residual stress analysis in orthogonal machining of standard and resulfurized AISI 316L steels', Journal of Materials Processing Technology, 96(1–3), pp. 225–233. doi: 10.1016/S0924-0136(99)00359-3.

Mahdavinejad, R. A. and Saeedy, S. (2011) 'Investigation of the influential parameters of machining of AISI 304 stainless steel', Sadhana - Academy Proceedings in Engineering Sciences, 36(6), pp. 963–970. doi: 10.1007/s12046-011-0055-z.

Manoj Kumar, B. V., Kumar, J. R. and Basu, B. (2007) Crater wear mechanisms of TiCN-Ni-WC cermets during dry machining, International Journal of Refractory Metals and Hard Materials. doi: 10.1016/j.ijrmhm.2006.12.001.

Marshall, D. B. et al. (1998) 'High-Temperature Stability of the Al2O3–LaPO4 System', Journal of the American Ceramic Society, 81(4), pp. 951–956.

Modern Metal Cutting: A Practical Handbook (1994). Sandvik Coromant.

O'Sullivan, D. and Cotterell, M. (2002) 'Machinability of austenitic stainless steel SS303', Journal of Materials Processing Technology, 124(1–2), pp. 153–159. doi: 10.1016/S0924-0136(02)00197-8.

Outeiro, J. C., Umbrello, D. and M'Saoubi, R. (2006) 'Experimental and numerical modelling of the residual stresses induced in orthogonal cutting of AISI 316L steel', International Journal of Machine Tools and Manufacture, 46(14), pp. 1786–1794. doi: 10.1016/j.ijmachtools.2005.11.013.

Peng, Y., Miao, H. and Peng, Z. (2013) 'Development of TiCN-based cermets: Mechanical properties and wear mechanism', International Journal of Refractory Metals and Hard Materials, 39, pp. 78–89. doi: 10.1016/j.ijrmhm.2012.07.001.

Philip Selvaraj, D. et al. (2014) 'Optimization of surface roughness, cutting force and tool wear of nitrogen alloyed duplex stainless steel in a dry turning process using Taguchi method', Measurement, 49(0), pp. 205–215. doi: http://dx.doi.org/10.1016/j.measurement.2013.11.037.

Philip Selvaraj, D. and Chandramohan, P. (2010) 'Optimization of surface roughness of AISI 304 austenitic stainless steel in dry turning operation using Taguchi design method', Journal of Engineering Science and Technology, 5(3), pp. 293–301. Available at: http://jestec.taylors.edu.my/Vol 5 Issue 3 September 10/Vol_5_3_293_301_DP_Selvaraj.pdf.

Prengel, H. G., Pfouts, W. R. and Santhanam, A. T. (1998) 'State of the art in hard coatings for carbide cutting tools', Surface and Coatings Technology, 102, pp. 183–190.

Rufe, P. D. (2013) Fundamentals of Modern Manufacturing. Third Edit. Edited by P. D. Rufe. Dearborn, Michigan: Society of Manufacturing Engineers.

Sharma, A. K., Tiwari, A. K. and Dixit, A. R. (2016) 'Effects of Minimum Quantity Lubrication (MQL) in machining processes using conventional and nanofluid based cutting fluids: A comprehensive review', Journal of Cleaner Production, 127, pp. 1–18. doi: 10.1016/J.JCLEPRO.2016.03.146.

Sreejith, P. S. and Ngoi, B. K. A. (2000) 'Dry machining: Machining of the future', Journal of Materials Processing Technology, 101(January 1999), pp. 287–291. doi: 10.1016/S0924-0136(00)00445-3.

Srivastava, A. K. and Das, K. (2010) 'The abrasive wear resistance of TIC and (Ti,W)C-reinforced Fe-17Mn austenitic steel matrix composites', Tribology International, 43(5–6), pp. 944–950. doi: 10.1016/j.triboint.2009.12.057.

Stephenson, D. A. and Agapiou, J. S. (2016) Metal Cutting Theory and Practice, Metal Cutting Theory and Practice.

Sushil, I., Amit, P. and Rohit, P. (2017) 'Machining Challenges in Stainless Steel – A Review', International Journal of Advance Research, Ideas and Innovations in Technology, 3(6), pp. 1395–1402. Available at: www.ijariit.com.

Tekiner, Z. and Yeşilyurt, S. (2004) 'Investigation of the cutting parameters depending on process sound during turning of AISI 304 austenitic stainless steel', Materials and Design, 25(6), pp. 507–513. doi: 10.1016/j.matdes.2003.12.011.

Wan, W. et al. (2012) 'Effects of Cr3C2 addition on the corrosion behavior of Ti(C, N)-based cermets', International Journal of Refractory Metals and Hard Materials, 31, pp. 179–186. doi: 10.1016/j.ijrmhm.2011.10.013.

Wang, J. et al. (2009) 'Effect of NbC on the microstructure and sinterability of Ti(C0.7, N0.3)-based cermets', International Journal of Refractory Metals and Hard Materials, 27(3), pp. 549–551. doi: 10.1016/j.ijrmhm.2008.07.003.

Whitney, E. D. (1994) Ceramic Cutting Tools. 1st Editio, William Andrew. 1st Editio. Edited by E. D. Whitney. New Jersey: Noyes Publications.

Wolfe, G. J., Petrosky, C. J. and Quinto, D. T. (1986) 'The role of hard coatings in carbide milling tools', Journal of Vacuum Science & Technology A, 2747(April 1986), pp. 2747–2754. doi: 10.1116/1.573673.

Xavior, M. A. and Adithan, M. (2009) 'Determining the influence of cutting fluids on tool wear and surface roughness during turning of AISI 304 austenitic stainless steel', Journal of Materials Processing Technology, 209(2), pp. 900–909. doi: 10.1016/j.jmatprotec.2008.02.068.

Xing, Y. et al. (2014) 'Cutting performance and wear mechanism of nanoscale and microscale textured Al2O3/TiC ceramic tools in dry cutting of hardened steel', International Journal of Refractory Metals and Hard Materials, 43, pp. 46–58. doi: 10.1016/j.ijrmhm.2013.10.019.

Xiong, J. et al. (2007) 'The effect of WC, Mo2C, TaC content on the microstructure and properties of ultra-fine TiC0.7N0.3 cermet', Materials & Design, 28(5), pp. 1689–1694. doi: 10.1016/j.matdes.2006.03.005.

Yamamoto, K. et al. (2003) 'Properties of (Ti , Cr , Al) N coatings with high Al content deposited by new plasma enhanced arc-cathode', 175, pp. 620–626. doi: 10.1016/S0257-8972.

Yang, W. et al. (2017) 'Structure and properties of PVD TiAlN and TiAlN/CrAlN coated Ti(C, N)-based cermets', Ceramics International, 43(2), pp. 1911–1915. doi: 10.1016/j.ceramint.2016.10.151.

Ying, X. et al. (2011) 'Effect of VC addition on the microstructure and properties of Ti(C,N)-based nano cermets', Rare Metals, 30(6), pp. 583–588. doi: 10.1007/s12598-011-0433-z.

Zhang, S., Li, J. F. and Wang, Y. W. (2012) 'Tool life and cutting forces in end milling Inconel 718 under dry and minimum quantity cooling lubrication cutting conditions', Journal of Cleaner Production, 32, pp. 81–87. doi: 10.1016/j.jclepro.2012.03.014.

Zhang, Y. et al. (2017) 'Experimental study on cutting performance of microwave sintered Ti(C, N)/Al2O3 cermet tool in the dry machining of hardened steel', International Journal of Advanced Manufacturing Technology, 91(9–12), pp. 3933–3941. doi: 10.1007/s00170-017-0062-2.

Zou, B. et al. (2014) 'Study of a hot-pressed sintering preparation of Ti(C_7N_3)-based composite cermets materials and their performance as cutting tools', Journal of Alloys and Compounds, 611, pp. 363–371. doi: 10.1016/j.jallcom.2014.05.150.

Zou, B. et al. (2015) 'Tool damage and machined-surface quality using hot-pressed sintering Ti(C_7N_3)/WC/TaC cermet cutting inserts for high-speed turning stainless steels', International Journal of Advanced Manufacturing Technology, 79(1–4), pp. 197–210. doi: 10.1007/s00170-015-6823-x.

Chapter 2 : Wear Mechanism and Performance Evaluation of Various Uncoated Cermet Tools

Complete Citation:

Copyright:

Author's Contributions:

Uttkarsh Patel	Conceptualization, Investigation, Formal analysis, Validation, Visualization, Methodology, Data Curation, Writing - Original Draft
Sushant Rawal	Conceptualization, Methodology, Validation, Supervision, Writing - Review & Editing
Abul Fazal M Arif	Conceptualization, Methodology, Project administration, Writing - Review & Editing
Stephen Veldhuis	Resources, Project administration, Funding acquisition, Supervision

Abstract

This research investigates wear morphology of a Ti(C,N)-based cermet tools used for the high-speed dry turning of austenitic stainless steel (AISI 304) specifically for finishing operation. The goal of this study is to investigate the influence of compositions from different cermet tools supplied by various manufacturers on microstructure, properties and tool wear morphology while finishing turning of AISI 304. A progressive wear study was performed at a fixed cutting length interval to measure the tool wear of different cermet tools. The tool wear and structure of cermet tools were examined by Scanning Electron Microscope (SEM). Tool material compositions and phases were determined using Energy-Dispersive X-ray Spectrometry (EDS) and X-ray diffraction (XRD), respectively. The results show that different elemental concentrations alter the microstructure of cermet tools by changing its core size and shape, which eventually shows the influence on mechanical properties and machining performance. The study also indicates that various elements are forming different compositions in cermet tools that play a critical role in determining their binding strength, heat resistance and lubricity during machining, which significantly affects the tool life.

Keywords: Cermet; 304 stainless steel; tool wear; notch; dry machining; high-speed machining

2.1 Introduction

Stainless steels are typically used to manufacture food processing and chemical equipment, as well as machinery parts that require high corrosion resistance (Groover, 2007). Stainless steels are known for their high work hardening rate, low thermal conductivity, high ductility, high tensile strength and high fracture toughness (Philip Selvaraj and Chandramohan, 2010). American Iron and Steel Institute (AISI) 304 austenitic stainless steel contains a minimum of 18% chromium to increase the hardness of the steel without compromising its ductility. Chromium content improves the grain refinement in the steel, which also increases its toughness and enhances the high-temperature strength of the steel. Stainless steel 304 also contains a minimum of 8% nickel to improve toughness, especially at low temperatures, reduce corrosion and minimize scratches. Nickel also imparts some heat resistance to the 304 stainless steel (whose thermal conductivity is three times lower than that of steel and five times lower than iron), which makes machining very challenging due to the high temperatures present in the cutting zone. Almost 80% of the generated heat is transferred into the tool, with its surface temperature reaching up to about 1000°C, which causes rapid tool wear due to diffusion and oxidization (Bapat et al., 2015). In addition, the high strain hardening rate of AISI 304 promotes the adhesion of stainless steel to the cutting tool surface, generating unstable chips and built-up edge (BUE) formation (Korkut et al., 2004).

High-speed machining is well-known in both die/mold and aerospace applications. The most commonly used materials in these applications are titanium, steels (including stainless

steel), and aluminium. Since each of these materials has its own unique attributes, their high-speed machining requires different approaches. However, undertaking high-speed machining presents further challenges, since the magnitude of all stress components increases along with cutting speed (M'Saoubi et al., 1999; Outeiro, Umbrello and M'Saoubi, 2006).

As of late, green or dry manufacturing has gained popularity in the manufacturing industry to meet environmental regulations and mitigate occupational health hazards. The major benefit of dry machining is that it leaves behind no atmosphere or water pollution and produces no swarf residue, which reduces associated disposal costs and health issues. In general, dry machining also reduces machining costs (Sreejith and Ngoi, 2000). Sharma et al. (Sharma, Tiwari and Dixit, 2016) assessed that cutting fluids used in the machining process make up approximately 16-20% of the total production costs in the manufacturing sector. The implementation of dry machining eliminates the need to use cutting fluid. However, this process also presents several drawbacks. The dry cutting condition does not allow the use of coolant; therefore, friction and adhesion between the tool and the chip are higher, and so is the temperature. This results in a higher wear rate and shorter tool life (Kramar et al., 2013).

Cemented carbide tools are most widely used for machining metal materials. As the cutting speed increases, so does the average cutting temperature at the tool-chip interface. When cutting speeds exceed 140 meters/minute, the temperature surpasses 500°C. The diffusion of elements throughout the tool-chip interface will begin at such high temperatures from the WC/Co or WC/TiC/Co carbide to stainless steel and vice versa. This phenomenon

causes rapid wear on the rake face of the tool and weakens the tool edge. In addition, the most commonly reported wear modes during the machining of stainless steel in carbide tools are adhesive and abrasive wear (Jianxin et al., 2011). Tekiner and Yeşilyurt (Tekiner and Yeşilyurt, 2004) used a WC P10 cemented carbide tool to machine AISI 304 at varying cutting speed, feed rate and depth of cut. During this study, the BUE was observed to decrease with the growth of cutting speed and increase along with feed rate. Korkut et al. in 2004 (Korkut et al., 2004) conducted experiments using a multilayer-coated (TiC, TiCN, Al_2O_3, TiN) cemented carbide tools on AISI 304 austenitic stainless steel by varying the cutting speed to 120, 150 and 180 m/min. They observed that the surface roughness values decrease as the cutting speed grows. Xavior et al. 2009 (Xavior and Adithan, 2009) investigated the effect of different cutting fluids on the tool wear and surface roughness during the turning of AISI 304 with a carbide tool. They determined that the cutting speed and feed have a more significant influence on tool wear than the cutting fluid. Yassmin et al. 2017 (Ahmed et al., 2017) investigated the effect of a build-up edge in the steady-state zone during the wet machining of AISI 304 with an uncoated carbide tool (WC-Co). Tensile residual stress decreased with the growth of BUE height and axial compressive stress. The surface roughness increased along with the growth of BUE. Korkut et al. in 2004 (Korkut et al., 2004) conducted experiments using a multilayer coated (TiC, TiCN, Al_2O_3, TiN) cemented carbide tool on AISI 304 austenitic stainless steel by varying the cutting speed to 120, 150 and 180 m/min. They observed that the surface roughness values decrease as the cutting speed grows. In summary, the above literature for carbide tools shows that most of

the work on carbide tools is finished by cooling or by various cooling techniques (max cutting speed 210m/min with coating and cooling techniques).

High-Speed Steel (HSS) tools are used to machine various alloys but reach catastrophic failure at cutting speeds greater than 45m/min as the chips become red hot. (Jiang et al., 1996). Diamond tools are used to machine many nonferrous materials due to excellent properties such as high hardness, and dimension stability during machining but are the most expensive cutting tool materials. However, they can't be used for machining stainless steel due to the high carbon affinity of stainless steel that draws the carbon out of the diamond. (Grzesik, 2017). Dorga et al. (Dogra et al., 2010) reported tool wear, chip formation and workpiece surface issues during hard turning with CBN. The issues related to ploughing arise due to a large nose radius and large negative chamfer angle.

Ceramics are non-metal materials. The advantages of ceramic tools include incredibly high resistance to abrasive wear and cratering, high-temperature hardness and compressive strength. Ceramics have excellent chemical stability and low affinity with ferrous metals (Whitney, 1994). However, low tensile strength, fracture toughness, thermal conductivity and thermal shock resistance limit the use of ceramics for machining steel alloys (Low, 2014).

Cermet is a composite material that consists of ceramic and metal. It is designed to possess higher temperature resistance, bending strength and fracture toughness as well as higher thermal shock resistance than oxide-based ceramics while retaining the ability to undergo plastic deformation like a metal (Gruss, 1987). Cermet tools are mainly composed of a

core-rim structure with a titanium carbon-nitride (C, N) forming a hard phase (core). Nickel or cobalt serves as a binder (matrix). The phase surrounding the core, or rim, has a similar crystalline structure as the core.
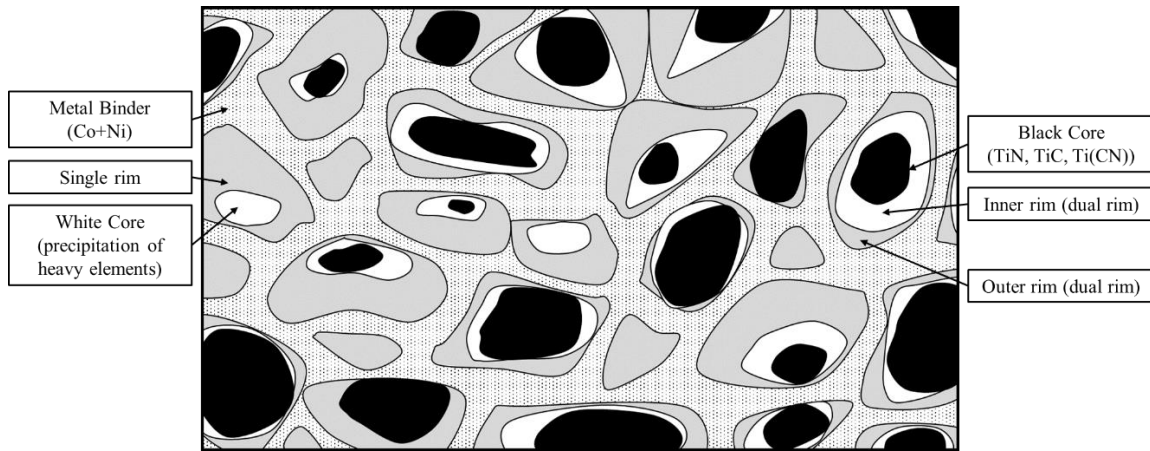
Figure 2.1 *Schematic SEM microstructure image (BSE) representation of Ti(C,N)-based commercial inserts*

The microstructural schematic image of a commercial cermet is shown in Figure 2.1. In Figure 2.1, black regions represent the cermet matrix cores that mostly contain Ti (C,N). This core binds with a metal binder such as cobalt (Co) and/or nickel (Ni) represented by the black dotted region. During the sintering process, a reaction between the core and binder forms a rim around the core. It can be a single or dual rim structure depending on the type of secondary carbide used in the production process and/or the manufacturing process (Ahn and Kang, 2000). In the case of a dual rim, the inner rims are bright rings containing heavy elements, whereas the outer rims, represented by grey loops surrounding the cores, may consist of solid solutions of Ti, W, and other secondary carbide elements(C, N). Stronger chemical bonds between the binder and the hard phases can be achieved by improving

wettability with the help of secondary carbides such as WC, VC, NbC, Cr_3C_2, TaC, Mo_2C (Peng, Miao and Peng, 2013).

Cermets are more sensitive to feed and have superior friction properties. The diffusion wear and thermal expansion coefficients are lower in cermet (Stephenson and Agapiou, 2016) than in WC (Tungsten carbide). Cermet outperforms coated carbide in terms of tool life by around 20% to 100% when used in appropriate applications. It works best with irons and steels that produces a continuous chip. Cermet can operate at a much higher surface cutting speed for more extended periods of time and can produce an excellent surface finish without the need for a coolant (Stephenson and Agapiou, 2016).

Zou et al., in 2014 (Zou et al., 2014) prepared a $Ti(C_7N_3)$ tool using various superfine WC and TaC particles. They accessed the performance of cermet as a cutting tool under cooling conditions at a maximum cutting speed of 350m/min. Chen et al. in 2015 (Xing et al., 2014) performed cutting and wear characteristics of Ti(C, N) cermet during turning hardened steel under dry cutting with 60–100 m/min cutting speed. Zou et al. 2015 (Zou et al., 2015) prepared a $Ti(C_7N_3)$/WC/TaC cermet and evaluated tool wear with the high-speed turning of 17-4PH martensitic (350~400 m/min) and 321 austenitic stainless steels (300~350 m/min) under cooling condition. Zhang et al. in 2017 (Zhang et al., 2017) prepared Ti(C, N)/Al2O3 cermet tool and investigated cutting performance and wear mechanism under dry cutting of hardened steel 40Cr (AISI 5140) for cutting speed of 120,180, and 240 m/min. They found the optimum cutting speed of 120m/min for metal removal, surface roughness and tool life.

Literature shows that many researchers have worked with cermet tools to machine various materials with different cutting parameters with cutting speeds up to 350m/min with various cooling methods. There is a scarcity of published work on the dry high-speed finishing machining of 304 stainless steel. AISI 304 is used in this experiment due to its severe machinability issues and also due to the fact that it comprises 72% of the market for stainless steel (Kulkarni, Sargade and More, 2018). The aim of this research work is to address this specific area and compare the performance of uncoated cermet tools from different manufacturers for dry high-speed finishing machining of 304 stainless steel. The study includes the effect of tool material composition on the microstructure, tool life and the tool wear mechanism for machining of 304 stainless steel under dry high-speed machining conditions.

2.2 Experimental Procedure
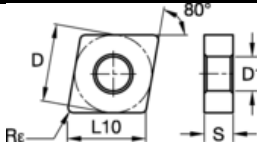
Dry high-speed machining tests were performed on a CNC turning machine OKUMA crown L1060. The workpiece material was AISI 304 steel with a hardness of 125 BHN. The mechanical properties and chemical composition of the workpiece are given in Table 2.1 ('ISO 15510-Stainless Steels-Chemical Composition: Stainless Steels 304', 2014).

Four different commercially available uncoated cermet tool inserts were investigated, each being of type CNMG 120408/CNMG 432. The details of these tools named Tool A, Tool B, Tool C and Tool D are given in Table 2.2. The machining tests were performed at a feed rate of 0.15 mm/rev, depth of cut of 0.4mm and cutting speed of 240 m/min.

Table 2.1 *Chemical composition and mechanical properties of AISI 304 stainless steel*

Chemical composition (%)								
C	Si	Mn	P	S	Cr	Ni	N	Balance
0.08	0.75	2.0_{max}	0.045_{max}	0.03_{max}	18-20	8-10.5	0.1_{max}	Fe(iron)

Mechanical properties						
Yield Strength	Tensile Strength	Elongation	Modulus of Elasticity	Shear Modulus	Hardness	Poisson's Ratio
215 MPa	505 MPa	70%	193-200 GPa	86 GPa	123 HB	0.29

Table 2.2 *Cutting tool's type, geometry, designation and hardness*

Tool label	Hardness (HV)	Tool geometry of the inserts CNMG 120408 / CNMG 432	
Tool A	1735 HV		D= 12.70mm
Tool B	1663 HV		L10= 12.90mm
			Rε=0.8mm
Tool C	1664 HV		D1=5.16mm
Tool D	1622 HV		S=4.76mm

Tool wear changes were characterized by volume wear measurements taken by a white light focus variation interference microscope (Alicona Infinite Focus G5 microscope,

Alicona Manufacturing Inc., Bartlett, IL, USA). A JEOL 6610LV Scanning Electron Microscope was used to capture the tool wear and edge geometry at different magnifications to observe the wear behavior at fixed machining intervals and to examine the cermet structure. Energy-dispersive X-ray spectroscopy (EDS) was used for compositional analysis. Tool life tests were conducted under the ISO 3685:1993 standard. Flank wear and notch wear were measured at fixed cutting length intervals by means of an optical microscope system that consisted of an X-Y table, a Mitutoyo digital micrometer and a KEYENCE-VHX 5000 digital microscope. A tool life criterion limit of 0.3mm was fixed based on the ISO 3685:1993 standard (Standardization, 2006). The hardness of different inserts was measured using a Vickers indenter. The structure of different cermet tools was studied by X-ray diffraction (XRD) (D8 Discover DAVINCI.DESIGN diffractometer, with Parallel Focus Goebel Mirror and Vantec 500 area detector) using a cobalt sealed tube source ($\lambda_{avg} = 1.79026$ Å). Samples were scanned in six steps at 22-112° range with an exposure time of 480s for each step.

2.3 Results and Discussion

Four uncoated commercial cermet tools were used in the current study. A reverse engineering approach was undertaken to identify various added secondary carbides in the cermet tool and evaluate the effects of the added secondary carbide on the microstructure, its effect on the wear mechanism and tool life during high-speed dry finish turning of 304 stainless steel.

2.3.1 Microstructure Analysis

The cermet microstructure morphology was studied using secondary and backscattered electrons (BSE) in the SEM. Figure 2.2 shows the SEM-BSE images of the microstructure of all cermet tools investigated in this study. The microstructure of all tools features a typical core-rim structure with black and white cores. Tools A and C show a rounded core structure displayed in Figure 2.2 (a) & (c), respectively. However, Tool A features finer cores and Tool C has a coarser core structure.
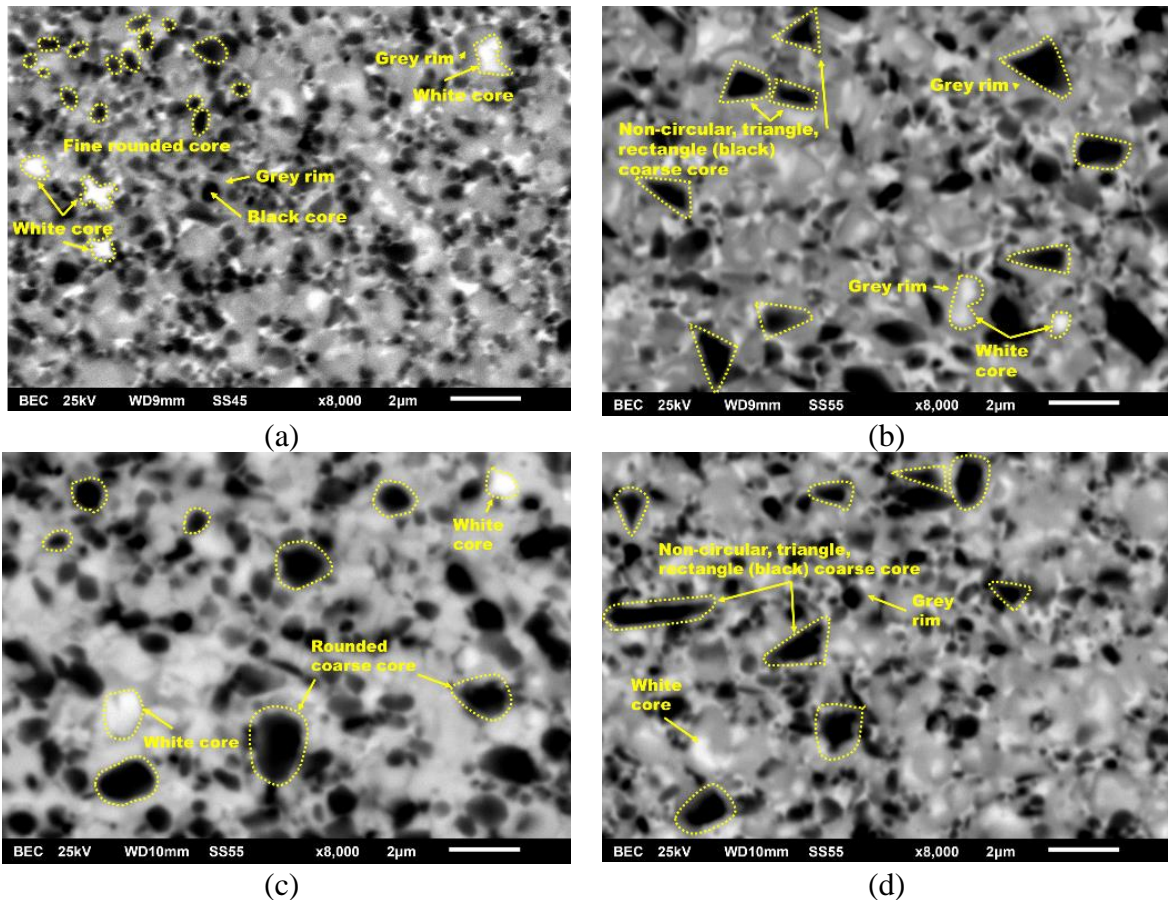
Figure 2.2 *Backscattered electron (BSE) SEM image of all Ti(C, N)-based cermet tools (a) Tool A, (b) Tool B, (c) Tool C, and (d) Tool D*

Tools B and D have non-circular, triangular and irregular coarse cores compared to Tool A as can be seen in Figure 2.2 (b) & (d), respectively. The elemental compositions were analyzed by means of EDS along with SEM. Table 2.3 shows the elemental weight % (wt.%) obtained by EDS of all four cermet tools, which are used to relate the effects of basic elemental composition on the microstructure of the tool material.

Table 2.3 *Elemental concentration (wt.%) of all cermet tools by EDS*

	Ti	W	Co	Ni	Nb	V	C	N	Mo	Ta	Others
Tool A	44.0	17.8	6.1	2.1	7.0	1.6	14.3	6.1			Balance
Tool B	36.7	22.7	5.3	5.9	5.0		15.0	5.2			Balance
Tool C	37.8	9.4	6.0	4.2	1.8	4.4	17.3	3.8	7.5	7.0	Balance
Tool D	38.2	20.1	7.3	7.0	5.1		14.8	3.7			Balance

The size of a cermet tool core depends on the manufacturing process and the presence of added secondary carbides like WC, NbC, MoC, TaC, and VC. However, the effects of all individual secondary carbides are different, and they are introduced into the tool to address specific issues. Literature states that tungsten carbide (WC) can be used to improve the wettability of hard carbide grains with the metal binders due to the low solubility in the binder (Kwon et al., 2004; Jun et al., 2009). Based on the EDS results from Table 2.3, the maximum concentration of tungsten (W) was found to be 22.7 wt.%, and the minimum was 9.4 W wt.% in Tool B and Tool C, respectively. For Tools A and D, it was 17.8 wt.% and 20.1 wt.%, respectively.
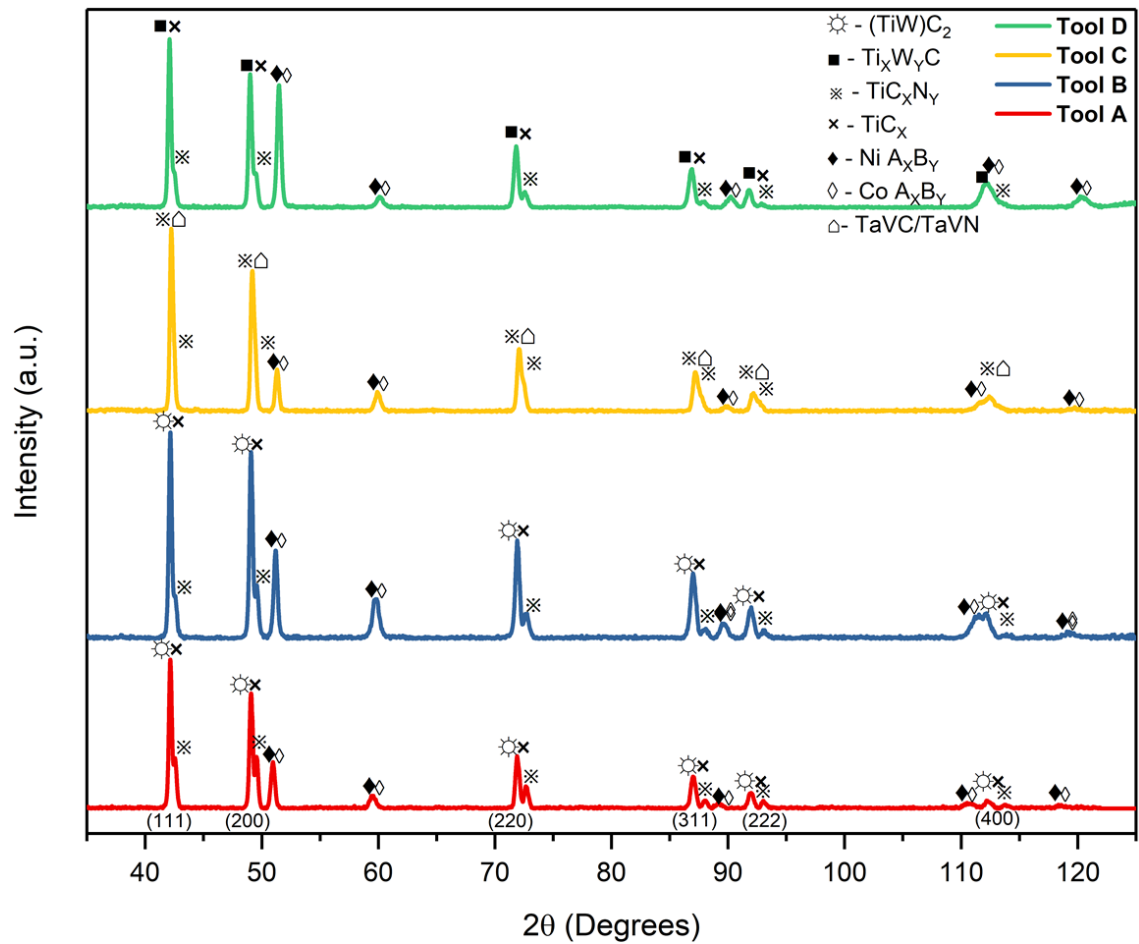
Figure 2.3 *Comparison of XRD patterns with phase identification of cermet tools Tool A,*

Tool B, Tool C and Tool D

The XRD results in Figure 2.3 shows that a major portion of tungsten (W) is dissolved in the binder forming a (TiW)C phase in Tools A, B, and D. While undergoing the sintering process, tungsten (W) quickly reacts with the metal binder due to the low heat formation energy of WC (Kwon et al., 2004) and later with the cores, to form a (TiW)C phase in Tools A, B, and D. The radii of (Ti) and tungsten (W) atoms are 1.47 and 1.41Å, respectively, but due to the low affinity between tungsten and nitrogen, the Ti(C,N) peak shifts to the low angles with the formation of the (Ti,W)C phase. The increase in WC content leads to

46

the splitting of the peak as can be seen in Figure 2.3. This result corresponds to the rim structure of the (Ti,W)C solid solution and to the Ti(C,N) cores. The rim structure is the major contributor to the observed (Ti,W)C major peak. It is also evident from Figure 2.3 that no (TiW)C phase is formed in Tool C due to the low amount of W (9.4 wt.%) as confirmed by EDS results. The amount of tungsten (W) dissolved in the metal binder was insufficient to react with the core material to form a (TiW)C phase.

(a)

(b)

(c)

(d)
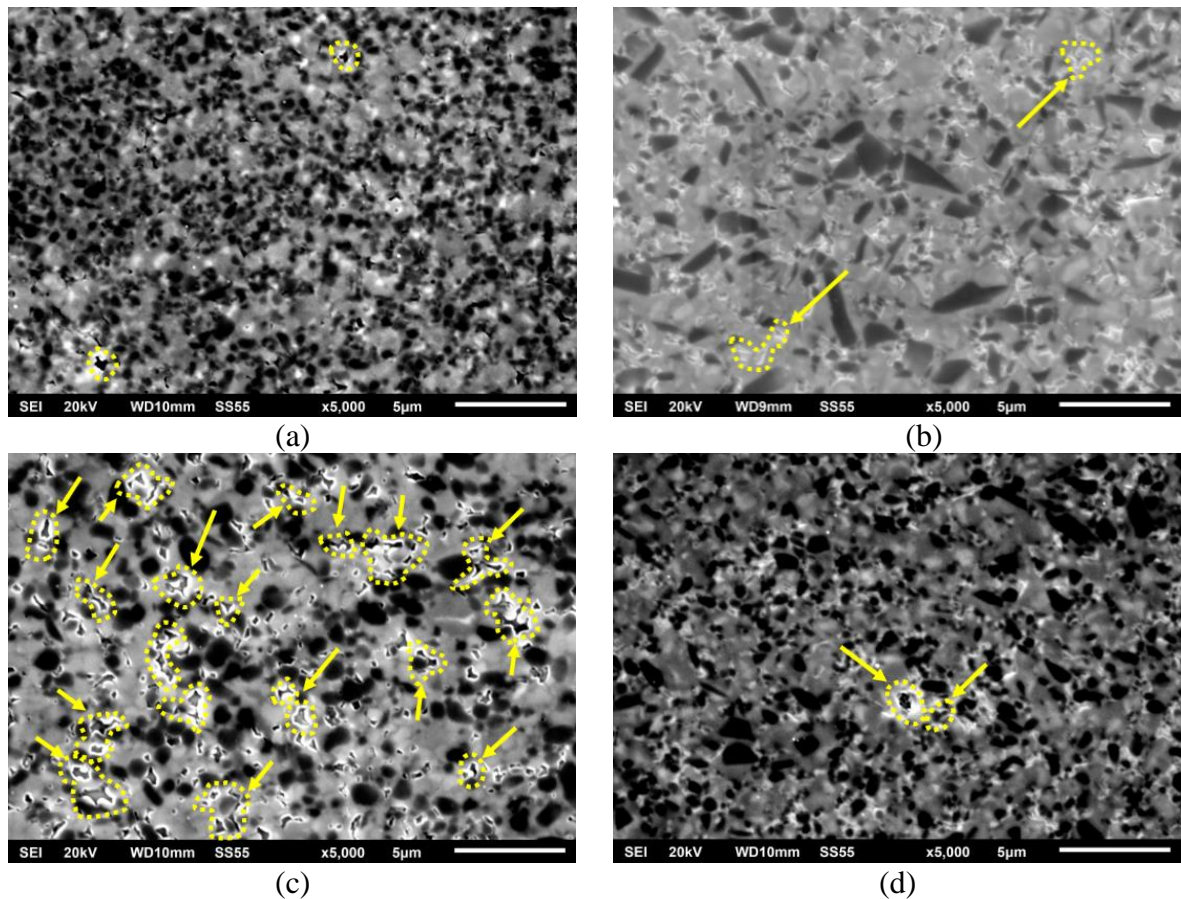
Figure 2.4 *Secondary electron SEM images of all Ti(C, N)-based cermet tool with their*

porosity marked in yellow in (a) Tool A, (b) Tool B, (c) Tool C, and (d) Tool D

Table 2.3 shows that Tool A & C contains 1.6 wt.% and 4.4 wt.% of vanadium (V), respectively. It is reported in the literature (Ying et al., 2011) that the presence of vanadium produces a rounded core and finer grains, as evident in Figure 2.4 (a) & (c). Lack of vanadium (V) in Tools B and D resulted in a coarse core with non-circular, triangular and rectangular, irregular coarse cores shapes. The addition of VC is responsible for reducing the grain size (Ying et al., 2011), but an excessive amount of VC does yield a finer grain. Grain size directly affects the hardness of the tool. According to the Hall-Petch theory, hardness increases as the grain size becomes more refined. In this study, Tool A has finer grains and maximum hardness compared to all other tools as given in Table 2.2 due to the limited presence of vanadium in Tool A (1.6 wt.%) compared to the other tools.

Tool A	black core	grey rim	white core
Ti	59.6	47.3	39.3
W	8.6	18.5	24.9
Nb	3.9	7.8	11.5
Co	3.3	4.5	1.9
Ni	1	1.6	0.6
C	7.4	12.5	13.3
N	15.2	6.5	6.8
V	1	1.4	1.8
Mo			
Ta			

(a)

Tool B	black core	grey rim	white core
Ti	63.6	37.9	34.6
W	11.7	29.3	32.1
Nb	6.4	10.8	13.2
Co	1.5	4.1	3.3
Ni	1.9	4.7	3.5
C	9.8	10.9	11.3
N	5.1	2.5	2
V			
Mo			
Ta			

(b)

Tool C	black core	grey rim	white core
Ti	67.1	39.3	23.6
W	4.4	12	12.9
Nb	4.1	5.6	6.5
Co	1.9	5.7	2.3
Ni	1.4	4.2	1.6
C	10.6	12.6	14.2
N	4.6	3.2	1.1
V	2.2	4.7	6.4
Mo	0.6	4.6	16.8
Ta	3.1	8.3	14.6

(c)

Tool D	black core	grey rim	white core
Ti	42.1	34.3	32.7
W	17.8	26	19.8
Nb	7.8	11.5	7.8
Co	9.6	7.7	14.6
Ni	9.4	7.5	14.6
C	9.9	10.9	8.8
N	3.5	2	1.7
V			
Mo			
Ta			

(d)

Figure 2.5 *Point EDS spectrum from core (blue spectra), grey rim (green spectra), and white regions (red spectra) of cermet tools (a) Tool A, (b) Tool B, (c) Tool C, (d) Tool D*

A secondary image of surface topography was captured in SEM, and point EDS spectra, as shown in Figure 2.5, were collected to measure the elemental variation and its effect on microstructure at three different locations: (i) the first at the core, represented in blue, (ii) the second at the rim represented in green and (iii) the third at the white represented in red.

Captured secondary SEM images show porosity at a different level in different inserts highlighted by yellow contours, as shown in Figure 2.4. Tool C features the maximum level of porosity and has a less dense structure compared to all other tools. This effect can be explained by the niobium (Nb) content in the tool material. Tool A has the maximum niobium (Nb) content of 7 wt.%, whereas Tools B and D have 5 wt.% and 5.1 wt.%, respectively. Tool C has the minimum niobium (Nb) content of 1.8wt.%, which is quite low compared to the other tools. It has been reported in the literature that NbC is used to lower the sintering temperature (Wang et al., 2009). As a result, more phases are formed at lower temperatures and the volume of the liquid phase increases from the addition of other secondary carbides to the liquid form. Additionally, at this liquid stage, most of the NbC is dissolved into the binder phase, as confirmed by the point EDS spectrum shown in Figure 2.5. Jun et al. Reported similar results (Wang et al., 2009) while comparing the effect of the added NbC on sinterability by varying the NbC content from 5 and 10wt.%. The reduction in porosity produces a denser tool material with improved mechanical properties. Huang et al. (Huang et al., 2008) reported that material grades containing less than 10wt% NbC provide more densification. However, increasing the NbC content beyond 30-40 wt.% can drastically decrease the densification. In the current study, Tool A has maximum

niobium (Nb) content of 7 wt.% as given in Table 2.3, resulting in the lower amount of porosity evident in Figure 2.4 and imparting high hardness to the tool material.

Molybdenum (Mo) is only observed in Tool C with a content of 7.5 wt.%. Literature shows that molybdenum (Mo) improves the wettability with the binder (Xiong et al., 2007) and can inhibit the core growth (Conforto, Mari and Cutard, 2004). The titanium (Ti) concentration in Tool C is drastically reduced by 41% and 65% in the grey and white region of the tool material compared to the core, as shown in Figure 2.5. This is the highest reduction of titanium (Ti) into the grey and white regions of the tool compared to all other tools. This may indicate that the presence of molybdenum (Mo) prevents the diffusion of titanium Ti from the boundary of the core, resulting in core growth inhibition as reported in the literature (Zhang, Liu and Rong, 2008).

The literature also mentions that NbC is used as a replacement for costly TaC in cermets (Wang et al., 2009). Tool C has niobium (Nb) content of 1.8 wt.% and tantalum (Ta) content of 7.0 wt.% as shown in Table 2.3, indicating that the manufacturer tried to use tantalum (Ta) as a replacement for niobium (Nb) to form the respective carbides. It is expected for TaC to increase the dissolution of secondary carbides and cores to reduce the grain size (Peng Wu, Yong Zheng, Yongle Zhao, 2010). However, instead of forming finer grains due to the presence of TaC, Tool C features a moderate core size as evident from Figure 2.2 (c). This can be explained by the effect of molybdenum (Mo) on core formation as discussed earlier, which prevents the core from dissolving into the binder. A similar effect was also reported in a study by Peng et al. (Peng Wu, Yong Zheng, Yongle Zhao, 2010) where grains agglomerated due to mass transportation resulting in diffusion and plastic flow of cores as

a result of tantalum (Ta) addition during the sintering process. The addition of 7wt.% of TaC increased the porosity of the material structure. This was also observed in the current study for Tool C that has 7wt.% tantalum (Ta), also as evident from Figure 2.4c for Tool C, indicating the highest amount of porosity amongst all the tools.

Figure 2.5 shows that more carbon is present more outside of the core, and it accumulates in the direction of the white rim area. Nitrogen content is greatest in the core itself but is low in the grey rim and white core areas. The core consists of TiCN and TiN only, whereas the grey rim area is formed by the dissolution of various secondary carbides such as CoAXBY and NiAXBY (A=Ti, B=W, V, Nb, Ta, Mo) with binders present in this region as evident from Figure 2.4 and Figure 2.5. Since the core contains TiCN, the maximum of N can be found in the core area but not in the grey and white regions due to the small size of the nitrogen atom. As a result, nitrogen (N) has a tendency to diffuse towards the core since this region is free from heavy atoms such as W, Ta, Mo, and Nb (Conforto, Mari and Cutard, 2004). Figure 2.5 also shows that most of the secondary carbides W, Nb, V, Mo and Ta are dissolved within the binder. The concentration of titanium (Ti) decreases drastically from the core to the rim and the white core in all tools. However, secondary carbides such as W, Nb, Mo, Ta exhibit the opposite trend, being richly concentrated in the white core region, which can be confirmed by the SEM BSE image colour contrast, where heavier elements are displayed in white. Additionally, it can be seen in Figure 2.5 that the concentration of binder is significantly reduced in the white core, meaning that the latter is produced by the precipitation of additional secondary carbides.

Figure 2.2 displays all images with the white cores in the tools. Since BSE images depict the chemical contrast, heavy atoms are outlined in a brighter colour compared to the light atoms resulting in the colour contrast for the BSE images. EDS spectrum in Figure 2.5 reveals that the added secondary carbides in all the tools can be mostly detected from the grey and white areas of the BSE-SEM images. This indicates that most of the secondary carbides are reacting with the binder to build up the grey rim responsible for holding the core within the matrix. The results of XRD in Figure 2.3 also confirm that all the secondary carbides form a new phase with the binder in having the same crystal structure as the major phases due to the dispersed molecules forming the secondary carbides with the binder metals or vice versa.

2.3.2 Tool Life Analysis

The cutting tests were performed to measure the tool performance and investigate wear morphology. Evaluation of tool life was based on an ISO 3685 standard, by which the flank wear and notch wear (length and width) were measured following a defined cutting interval that reached a fail criterion of 300μm by flank or notch wear. The tool performance was evaluated based on the flank wear and tool failure images as shown in Figure 2.6. Tool performance based on the notch wear length and width represented by the 3D wear volume view is shown in Figure 2.7. All tools except Tool B failed by notch length and Tool B failed by notch width. Notching was observed in all tools after a machining length of 100m, as observed with a digital microscope.
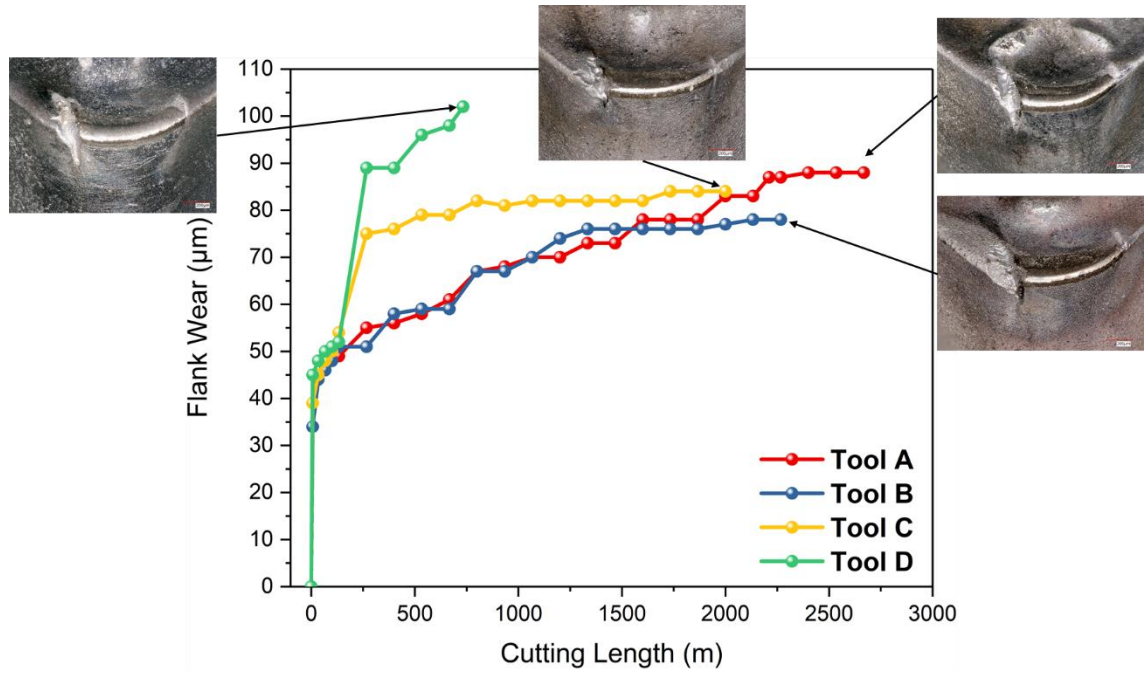
Figure 2.6 *Tool flank wear progression with cutting length*

(a)   (b)
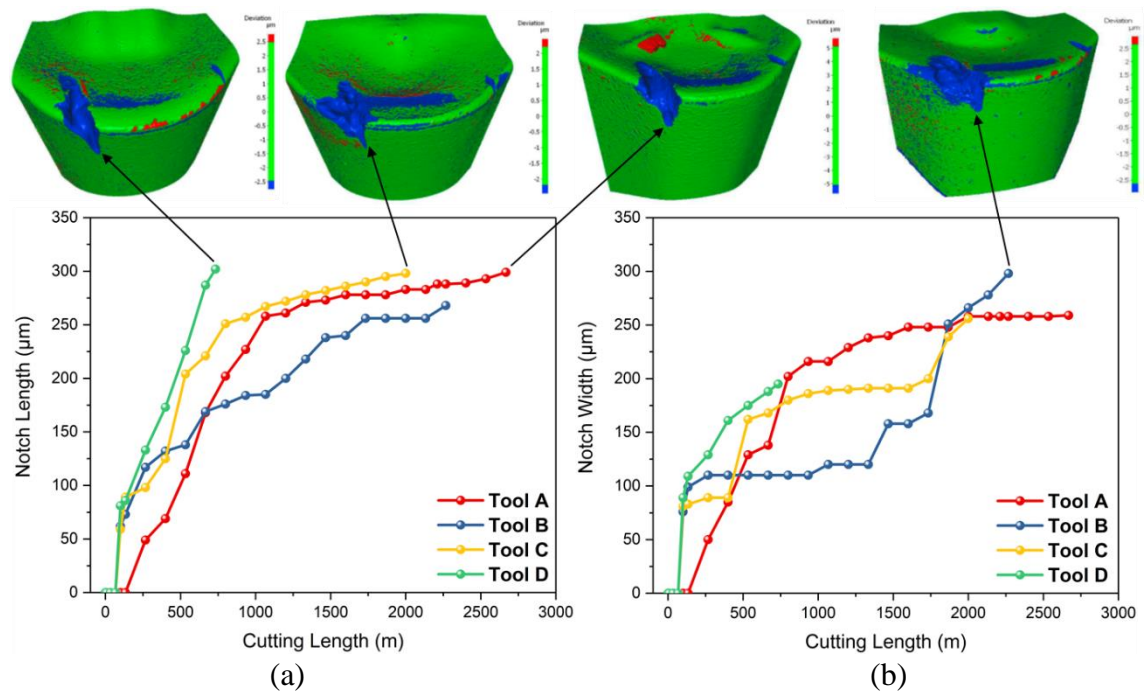
Figure 2.7 *Tool notch wear progression with machining length: (a) notch length and (b)*

notch width

Tool A: Tool A exhibits excellent wear behavior from the beginning as compared to the other tools. Its notch wear had a length and width of around 50μm at 267m of cut, while its flank wear was 55μm. Tool A also has the best initial wear resistance out of all the tools. After a machining length of 1067m, the notch wear enters a steady wear zone. The notch wear rate slowed down following 1067m of machining, reaching the failure criteria at 2668m of machining, at which the flank wear was the only 88μm. Overall flank wear increased rapidly until reaching 60μm at 533m of machining and remained uniform until failure.

Tool B: In Tool B, the initial notch was around 62μm long and 76μm wide after a cutting length of 100m, at which the flank wear was 48μm. The notch wear length of Tool B facilitated rapid initial notch wear. Notch wear length increased rapidly to 169μm until 667m of cut, with flank wear of 59μm. After that, it entered a steady zone where the wear rate was stable. The tool reached the failing stage at a machining length of 2267m. Notch wear width of Tool B grows rapidly to 99μm until 133m of machining length. After that, it enters the stable wear zone. Notch width increased slowly until 1733m of machining length and the tool reached failure at a flank wear higher than 76μm. The wear rate accelerated and reached the tool failure stage at a notch width of 300μm, while the flank wear was only 78μm at a machining length of 2267m.

Tool C: In Tool C, the initial notch was around 60μm long and 80μm wide after a cutting length of 100m with flank wear of 50μm. The notch length of Tool C began to tremendously increase from 98μm to 125μm and then 204μm after machining length of 400m, 533m, and 667m respectively, while the flank wear remained steady from 75μm to 79μm. The notch

54

wear width of Tool C increased rapidly to 180μm until 800m of machining length, while the flank wear was 82μm. After that, it entered the steady zone and progressed slowly until reaching the failure criteria at 2000m of machining with flank wear of 84μm.

Tool D: Tool D's notch was 80μm long and 90□m wide, 50% larger than all the other tools. Flank wear was 50μm after a machining length of 100m, which is the same as for the other tools. Tool D rapidly wore out from 90μm to 302μm by notch wear at a machining length between 133m to 733m. Flank wear at the failure stage was 102μm, which is approximately 20μm more than that observed for the other tools. Overall flank wear rapidly increased to 75μm at 267m of machining length and then slowly grew until failure.

2.3.3 Discussion on Wear Mechanisms

2.3.3.1 Pitting Mechanism

Figure 2.8 shows the SEM images of all tools at different stages after a machining length of 7m, 34m, and 133m. It can be observed that, after 7m of machining, tools do not exhibit any chipping or significant geometry changes. However, there was a slight marring of the tool surface at a depth of cut (DOC) interface area that formed some pits on the surface of all tools. These pits might have occurred due to the removal of the carbide grains from the tool surfaces. The removal of carbide grains might occur due to a loss of compressive residual stress within the binders, since plastic deformation extracts the binder from the cermet matrix structure, as was first observed by Larsen-Basse (Larsen-Basse, 1985). The repetitive loading and sliding with the workpiece material at the same location of the tool might have resulted in the removal of small carbide fragments and formed pits.
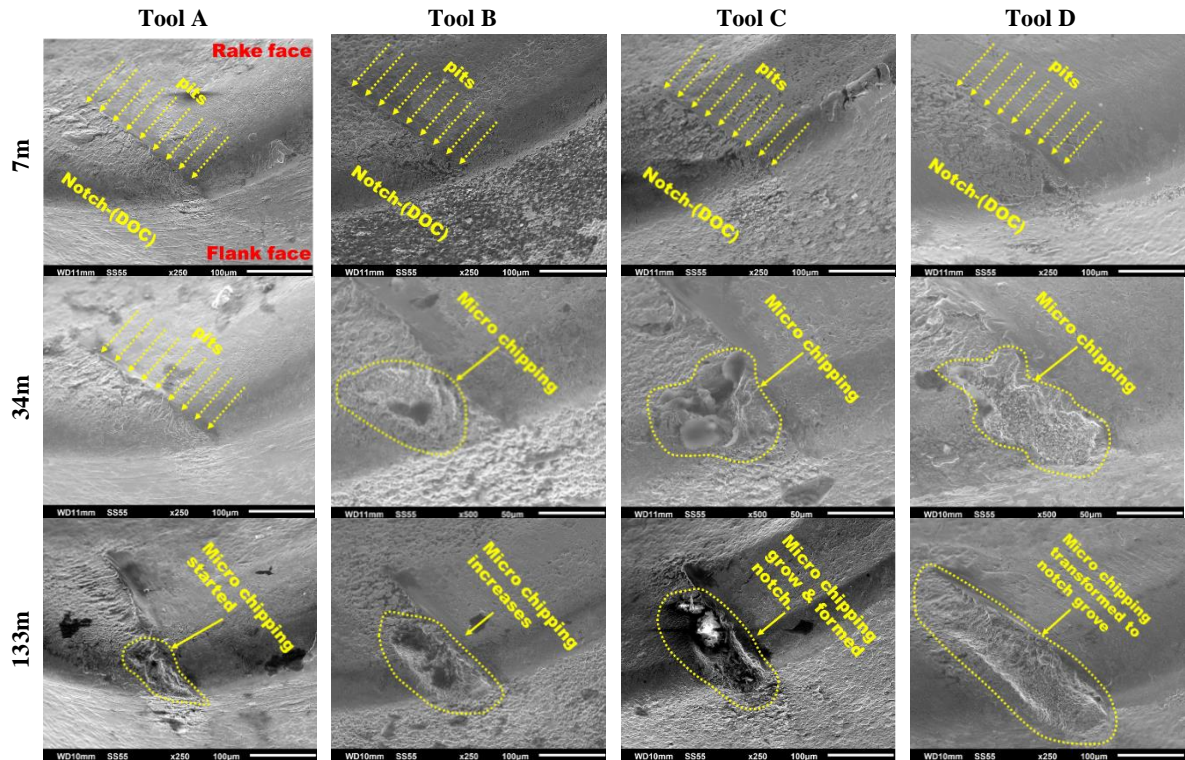
Figure 2.8 *Secondary electron SEM images of all Ti(C,N)-based cermet tool after*

machining lengths of 7m, 34m and 133m showing microchipping and notch generation

2.3.3.2 Microchipping & Furrowing Mechanism

After a machining length of 34m, the DOC area surface of the tool become increasingly

marred and all tools except Tool A exhibit microchipping, as evident from Figure 2.8. This

microchipping occurrence can be explained by grains falling out and leaving small cavities

in the affected area. This happens through a furrowing effect on the tool surface. A newly

machined surface experiences compression during the first machining pass, and due to the

high ductility of 304 stainless steel, these top machined surfaces become work hardened.

Therefore, when the tool enters the second pass, its work-hardened surface is compressed

further, generating burrs which deform and become work-hardened at this stage of chip

formation. These excessively work-hardened burrs will rub against the tool at the bottom of the depth of cut interface area, further wearing out this region of the tool. Following the running-in stage, some carbide grains will begin to detach, generating small cavities on the tool surface, which then becomes characterized by microchipping at a depth of cut tool-chip interface area. This is also known as the notching of the tool and may occur due to the development of surface and subsurface microcracks, which break up the structure of the cermet tools, ultimately leading to grain removal.

After a machining length of 133m, the first microchipping was observed in Tool A whereas a significant amount was observed for the rest of the tools. Chipping becomes more dominant with an increase in the machining length. In Tool D, chips turn into grooves whose length increases along the rake face of the tool. This can be attributed to the amount of the binder content within the tool; as evident from Table 2.3, the binder (Co+Ni) content in Tool D is highest (14.3wt.%). Meanwhile, in Tools A, B and C, the binder content is 8.2, 11.2, and 10.2 wt.%, respectively. Therefore, the lower binder (Co+Ni) content level results in better tool life for these Tools as compared to Tool D, as shown in Figure 2.7. Tool D with a maximum nickel (Ni) binder content of 7wt.% has the maximum chemical affinity with the nickel (Ni) present in the 304 stainless steel. It has been reported in the literature that due to the high temperature and pressure during the machining process at the tool-chip interface area, nickel (Ni) (Zhu, Zhang and Ding, 2013) diffuses from the tool to the workpiece or the chip. This results in the loss of some binder content from the tool, weakening the support for the carbide grains and may have resulted in the removal of the carbide grains as the chip slides along the tool surface.

2.3.3.3   Notch Grooving

The continuation of the machining test increased the notch groove length as well as width as shown in Figure 2.7 (a) and (b), respectively, for all four cermet tools. This expanded notch began to be filled with workpiece material. New material continuously pushed the old material during the machining process and began to fill in the voids on the surface, creating another material flow from the notch area, as shown in Figure 2.9. This material in the notch was coming from a furrowing effect described earlier. When the contact surface in the worn area expands, it will begin to deform in this region due to the curved groove material. this will lead to an increase in the temperature in this notch region as compared to rest of the tool.

| (a) | (b) | (c) | (d) |
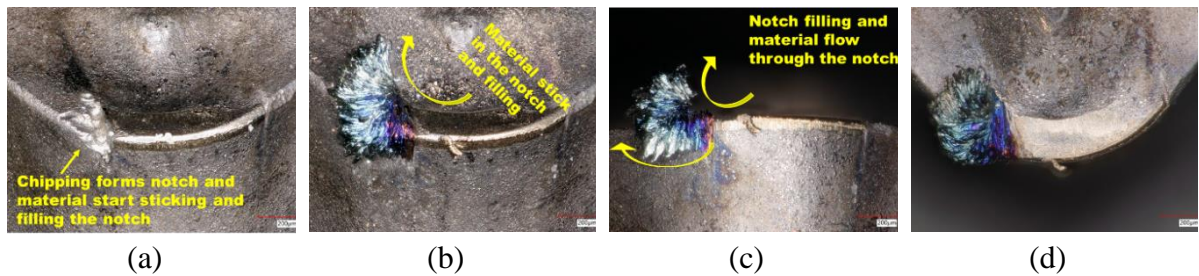
Figure 2.9 *Sticking and filling mechanism of workpiece material in the DOC notch groove formed by chipping (a) notch grove where the workpiece material sticking, (b) sticking, filling, and sliding of workpiece material in the notch, (c) side view of the notch filling and sliding mechanism, (d) top view of the notch and insert*

The temperature in this area remained relatively high compared to the rake face of the tool, since the rake face has a larger cross-section to dissipate the generated heat through the fast-flowing chip. A linear regression of volumetric wear of all tools is shown in Figure 2.10 with the R-square (COD) value of 99% for Tool D and 96% for the rest of the tools. Wear volume for all the cermet tools increased almost linearly along with cutting length as the area of contact with the tool grew as shown in Figure 2.10. The temperature is very high

in this region, as a result, the binder becomes softer, and the poorly supported carbide grains may be squeezed out of the binder. Over time, this phenomenon causes severe notch wear, with the notch getting wider, deeper and longer, ultimately leading to tool failure.
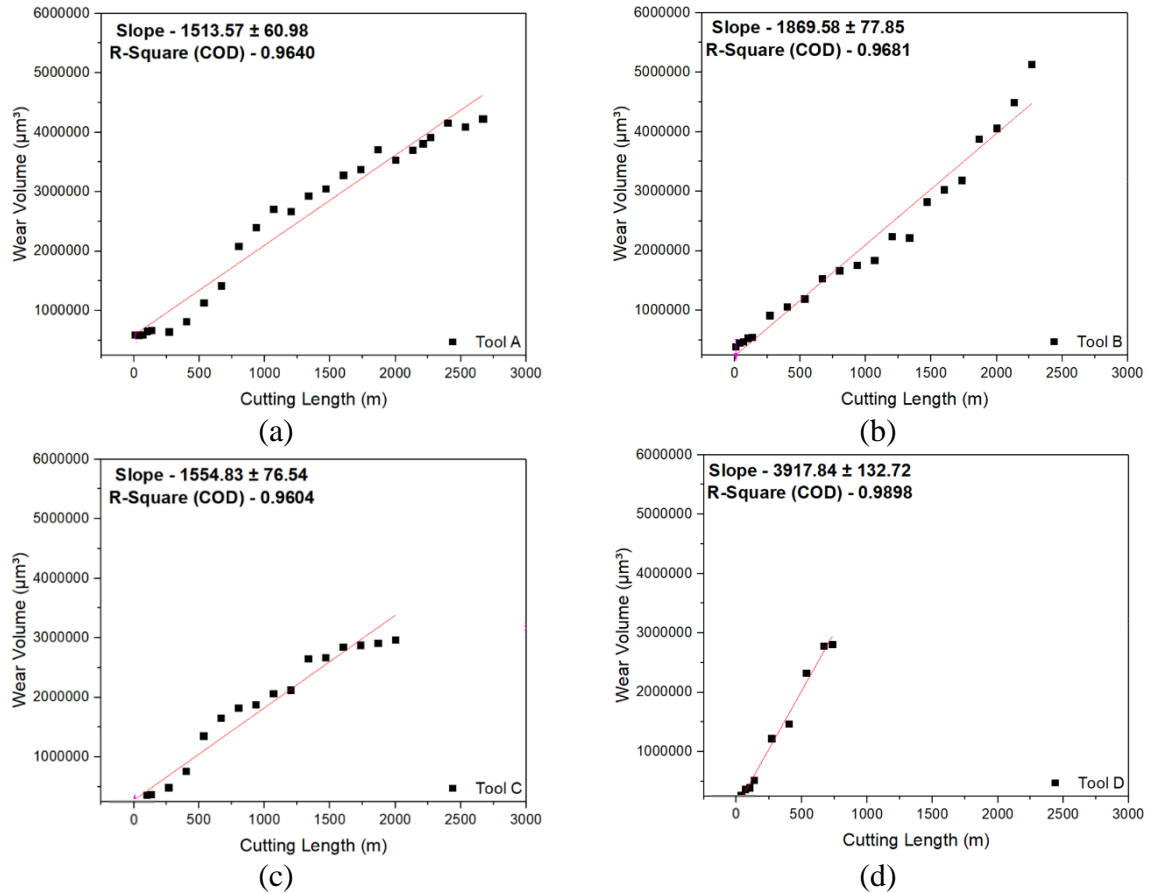
Figure 2.10 *Linear regression of wear volume showing wear volume rate with machining length for (a) Tool A, (b) Tool B, (c) Tool C, and (d) Tool D*

2.3.4 Effect of Compositions on Tool Performance

The wt.% of different phases (TiW)C, TiCN, and TiC calculated by Topas software from the XRD raw data are shown in Table 2.4. It can be observed that Tool A contains the highest amount of phase (TiW)C. Kim 2011 reported that, in most cermet systems, the fracture of material due to crack propagation is mostly initiated from the high strained core–

rim interface regions (Kim, Seo and Kang, 2011). If a larger proportion of core/rim structures are covered by (TiW)C, then the core eliminates this internal stress on the interface. As a result, the higher content of (TiW)C phase leads to high fracture toughness (Kim et al., 2012; Oh et al., 2015), and also increases the hardness of the cermet tool. Although WC has a lower hardness compared to TiCN, the high solubility of the binders and their improved sinterability due to the addition of WC improves the hardness of the cermet material. Tool A has a high content of (TiW)C. As a result, it is resistant to microchipping up to a 133m machining length, whereas all other tools exhibited microchipping at a machining length of 34m, as evident from Figure 2.8. The delayed microchipping of the tool during the initial stage of machining improved the tool life for Tool A as evident from Figure 2.7(a). Tool C shows no evidence of the (TiW)C phase being present, and thus has a relatively lower tool life as compared to the other cermet tools, but a longer tool life than Tool D, which does possess a (TiW)C phase. However, it performed more poorly due to the higher amount of binder present in the tool as discussed earlier.

Table 2.4 Wt.% of phases (TiW)C, TiCN, and TiC

	(TiW)C wt.%	TiCN wt.%	TiC wt.%
Tool A	20.5	32.2	47.3
Tool B	17.5	22.5	59.5
Tool C	-	100.0	-
Tool D	18.2	20.8	61.1

The hard TiCN grain phase responsible for lower wear resistance and shorter tool life was found to be the lowest in Tool D, as can be seen in Figure 2.7. Tool A had the highest TiCN phase content after Tool C. However, Tool C does not feature the highest tool life because of the absence of the (TiW)C phase in the tool, which plays a critical role in keeping together the hard TiCN core grains. Tool A has the highest tool life as it has the highest amount of wear-resistant TiCN particles as represented by the black area along with (TiW)C particles represented by the grey area, as shown by the SEM images in Figure 2.2. The (TiW)C particles play a critical role as a rim that encloses the hard TiCN grains.

As discussed earlier, NbC is used to lower the sintering temperature and increase the densification of the cermet tool. However, in terms of the mechanical and machining aspects, NbC is known to improve the thermal shock resistance of the material. The high melting temperature of NbC facilitates control of the material's thermal softening while at the same time also improves its adhesive wear resistance. Kelly et al. (Kelly and Rowcliffe, 1967) reported that at a temperature beyond 1000°C, the yield strength of NbC is higher than that of the WC. Since the hardness of a material depends on temperature, the microhardness of WC drops at 500-700 °C (Lee, 1983), while the same drop for NbC occurs between 900-1000 °C (Kumashiro, Nagai and Katō, 1982). So, the literature reports that NbC has a higher hot hardness compared to WC. Woydt et al. (Woydt and Mohrbacher, 2014) reported that some NbC metal grades are present in the cermet tool material, such as NbC-Co or NbC-Ni. When the temperature is reached at 400°C, the friction decreases with an increase in the sliding speed. And as the cutting speed grows, the niobium (Nb) metal phases help reduce the tool wear. Tool A, with maximum niobium (Nb) content of 7wt%

as shown in Table 2.3, features the highest tool life (Figure 2.7 (a)) and best wear resistance out of all the tools, which can be attributed to the formation of a secondary carbide with niobium (Nb).

As explained earlier, the addition of VC is responsible for the fine grain structure of the cermet material. Tools A and C have a 1.6 wt.% and 4.4 wt.% of vanadium (V), respectively, in Table 2.3. It was reported in the literature (Ying et al., 2011) that excessive vanadium (V) content, more than 1 wt.%, will not result in finer grains. Lower vanadium (V) content (≤1%wt) may result in fine grains. As the interface between the hard phase (TiCN) and binder (Co/Ni) phase increases, the mean free path of the binder phases is reduced, which will impart high hardness to the binder phase. Tool A has a finer grain structure and maximum hardness, whereas Tool C has a coarser grain structure and lower hardness values, as evident from Figure 2.2 and Table 2.2, respectively. The structure of Tool A as shown in Figure 2.4 is less porous compared to that of other tools, thereby reducing the material bearing load volume (Huang, 1995) and resulting in a dense structure with a higher hardness value. In general, a material with a high hardness value is usually more wear-resistant (Jia and Fischer, 1997). Milman et al. reported that the hardness of WC–Co decreases with increasing temperature, increasing cobalt content and increasing WC grain size (Milman, Luyckx and Northrop, 1999). Hence, Tool A has a longer tool life compared to Tool C as can be seen in Figure 2.7 (a), due to its finer grain structure, high hardness values and lower binder content as compared to the other cermet tools.

Table 2.3 shows that Tool C contains 7.5wt.% of molybdenum (Mo). It is reported in the literature that during dry machining, molybdenum (Mo) reacts with oxygen at temperatures

greater than 520 °C to form MoO_3 and MoO_2 oxides (Yang et al., 2017). These oxides are very similar in structure to graphite and possess self-lubricating properties in the dry turning condition similar to solid lubricants (Broniszewski et al., 2013; Fang et al., 2014). The friction coefficient at the tool chip interface is decreased as a result. Due to this effect, the wear rate of Tool C becomes low as shown in Figure 2.10 (c). It is lower compared to all other tools except Tool A, which demonstrates the low volume wear rate of the Tool C, almost the same as that of the Tool A. However, since the tool material hardness is not same, (1663 HV in Tool C and 1735 HV in Tool A) the tool with the greater hardness is expected to have the longest tool life. However, the wear volume of Tool A and Tool C are the same.

During the sintering process, vanadium (V) and nitrogen (N) replace tantalum (Ta) and carbon (C) in TaC to form the TaVCN and TaVN phases, as confirmed by XRD in Figure 2.3. These phases show the FM-3M (225) space group and are structured in a cubic lattice, which is like the core structure of TiCN, TiC and the (TiW)C rim. Vanadium and Tantalum form an oxide (V_2O_3, V_2O_5, Ta_2O_5 and Ta_4O) that acts as a lubricant during the machining process. In addition, V_2O_5 melts and acts like a liquid lubricant at temperatures greater than 686°C (Jun-hua et al., 2012; Yu, Huang and Xu, 2015). Consequently, these lubricants decrease friction and reduce the wear of the tools. Tool C contains tantalum (Ta), whereas Tools A and C both contain vanadium (V) as shown in Table 2.3. These two Tools, A and C, have a low wear volume rate (Figure 2.10) and represent almost the same wear volume rate may be due to the lubricating effect of the above oxides during the machining process.

2.4   Conclusions

The cermet tools with the same geometry but different compositions from different manufacturers were studied to examine the role of constituents on the tool performance during dry high-speed machining of 304 stainless steel. The summary of the noteworthy findings is:

- Wear progression: Pitting wear is initially observed in all tools at 7m of cutting length, due to the loss of binding strength of the binder material (Co and Ni) causing the elimination of the grain. All the tools except Tool A begin to chip due to the furrowing effect that may be caused by harden burr (formed by work-harden layer from the previous machined surface) on the tool surface at a cutting length between 34m and 133m. The continuation of this process results in notch chipping (material removal from notch) and transforms into a groove causing the workpiece material to fill and flow through it. This material flow in the notch grooves intensifies the notch wear and ultimately causes tool failure.

- The higher binder content (Co and Ni) accelerates the notch wear and causes the tool to fail. In addition, as the nickel (Ni) content increases, the rate of its diffusion into the stainless-steel workpiece during machining increases, resulting in lower tool life for Tool D.

- Tungsten(W) is present in all tools and forms (TiW)C phase, with the exception of the Tool C, which has a very low amount of W. (TiW)C phase plays a crucial role

as it forms a set of rims that holds ceramic (TiCN) cores imparting higher wear resistance and tool life to the tools.

- Tantalum, molybdenum, vanadium, tungsten, and niobium may have resulted in the precipitation of secondary carbides as evident from the EDS spectrum taken at the white core in BSE SEM images.

- The presence of a lower amount of vanadium results in the rounded and fine core for Tool A and Tool C. The absence of vanadium from Tool B and Tool D results in irregular core shapes such as non-circular, triangular and rectangular cores for these tools.

- Vanadium and tantalum may form lubricious oxides during the machining process, thereby reducing the wear volume rate and higher tool life for Tool A and Tool C. However, the excessive content of tantalum in Tool C has an adverse effect that results in the increase of the porosity due to agglomeration.

- The presence of niobium provides high hot hardness by forming secondary carbides, reduces porosity and helps in improving the tool performance.

- Molybdenum inhibits core growth and makes the core coarser, that may reduce the hardness of Tool C. However, molybdenum also forms lubricating oxides, that may reduce friction and wear volume during the machining process, as observed for Tool C.

2.5 Acknowledgment

2.6 References

Ahmed, Y. S. et al. (2017) 'Effect of built-up edge formation during stable state of wear in AISI 304 stainless steel on machining performance and surface integrity of the machined part', Materials, 10(11), pp. 1–15. doi: 10.3390/ma10111230.

Ahn, S. and Kang, S. (2000) 'Formation of Core/Rim Structures in Ti (C,N)-WC-Ni Cermets via a Dissolution and Pricipitation Process', Journal of American Ceramical Society, 83, pp. 1489–1494. doi: 10.1111/j.1151-2916.2000.tb01415.x.

Bapat, P. S. et al. (2015) 'A Numerical Model to Obtain Temperature Distribution During Hard Turning of AISI 52100 Steel', Materials Today: Proceedings, 2(4–5), pp. 1907–1914. doi: 10.1016/j.matpr.2015.07.150.

Broniszewski, K. et al. (2013) 'Al2O3-Mo cutting tools for machining hardened stainless steel', Wear, 303(1–2), pp. 87–91. doi: 10.1016/j.wear.2013.03.002.

Conforto, E., Mari, D. and Cutard, T. (2004) 'The role of molybdenum in the hard-phase grains of (Ti, Mo)(C, N)-Co cermets', Philosophical Magazine, 84(17), pp. 1717–1733. doi: 10.1080/14786430310001659516.

Dogra, M. et al. (2010) 'Tool wear, chip formation and workpiece surface issues in CBN hard turning: A review', International Journal of Precision Engineering and Manufacturing, 11(2), pp. 341–358. doi: 10.1007/s12541-010-0040-1.

Fang, Y. et al. (2014) 'Influence of structural parameters on the tribological properties of Al2O3/Mo laminated nanocomposites', Wear, 320(1), pp. 152–160. doi: 10.1016/j.wear.2014.09.003.

Groover, M. P. (2007) Fundamentals of Modern Manufacturing. Third Edit. John Wiley & Sons.

Gruss, W. W. (1987) Turning and milling of steel with cermet cutting tools. Scottsdale, AZ: Proceedings of ASM Tool Materials for High-Speed Machining Symposium.

Grzesik, W. (2017) 'Cutting Tool Materials', in Advanced Machining Processes of Metallic Materials, pp. 35–63. doi: 10.1016/B978-0-444-63711-6.00004-1.

Huang, P. (1995) Principle of powder metallurgy. Beijing: Metallurgical Industry Press.

Huang, S. G. et al. (2008) 'NbC as grain growth inhibitor and carbide in WC-Co hardmetals', International Journal of Refractory Metals and Hard Materials, 26(5), pp. 389–395. doi: 10.1016/j.ijrmhm.2007.09.003.

'ISO 15510-Stainless Steels-Chemical Composition: Stainless Steels 304' (2014). Geneva, Switzerland: International Organization for Standardization. Available at: www.iso.org.

Jia, K. and Fischer, T. E. (1997) 'Sliding wear of conventional and nanostructured cemented carbides', Wear, 203–204, pp. 310–318. doi: 10.1016/S0043-1648(96)07423-6.

Jiang, L. et al. (1996) 'Active wear and failure mechanisms of TiN-coated high speed steel and TiN-coated cemented carbide tools when machining powder metallurgically made stainless steels', Metallurgical and Materials Transactions A: Physical Metallurgy and Materials Science, 27(9), pp. 2796–2808. doi: 10.1007/BF02652372.

Jianxin, D. et al. (2011) 'Wear mechanisms of cemented carbide tools in dry cutting of precipitation hardening semi-austenitic stainless steels', Wear, 270(7–8), pp. 520–527. doi: 10.1016/j.wear.2011.01.006.

Jun-hua, X. et al. (2012) 'Microstructures, mechannical properties and friction properties of TiVCN composite films', Jinshu Xuebao/Acta Metallurgica Sinica, 48(5), pp. 555–560. doi: 10.3724/SP.J.1037.2011.00724.

Jun, W. et al. (2009) 'Effect of WC on the microstructure and mechanical properties in the Ti(C0.7N0.3)-xWC-Mo2C-(Co, Ni) system', International Journal of Refractory Metals and Hard Materials, 27(1), pp. 9–13. doi: 10.1016/j.ijrmhm.2008.01.010.

Kelly, A. and Rowcliffe, D. J. (1967) 'Deformation of Poly crystalline Transition Metal Carbides', Journal of the American Ceramic Society, 50(5), pp. 253–256. doi: 10.1111/j.1151-2916.1967.tb15098.x.

Kim, J., Seo, M. and Kang, S. (2011) 'Microstructure and mechanical properties of Ti-based solid-solution cermets', Materials Science and Engineering A, 528(6), pp. 2517–2521. doi: 10.1016/j.msea.2010.11.076.

Kim, Y. S. et al. (2012) 'Tool performance of new wear-resistant cermets', International Journal of Precision Engineering and Manufacturing, 13(6), pp. 941–946. doi: 10.1007/s12541-012-0122-3.

Korkut, I. et al. (2004) 'Determination of optimum cutting parameters during machining of AISI 304 austenitic stainless steel', Materials and Design, 25(4), pp. 303–305. doi: 10.1016/j.matdes.2003.10.011.

Kramar, D. et al. (2013) 'The machinability of nickel-based alloys in high-pressure jet assisted (HPJA) turning', Metalurgija, 52(4), pp. 512–514.

Kulkarni, A., Sargade, V. and More, C. (2018) 'Machinability Investigation of AISI 304 Austenitic Stainless Steels using Multilayer AlTiN/TiAlN Coated Carbide Inserts', Procedia Manufacturing, 20, pp. 548–553. doi: 10.1016/j.promfg.2018.02.082.

Kumashiro, Y., Nagai, Y. and Katō, H. (1982) 'The Vickers micro-hardness of NbC, ZrC and TaC single crystals up to 1500°C', Journal of Materials Science Letters, 1(2), pp. 49–52. doi: 10.1007/BF00731023.

Kwon, W. T. et al. (2004) 'Effect of WC and group IV carbides on the cutting performance of Ti(C,N) cermet tools', International Journal of Machine Tools and Manufacture, 44(4), pp. 341–346. doi: 10.1016/j.ijmachtools.2003.10.023.

Larsen-Basse, J. (1985) 'Binder extrusion in sliding wear of WC-Co alloys', Wear, 105(3), pp. 247–256. doi: 10.1016/0043-1648(85)90071-7.

Lee, M. (1983) 'High temperature hardness of tungsten carbide', Metallurgical Transactions A, 14(8), pp. 1625–1629. doi: 10.1007/BF02654390.

Low, I. M. (2014) Advances in ceramic matrix composites, Advances in Ceramic Matrix Composites. Cambridge, UK: Woodhead Publishing. doi: 10.1533/9780857098825.

M'Saoubi, R. et al. (1999) 'Residual stress analysis in orthogonal machining of standard and resulfurized AISI 316L steels', Journal of Materials Processing Technology, 96(1–3), pp. 225–233. doi: 10.1016/S0924-0136(99)00359-3.

Milman, Y. V., Luyckx, S. and Northrop, I. (1999) 'Influence of temperature, grain size and cobalt content on the hardness of WC-Co alloys', International Journal of Refractory Metals and Hard Materials, 17(1), pp. 39–44. doi: 10.1016/S0263-4368(98)00038-9.

Oh, S. W. et al. (2015) 'Investigation into the microstructure and cutting performance of (Ti,Ta,W)(CN)-Co/Ni cermets', International Journal of Refractory Metals and Hard Materials, 53, pp. 36–40. doi: 10.1016/j.ijrmhm.2015.04.017.

Outeiro, J. C., Umbrello, D. and M'Saoubi, R. (2006) 'Experimental and numerical modelling of the residual stresses induced in orthogonal cutting of AISI 316L steel', International Journal of Machine Tools and Manufacture, 46(14), pp. 1786–1794. doi: 10.1016/j.ijmachtools.2005.11.013.

Peng Wu, Yong Zheng, Yongle Zhao, H. Y. (2010) 'Effect of TaC addition on the microstructures and mechanical properties of Ti(C, N)-based cermets', Materials and Design, 31(7), pp. 3537–3541. doi: 10.1016/j.matdes.2010.01.047.

Peng, Y., Miao, H. and Peng, Z. (2013) 'Development of TiCN-based cermets: Mechanical properties and wear mechanism', International Journal of Refractory Metals and Hard Materials, 39, pp. 78–89. doi: 10.1016/j.ijrmhm.2012.07.001.

Philip Selvaraj, D. and Chandramohan, P. (2010) 'Optimization of surface roughness of AISI 304 austenitic stainless steel in dry turning operation using Taguchi design method', Journal of Engineering Science and Technology, 5(3), pp. 293–301. Available at: http://jestec.taylors.edu.my/Vol 5 Issue 3 September 10/Vol_5_3_293_301_DP_Selvaraj.pdf.

Sharma, A. K., Tiwari, A. K. and Dixit, A. R. (2016) 'Effects of Minimum Quantity Lubrication (MQL) in machining processes using conventional and nanofluid based cutting fluids: A comprehensive review', Journal of Cleaner Production, 127, pp. 1–18. doi: 10.1016/j.jclepro.2016.03.146.

Sreejith, P. S. and Ngoi, B. K. A. (2000) 'Dry machining: Machining of the future', Journal of Materials Processing Technology, 101(January 1999), pp. 287–291. doi: 10.1016/S0924-0136(00)00445-3.

Standardization, F. O. R. (2006) 'IS0 3685:Tool-life testing with single-point turning tools'.

Stephenson, D. A. and Agapiou, J. S. (2016) Metal cutting theory and practice, Third edition. Third Edit, Metal Cutting Theory and Practice, Third Edition. Third Edit. CRC Press, Taylor & Francis Group. doi: 10.1201/b19559.

Tekiner, Z. and Yeşilyurt, S. (2004) 'Investigation of the cutting parameters depending on process sound during turning of AISI 304 austenitic stainless steel', Materials and Design, 25(6), pp. 507–513. doi: 10.1016/j.matdes.2003.12.011.

Wang, J. et al. (2009) 'Effect of NbC on the microstructure and sinterability of Ti(C0.7, N0.3)-based cermets', International Journal of Refractory Metals and Hard Materials, 27(3), pp. 549–551. doi: 10.1016/j.ijrmhm.2008.07.003.

Whitney, E. D. (1994) Ceramic Cutting Tools. 1st Editio, William Andrew. 1st Editio. Edited by E. D. Whitney. New Jersey: Noyes Publications.

Woydt, M. and Mohrbacher, H. (2014) 'The tribological and mechanical properties of niobium carbides (NbC) bonded with cobalt or Fe3Al', Wear, 321, pp. 1–7. doi: 10.1016/j.wear.2014.09.007.

Xavior, M. A. and Adithan, M. (2009) 'Determining the influence of cutting fluids on tool wear and surface roughness during turning of AISI 304 austenitic stainless steel', Journal of Materials Processing Technology, 209(2), pp. 900–909. doi: 10.1016/j.jmatprotec.2008.02.068.

Xing, Y. et al. (2014) 'Cutting performance and wear mechanism of nanoscale and microscale textured Al2O3/TiC ceramic tools in dry cutting of hardened steel', International Journal of Refractory Metals and Hard Materials, 43, pp. 46–58. doi: 10.1016/j.ijrmhm.2013.10.019.

Xiong, J. et al. (2007) 'The effect of WC, Mo2C, TaC content on the microstructure and properties of ultra-fine TiC0.7N0.3 cermet', Materials & Design, 28(5), pp. 1689–1694. doi: 10.1016/j.matdes.2006.03.005.

Yang, T. et al. (2017) 'Cutting wear, microstructure and mechanical properties of (Ti0.5,W0.5)C-based cermet inserts containing Mo2C', International Journal of Refractory Metals and Hard Materials, 68(July), pp. 151–158. doi: 10.1016/j.ijrmhm.2017.07.011.

Ying, X. et al. (2011) 'Effect of VC addition on the microstructure and properties of Ti(C,N)-based nano cermets', Rare Metals, 30(6), pp. 583–588. doi: 10.1007/s12598-011-0433-z.

Yu, L., Huang, T. and Xu, J. (2015) 'Effect of vanadium content on microstructure, mechanical and tribological properties of TaVCN composite films', Fenmo Yejin Cailiao Kexue yu Gongcheng/Materials Science and Engineering of Powder Metallurgy, 20(1).

Zhang, X., Liu, N. and Rong, C. (2008) 'Effect of molybdenum content on the microstructure and mechanical properties of ultra-fine Ti(C, N) based cermets', Materials Characterization, 59(12), pp. 1690–1696. doi: 10.1016/j.matchar.2008.03.008.

Zhang, Y. et al. (2017) 'Experimental study on cutting performance of microwave sintered Ti(C, N)/Al2O3 cermet tool in the dry machining of hardened steel', International Journal of Advanced Manufacturing Technology, 91(9–12), pp. 3933–3941. doi: 10.1007/s00170-017-0062-2.

Zhu, D., Zhang, X. and Ding, H. (2013) 'Tool wear characteristics in machining of nickel-based superalloys', International Journal of Machine Tools and Manufacture, 64, pp. 60–77. doi: 10.1016/j.ijmachtools.2012.08.001.

Zou, B. et al. (2014) 'Study of a hot-pressed sintering preparation of Ti(C7N3)-based composite cermets materials and their performance as cutting tools', Journal of Alloys and Compounds, 611, pp. 363–371. doi: 10.1016/j.jallcom.2014.05.150.

Zou, B. et al. (2015) 'Tool damage and machined-surface quality using hot-pressed sintering Ti(C7N3)/WC/TaC cermet cutting inserts for high-speed turning stainless steels', International Journal of Advanced Manufacturing Technology, 79(1–4), pp. 197–210. doi: 10.1007/s00170-015-6823-x.

Chapter 3 : Data Set and Methodology

Complete citation:

U. Patel, S. Rawal, A.F.M. Arif, S. Veldhuis, Dataset and methodology on identification and correlation of secondary carbides with microstructure, wear mechanism, and tool performance for different CERMET grades during high-speed dry finish turning of AISI 304 stainless steel, Data in Brief. (2020) 105753. https://doi.org/https://doi.org/10.1016/j.dib.2020.105753.

Copyright:

Author's Contributions:

Uttkarsh Patel	Conceptualization, Investigation, Formal analysis, Validation, Visualization, Methodology, Data Curation, Writing - Original Draft
Sushant Rawal	Conceptualization, Methodology, Validation, Supervision, Writing - Review & Editing
Abul Fazal M Arif	Conceptualization, Methodology, Project administration, Writing - Review & Editing
Stephen Veldhuis	Resources, Project administration, Funding acquisition, Supervision

Abstract

The aim of this research is to utilize a reverse engineering approach for the identification of the elements and phases available in the commercial CERMET inserts with the help of characterization techniques such as Scanning Electron Microscope (SEM), Energy-dispersive X-ray spectroscopy (EDS), and X-Ray Deposition (XRD). Four commercial CERMET inserts were investigated in this research work, and the effect of the composition and phases are related to its tool wear mechanism and performance. Each CERMET insert is used to perform a turning process on a CNC lathe for machining Stainless Steel (SS) under the dry condition at a fixed cutting length interval. Once it completes machining for a fixed cutting length, the CERMET insert is taken out to investigate its wear mechanism with the help of SEM, EDS, XRD and using a focus-variation microscope (Alicona). A correlation analysis is performed to relate progressive tool wear mechanisms with elements and their relevant phases of various carbides. The approach of correlating wear property with the phase content will contribute to the understanding of the wear mechanism under such extreme machining conditions. It will serve as a reference for the improvement of the performance of these CERMET inserts for such harsh machining conditions by the development of protective coatings for these CERMET inserts based on the identification of the composition and phases that improves tool life and reduces wear. The data related to this research work can be found at "https://doi.org/10.1016/j.wear.2020.203285" (Patel et al., 2020).

3.1 Specifications Table

Subject	Ceramics and Composites
Specific subject area	Influence of the composition and phases available in commercial CERMET inserts on its wear mechanism and tool life for machining stainless steel
Type of data	Table (Procedure steps for the polishing).
	Images (SEM images, and microscopic images).
	Graphs (EDS point spectra)
How data were acquired	The following experimental techniques were used to acquire data:
	• Scanning Electron Microscope (SEM): - Using "JEOL 6610LV" for SEM images and Elemental identification (EDS). (ref. Figure 3.1, Figure 3.2, and Figure 3.3)
	• X-Ray Diffraction (XRD): - Bruker D8 discover with cobalt source.
	• CNC turning lathe: - OKUMA crown L1060 for Tool life test and tool wear test
	• Digital Images: - KEYENCE-VHX 5000 digital microscope to capture tool wear from various orientations (ref. Figure 3.4)
	• 3D Scan Microscope: - Alicona Infinite Focus G5 microscope to capture 3D wear volume (ref. Figure 3.5)
Data format	Raw data for microstructure SEM images, XRD, and EDS.
	Tool life with flank wear and notch wear are collected and prepared as graphs.
	Volume wear data for the CERMET inserts was measured by the software of Alicona Infinite Focus G5 microscope, analyzed and prepared as graphs.

Parameters for data collection	SEM:
	Electron beam: 20-25KeV
	Spot size: 55
	WD: 10-12mm
	XRD:
	Cobalt sealed tube source ($\lambda_{avg} = 1.79026$Å)
	Power settings: 35kV, 45mA
	Scan at six steps in 22-112˚ range, Exposure time: 480s/step.
	CNC turning lathe:
	Cutting speed: 240m/min
	Depth of cut: 0.4mm
	Feed:0.15 mm/rev
Description of data collection	Four commercial CERMET inserts were investigated in this research work. Each new CERMET insert was scanned before the start of the experiment to compare it later with its machined tool surface. The machining test was performed at a fixed cutting interval. The SEM images were captured to keep track of tool wear and to understand the tool microstructure, and EDS was performed at the fixed cutting interval to identify its composition. XRD was done to determine the relevant phases present, and a 3D scan was taken using a focus variation microscope (Alicona) to measure the wear volume after each cutting interval. A digital microscope was also utilized to measure flank wear and notch wear.

Data source location	SEM: (Figure 3.1, Figure 3.2, and Figure 3.3)
	Institution: Canadian Centre for Electron Microscopy (CCEM) Facility, McMaster University
	City/Town/Region: A.N. Bourns Science Building, 1280 Main St W, Hamilton, ON, L8S 4M1
	Country: Canada
	XRD:
	Institution: McMaster Analytical X-Ray Diffraction (MAX) Facility, McMaster University
	City/Town/Region: A.N. Bourns Science Building, 1280 Main St W, Hamilton, ON, L8S 4M1
	Country: Canada
	Tool life:
	Institution: McMaster Manufacturing Research Institute (MMRI), McMaster University
	City/Town/Region: John Hodgins Engineering Building, 1280 Main St W, Hamilton, ON L8S 4L7
	Country: Canada
	Digital microscope image & 3D scan images (Figure 3.4 and Figure 3.5)
	Institution: McMaster Manufacturing Research Institute (MMRI), McMaster University
	City/Town/Region: John Hodgins Engineering Building, 1280 Main St W, Hamilton, ON L8S 4L7
	Country: Canada
Data accessibility	In a public repository:
	Repository name: [Mendeley Data]
	Data identification number: [10.17632/xg2rngb8xn.1]
	Direct URL to data:
	[https://dx.doi.org/10.17632/xg2rngb8xn.1]

Related research article	Author's name: Uttkarsh S. Patel, Sushant K. Rawal, A.F.M. Arif, Stephen C. Veldhuis
	Title: Influence of secondary carbides on microstructure, wear mechanism, and tool performance for different CERMET grades during high-speed dry finish turning of AISI 304 stainless steel (Patel *et al.*, 2020).
	Journal: Wear
	Volume: 452–453
	Year: 2020
	DOI: https://doi.org/10.1016/j.wear.2020.203285

3.2 Value of the Data

- These data provide a comprehensive comparison and explanation on the effect of various tool compositions and phases on the wear mechanism and tool life for dry machining of stainless steel by four different commercial CERMET inserts.

- These data will provide a reference for the manufacturing sector on the identification and selection of appropriate CERMET inserts based on tool life for dry machining of stainless steel.

- These data will be used for the development of protective coatings for these CERMET inserts based on the identification of the composition and phases that improve tool life and reduces wear.

- These data can serve as a benchmark for CERMET insert to be explored for additional machining applications for different materials in similar dry machining conditions.

3.3 Data Description

Data presented in the article is on the comparison of wear mechanism and tool life for dry machining of stainless steel by four different commercial CERMET inserts. The experiments were performed to identify the various elements present in CERMET inserts, evaluate their effect on microstructure, and relate it to its wear mechanism and tool performance.

In the first step, new CERMET inserts were used to capture microstructure (Figure 3.1 and Figure 3.2) and EDS results (Figure 2.5). In the second step, an XRD test was performed to identify the phases related to these elements. The wt.% of major phases were calculated using the Topas software. A machining test was performed at a fixed interval to measure and quantify the tool wear under an optical microscope and a focus variation microscope (Alicona). The collected data was used to prepare a tool life graph. SEM images were also taken to investigate the progressive wear mechanism, as shown in Figure 3.3. The 3D wear volume images were taken by scanning the CERMET insert in Alicona (Figure 3.5) and presented as linear regression to compare the tool wear.

3.4 Experimental Design, Materials, and Methods

3.4.1 Sample Preparation for SEM:

The samples were mounted in Bakelite (hot mount) and polished with the help of an auto polisher to make it flat and smooth mirror finished using the following steps as given in Table 3.1.

Table 3.1 Steps to polish the CERMET inserts/coupons

Step No.	Surface	Suspension	Lubrication	Time (min)
1.	Piano 120		Water	2:30
2.	Piano 600		Water	2:30
3.	Plan	DP-A 15μm	Blue	2:30
4.	Allegro	DP-A 9μm	Blue	4:00
5.	Dur	DP-A 3μm	Blue	4:00
6.	Dur	DP-A 1μm	Blue	6:00
7.	Chem	OP-S		2:00

Once samples were mirror polished, they were unmounted and placed on an SEM fixture for the SEM characterization.

3.4.2 Scanning Electron Microscopy (SEM) Images:

JEOL 6610LV SEM instrument was used to obtain the microstructure images of the CERMET inserts. The polished CERMET inserts were coated with the carbon/gold, and nickel paste was applied to create a path for the electron to pass through it so the charging effect can be minimized and more clear and sharper image can be obtained. A backscattered electron (BSE) mode was used to capture chemical (atomic) contrast, which can help to identify core, rim and binder compounds in the CERMET inserts, as shown in Figure 3.1.

BEC 20kV WD10mm SS55 x8,000 2μm (a)

BEC 20kV WD10mm SS55 x8,000 2μm (b)

BEC 20kV WD10mm SS55 x8,000 2μm (c)

BEC 20kV WD10mm SS55 x8,000 2μm (d)
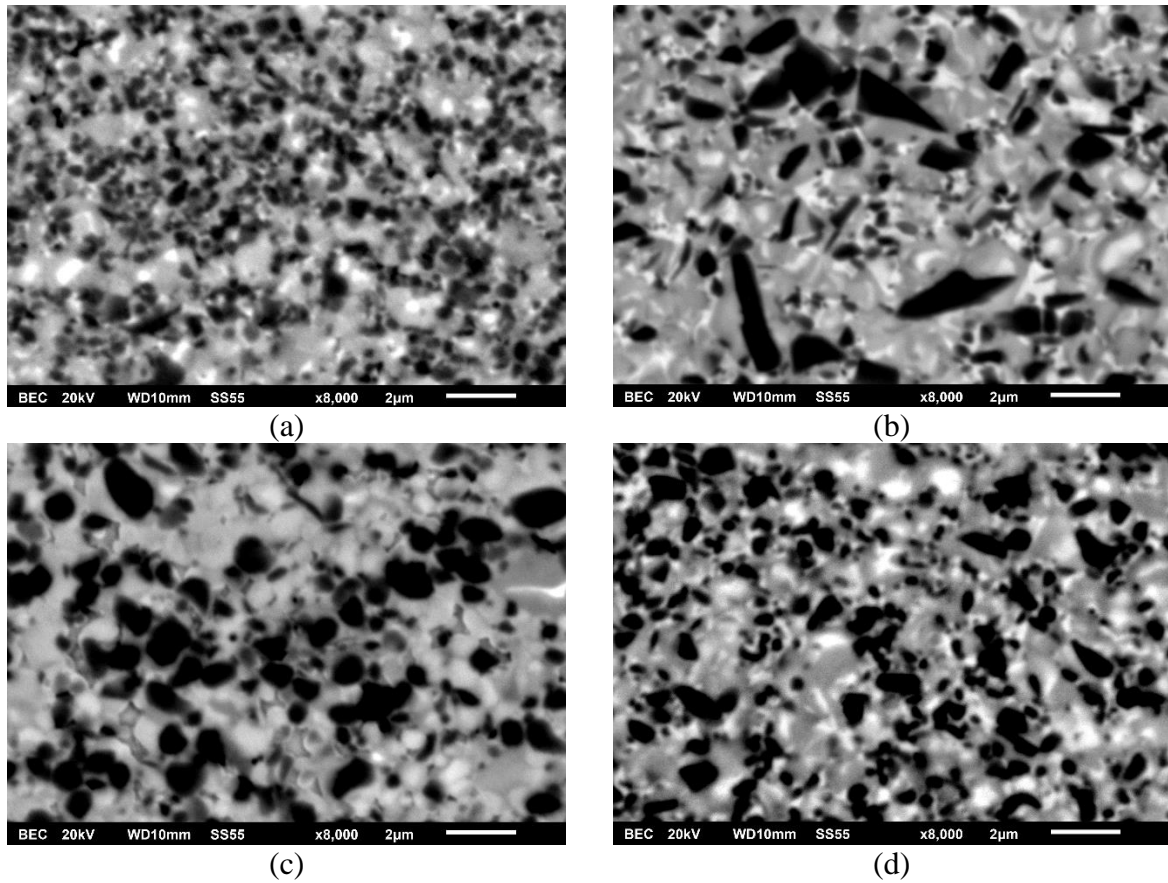
Figure 3.1 *Backscattered electron (BSE) SEM images of all CERMET tools (a) Tool A, (b)*

Tool B, (c) Tool C, and (d) Tool D

To capture the surface topography, BSE mode was changed to secondary electron mode, and the same procedure as above was followed, and the images, as shown in Figure 3.2, were obtained.

3.4.3 Energy-Dispersive X-ray Spectroscopy (EDS)

Polished CERMET inserts were loaded into the chamber and brought near to the detector until the working distance is 10-12mm. The EDS detector and software available to operate the equipment were used to collect X-rays at a minimum of 20KeV from the sample surface

to excite X-rays from all the elements. The software was used to keep the dead time around 30%. The data was acquired and processed by the software to get the EDS spectrum, as shown in Figure 2.5.

SEI 20kV WD10mm SS55 x6,000 2μm
(a)

SEI 20kV WD10mm SS55 x6,000 2μm
(b)

SEI 20kV WD10mm SS55 x6,000 2μm
(c)

SEI 20kV WD10mm SS55 x6,000 2μm
(d)
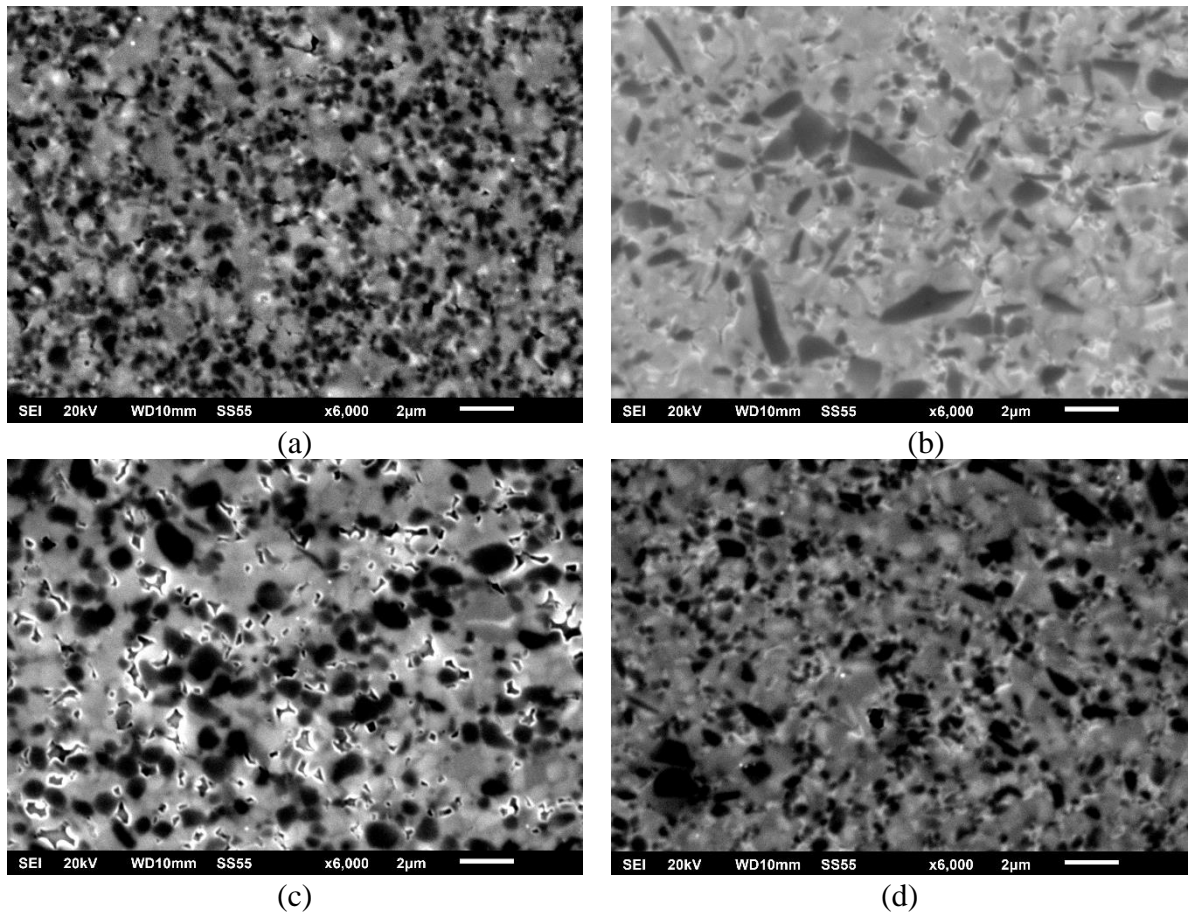
Figure 3.2 *Secondary electron SEM images of all CERMET tools (a) Tool A, (b) Tool B, (c) Tool C, and (d) Tool D*

The investigation of elemental concentration (wt.%) of all CERMET tools by using JEOL 6610LV SEM device with the help of EDS, which allows the user to identify the various elements and their concentration are summarized in Table 2.3.

3.4.4 X-Ray Diffraction (XRD):

Once the elements are confirmed, the same samples were used to perform the XRD for phase identification. The samples were mounted on the Bruker D8 discover with a cobalt source having a wavelength of λ_{avg}= 1.79026Å, and power settings: 35kV, 45mA. The data was collected through the scanning performed at 2θ values from 22° to 112° and at an increment of 18.

Software "DIFFRAC.EVA V4.2.1" (Bruker Corporation) was used to merge all frame and mask it to remove noise. A 1-dimension XRD spectra were created by using the tool "integrate cursor," and an intensity v/s 2θ plot was generated. The "export partial scan" tool was used to flatten and export the intensity plot by removing background noise.

The exported plot was saved as an XY file, and the data was used in the origin software to create a plot graph and stack multiple plots into a single graph for comparison, as shown in Figure 2.3.

The same "DIFFRAC.EVA" software was used to search and identify phases from the database and match them with the XRD intensity plot data for all CERMET tools. In this case, ICDD PDF-4+ 2019 database was matched with CERMET tools, and peaks, along with its orientations for the identification of the respective phases, as showed in Figure 2.3.

TOPAS software was used to measure the wt.% of phases identified by XRD. A CIFs file related to the phase for which we want to measure the wt.% is required and can be downloaded from the "ICSD Web-Inorganic Crystal Structure Database." The CIFs files for the respective phases were downloaded and matched with the XRD raw data files using

TOPAS, and the wt.% of phases results were summarized in Table 2.4 of the article (Patel et al., 2020).

3.4.5 Tool Life and Wear Test:

The tool life test for four different commercial uncoated inserts (CNMG 12408/CNMG 432) was performed using CNC OKUMA crown L1060 turning the machine on AISI 304 stainless steel workpiece. The feed rate of 0.15 mm/rev, depth of cut of 0.4mm and cutting speed of 240 m/min were used for the test. The machining was done for a fixed interval, and the inserts were examined for flank wear measurement along with notch length and width measurement. The data were measured and recorded in an MS Excel sheet, and the test was run until the tool reached the failure criteria of 300μm for either notch or flank wear. The collected data were processed in the origin software to prepare the tool life curves, as shown in Figure 2.6 and Figure 2.7. The images collected at several intervals with the digital microscope (KEYENCE-VHX 5000 digital microscope) and focus variation (3D scan with Alicona Infinite Focus G5) were plotted on the same graph to get an idea about tool wear condition at a particular stage. Figure 2.6 shows the tool flank wear progression, and Figure 2.7 shows notch wear progression with respect to the cutting length.

3.4.6 Progressive Wear Assessment:

SEM examination was done at several intervals (7m, 34m, 67m, 100m, 133m, and after every additional 133m until failure of the tool) on all the four CERMET tools during the

tool life test. The samples were mounted on the tool holder with 45˚degree inclined studs to track the wear progression, as shown in Figure 3.3, as examined by SEM. The images were taken at 20KeV, at a spot size of 55 and a working distance of 11mm at a magnification of 120X
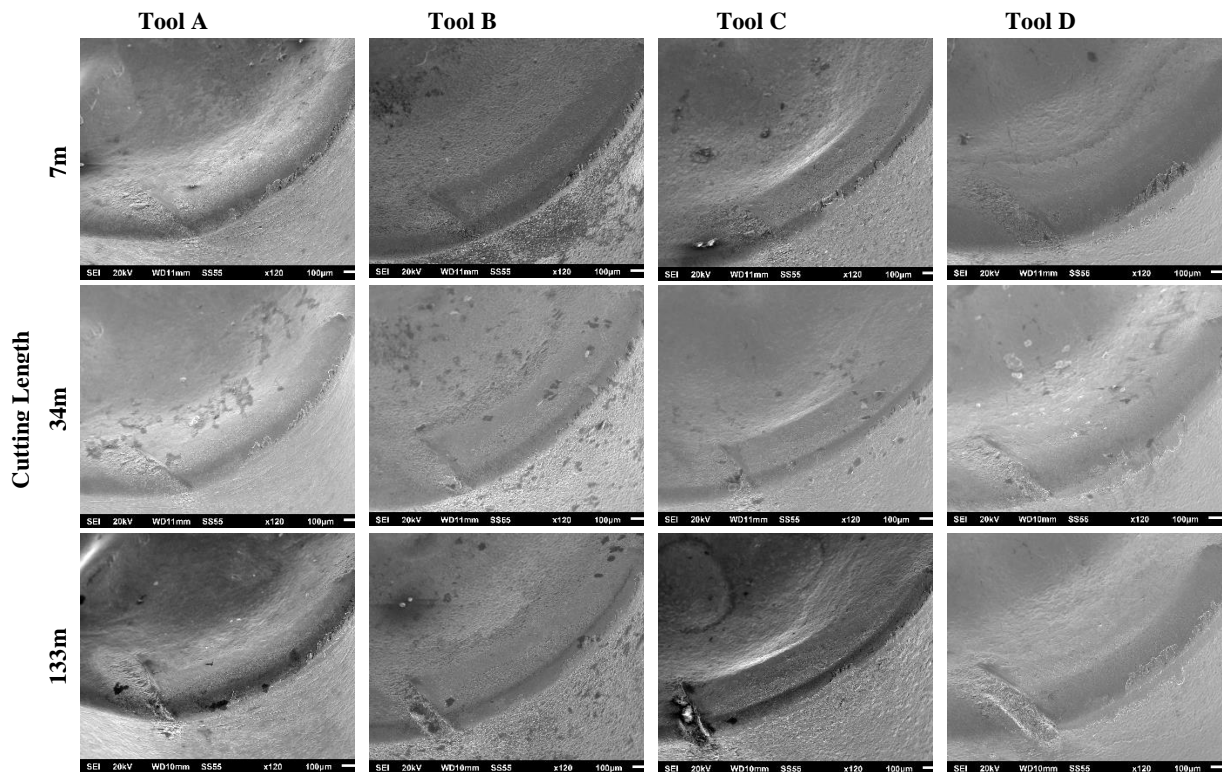
Figure 3.3 *Secondary electron SEM images of all CERMET tools after machining lengths of 7m, 34m and 133m showing microchipping and notch generation*

The CERMET tools were taken out of the CNC turning lathe and examined under the microscope without any cleaning or allowing the external interface to see the sticking material on the tools. The CERMET tools were examined under the digital microscope (KEYENCE-VHX 5000 digital microscope), and images were taken at a different angle to examine the tool and wear mechanism. Figure 3.4 shows the sticking and notch filling

87

mechanism with the workpiece material on the tools, as observed under an optical microscope.

(a)   (b)   (c)
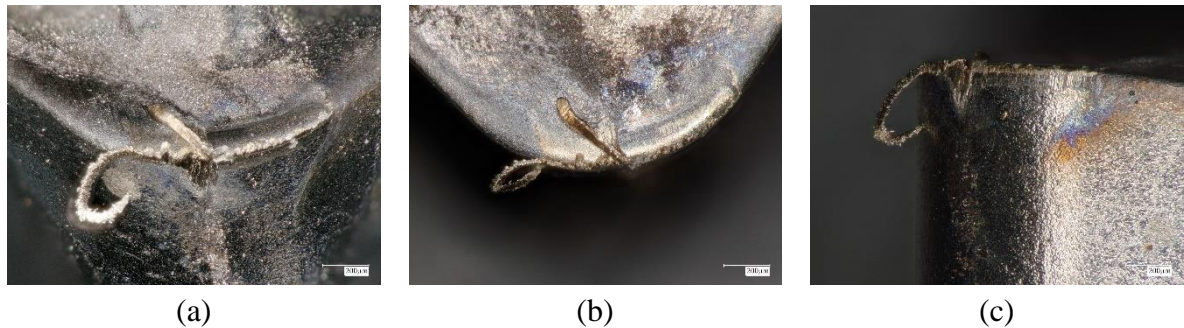
Figure 3.4 Optical microscope image of sticking and filling mechanism of workpiece material in the DOC notch groove formed on the CERMET tool by chipping (a) inclined view of notch groove where the workpiece material stick and form chip, (b) Rake view (c) side view (1600m)

3.4.7 3D Wear Volume Measurement and Comparison:

The wear volume was measured using the Alicona Infinite Focus G5 microscope. First, the new CERMET tools before machining were scanned and examined with Alicona. The CERMET tools, after every fixed interval during the machining test, were scanned under Alicona again. The scanned CERMET tools were used to compare and calculate the wear volume with respect to new CERMET tools. By applying the proper alignment of two data sets, the software in Alicona shows the peaks and valleys with respect to the reference scan (new/fresh tool). The software then calculates the volume of the valley (wear, chipping) and peak (sticking of material, BUE). The illustration is shown in Figure 3.5. The collected

wear volume data was plotted with respect to cutting length, and linear regression analysis was performed with the help of origin software, as shown in Figure 2.10.
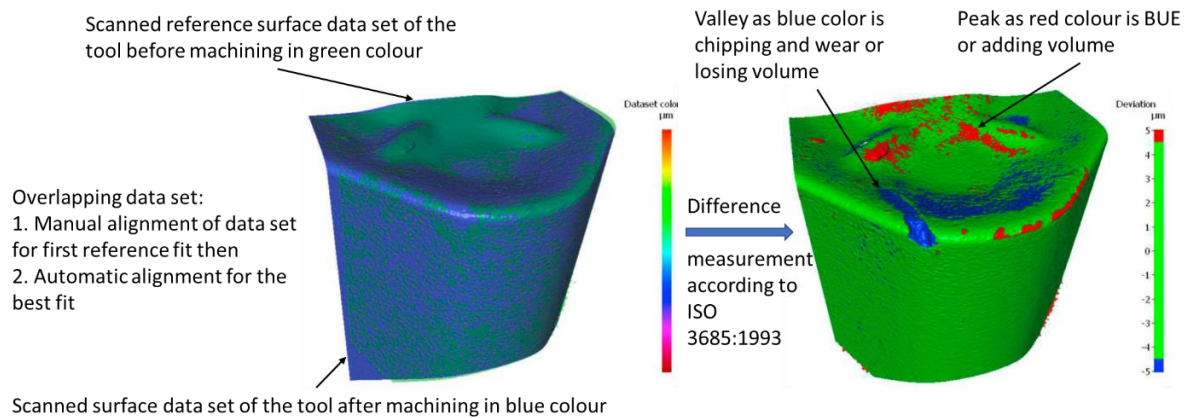
Figure 3.5 Illustration of the methodology used to identify three-dimensional wear volume

3.5 Acknowledgment

3.6 References

Patel, U. S. et al. (2020) 'Influence of secondary carbides on microstructure, wear mechanism, and tool performance for different cermet grades during high-speed dry finish turning of AISI 304 stainless steel', Wear, 452–453, p. 203285. doi: 10.1016/j.wear.2020.203285.

Chapter 4 : Wear Mechanism and Performance Evaluation of Various Commercial PVD coatings

Complete citation:

U. Patel, S. Rawal, B Bose, A.F.M. Arif, S. Veldhuis, Performance Evaluations of Ti-based PVD coatings deposited on cermet tools for high-speed dry finish turning of AISI 304 stainless steel, Submitted to the "Wear" journal, July 2021.

Copyright:

Author's Contributions:

Uttkarsh Patel	Conceptualization, Investigation, Formal analysis, Validation, Visualization, Methodology, Data Curation, Writing - Original Draft
Sushant Rawal	Conceptualization, Methodology, Validation, Supervision, Writing - Review & Editing
Bipasha Bose	Methodology, Validation, Writing - Review & Editing
Abul Fazal M Arif	Conceptualization, Methodology, Project administration, Writing - Review & Editing
Stephen Veldhuis	Resources, Project administration, Funding acquisition, Supervision

Abstract

The aim of this research work is to develop and compare in-house Ti-based coatings with commercial coatings for cermet tools, specifically for the high-speed dry turning of Austenitic stainless steel (AISI 304). In the present study, commercial Ti-based coated cermet tools from different manufacturers are used to evaluate and compare the performance of commercial coatings. This research focuses on the investigation of the performance for the various commercial coatings on cermet tools based on the mico-mechanical properties, tool performance and surface roughness. The results are used to develop a range of in-house Ti-based PVD coatings with different compositions and compare their performance with similar commercial coatings. A Scanning Electron Microscope (SEM) was utilized to conduct a progressive wear study. Coating surface topography and structure were investigated using Atomic Force Microscopy (AFM). The compositions of coating materials and tribo films were determined using Energy-Dispersive X-ray Spectrometry (EDS) and X-ray photoelectron spectroscopy. The results of this research demonstrate that the compositions of various coatings affect the micro-mechanical properties and significantly influence the tool life and wear morphology. The performance of in-house Ti-based coatings with a similar composition to commercial coatings was better than the latter, depending upon their micro-mechanical properties.

Keywords: PVD; Coating; Cermet; 304 stainless steel; tool wear; dry machining; high-speed machining

4.1 Introduction

Stainless steels are widely used in sectors that demand high corrosion resistance without compromising the mechanical strength at elevated temperatures. Stainless steels have a tendency of severe adhesion or galling (high ductility). Therefore, the cutting tool material must be tougher, and its coating must have anti-adhesion properties. Stainless steels have a higher possibility of strain hardening, which results in the notching and the chipping of the cutting tool. Stainless steels are also lower in thermal conductivity. Therefore, less heat will be dissipated through the workpiece and formed chips, and the majority of the heat will be absorbed by the cutting tool. For these reasons, the hot hardness of the cutting tools is very important.

Dry and high-speed machining is preferred by manufacturing sectors because of its several advantages, like cost-effectiveness, operator's health and safety, low instrument clean up, wet scrap handling and cost, as well as the environmental perspective. The dry machining process increases heat generation during cutting, and, therefore, the majority of the tools fail due to low sustainability at high temperatures.

The cutting fluid used during wet machining results in pollution and have a considerable environmental impact (Noordin et al., 2001; Stanford et al., 2009). Carbide tools suffer severe tool wear and breakage, which limits cutting speed. It was also observed that coated carbide tools undergo adhesive wear, oxidation wear, and diffusion wear as a result of the coating cracking (Noordin, Venkatesh and Sharif, 2007; Suresh, Basavarajappa and Gaitonde, 2015). Ceramic tools are the most effective tools when it comes to performing

under high cutting temperatures. However, they are poor in terms of crack resistance and toughness. Ceramic tools undergo catastrophic failures due to the high brittleness of ceramic constituents (Ghani, Choudhury and Masjuki, 2004; Noordin, Venkatesh and Sharif, 2007; Zhang et al., 2017). A lower thermal conductivity of ceramic tools tends to favour adhesive wear (Chen, Xu and Xiao, 2015). Cermet tools have higher transverse rupture strength and fracture toughness than ceramics and greater oxidation resistance and wear resistance than cemented carbide tools (Peng, Miao and Peng, 2013). Therefore, nowadays, advanced composite tools referred to as CERMET are developed to adopt the property of ceramic-like wear resistance and hardness and enhance mechanical properties like toughness by using metal as a binder. The ceramic matrix that is predominant in the cermet tool protects the tool at elevated temperatures when it undergoes a small amount of plastic deformation, and there is no effect on the metal phase for deformation. This is the major advantage of cermet tools and, as a result, are a better alternative cutting tools (Sarjana et al., 2020a).

The authors reported and discussed in detail cermet microstructure, the role of various secondary carbides, and their effect on microstructure (U. S. Patel et al., 2020). The authors found that a higher binder content accelerates the notch wear, and high nickel (Ni) content increases the diffusion of the tool. Cermet cores are bonded and covered with rims which play a crucial role in holding the cores together and increase the wear resistance and reduce crack initiation. The presence of tungsten (W) as a key element found in the cermet formed (TiW)C phase as a rim was found to reduce wear. However, other secondary carbides also

contributed to other aspects of the tool's microstructure as mentioned in the article (U. S. Patel et al., 2020).

Ghani et al. 2004 found cracks, chipping, and fractures cermet tools during the milling of hardened AISI H13 tool steel but found that cermet tools performed better than carbide tools (Ghani, Choudhury and Masjuki, 2004). Zou et al. 2014 observed cracking, and severe notch wear of $Ti(C_7N_3)$ based cermets while performing the turning operation of 17-4PH martensitic stainless steel (Zou et al., 2014). Zou, Bin et al. 2015 reported crater wear, cracks, notch wear, adhesion wear, and abrasion wear of $Ti(C_7N_3)/WC/TaC$ cermet during machining 321 austenitic stainless steel and 17-4PH martensitic stainless steel under various cutting conditions (Zou et al., 2015). Zhang et al. 2017 found cracking and micro-chipping of cermet tool during dry cutting of hardened steel 40Cr (AISI 5140) (Zhang et al., 2017). Sarjana et al. 2020 also found cermet tool failure due to chipping, notching, fracture, and catastrophic failure during the turning of high strength low alloy AISI 4340 steel (Sarjana et al., 2020). The authors also found pitting wear and microchipping during the early stage of machining stainless steel 304 under the dry cutting condition which progressed to notch chipping and formed a notch groove and reported the causes in detail. This chipping of the notch at a depth of the cut region resulted in dominant tool wear. However, flank wear was not observed as a major tool wear mechanism which can be attributed to the unique property of ceramics that resist wear (U. S. Patel et al., 2020).

Tools can be protected and tool life can be improved by adding a protective layer such as PVD coatings. These coatings can protect cutting tools during the machining application against excessive tool wear and damage, which can ultimately help to improve the tool life

and lower machining costs. Nowadays majority of the commercial cutting tools for machining are PVD-coated (Ortner, Ettmayer and Kolaska, 2014).

The first commercial PVD coating developed was TiN, for high-speed steel drills around 1980 and later on carbide inserts for the milling process (Wolfe, Petrosky and Quinto, 1986). Moreover, other binary and ternary coatings of Ti, Al, and Cr were prepared over time (Yamamoto et al., 2003; Kalss et al., 2006; Patel et al., 2016). A new scope of manufacturing functional coatings was opened in the mid-1990s with the advancement of nanostructure coatings designed at the atomic level.

PVD coated machine tools like WC/Co with sharp or prepared edges can be used mainly for machining stainless steel and other high-temperature alloys like Ni, Ti, Al alloys. The PVD process involves an intense ion bombardment that develops the compressive stress in the film, which may lead to high hardness of the tool coating. Moreover, with the increased cutting speed, the coating's stress dependant component of hardness is eliminated, and, therefore, PVD coatings can retain the functional hardness over the wide range of machining conditions (Breidenstein and Denkena, 2013).

Vandierendonck and Van Stappen 1997 (Vandierendonck and Van Stappen, 1997) investigated the performance of TiN (PVD), (Ti, Al)N (PVD), TiN (PCVD), and a multilayer $TiN/A_2O_3/TiN$ (PCVD) coated cermet for turning and milling applications with various workpiece materials. They found (Ti, Al)N (PVD) coating is best for milling applications because of the lower thermal conductivity of the (Ti, Al)N coating. TiN (both PVD and PCVD) coatings showed improvement in tool life for the turning process. They

also observed build-up at the edge of the cutting tool and coating delamination on the sharp cutting edge of the tool. Soković and Bahor 1998 (Soković and Bahor, 1998) designed a statistical model and showed relation to regression analysis to obtain an experimental result of roughness value and showed that with the conventional finish machining the roughness can be achieved and coating (TiN - outsourced) can be wear-resistant and improve the performance and increase the stability of the cutting process. Dolinšek and Soković 1998 (Dolinšek and Soković, 1998) used uncoated and coated (TiN-outsourced) cermet tools to investigate the effect of coating on identification parameters in turning. They found that coated tools showed a decrease in input and output energies and their parameters. D'Errico, Calzavarini, and Vicenzi 1998 (D'Errico, Calzavarini and Vicenzi, 1998) tested TiN and Ti(C,N) coating for machining AISI-SAE1045 steel under dry condition. They found that some coatings did not perform efficiently as a barrier to the wear mechanism, which becomes more severe in interrupted turning, resulting in diffusion and chipping as dominant wear.

Dobrzański and Gołombek 2005 (Dobrzański and Gołombek, 2005) compared tool life of cemented carbide and cermet inserts with different PVD TiN + gradient layer (Ti,Al,Si)N + TiN, TiN + multilayer (Ti,Al,Si)N + TiN, TiN + TiC + TiN coatings. Cermet provided higher tool life and lower surface roughness compared to the cemented carbide tools. The presence of Al and Si as a solid secondary solution alternating with the pure TiN resulted in the improvement in the adhesion of coating and substrate and improved hardness. DOC notch chipping was also observed while machining C45E steel under dry turning. Noordin, Venkatesh, and Sharif 2007 (Noordin, Venkatesh and Sharif, 2007) machined martensitic

stainless tool steel 43-45 HRC with coated cermet and carbide under dry conditions and found that coating fracture caused tool edge chipping, flaking, and rapid crater wear. Li et al. 2017 (Li et al., 2017) used various WC contents as the substrate of TiAlCrN coatings and found that grains of TiAlCrN columnar structure become finer with the increase in WC content, and adhesion strength of the coating decreases, resulting in poorer coated tool performance. Kaladhar 2019 (Kaladhar, 2019) used a standard orthogonal array L16 for choosing different parameters. The author compared the performance of PVD and CVD coated carbide and cermet tools from different manufacturers focusing on MRR and surface roughness. Tiwari et al. 2020 (Tiwari et al., 2020) used multi-layered coated (TiN/TiCN/TiN) cermet (golden colour) inserts in the dry-hard turning of AISI 4340 steel. The author's work focused on MRR, surface roughness, and chip reduction coefficient. The surface roughness was (Ra) found in the range 0.212-1.452µm, and MRR increased linearly with an upturn in the radial depth of cut.

There are various coatings with the combination of different compounds that have been developed over time. Kalss et al. 2006 (Kalss et al., 2006) used Al-based Ti free coatings AlTiN and AlCrN on carbide tools for milling and drilling and compared the performance with the Ti-based hard PVD coating. High Al content based AlCrN coating showed improvement with excellent oxidation and wear behaviour. Kulkarni, Sargade, and More 2018 (Kulkarni, Sargade and More, 2018) used AlTiN/TiAlN multilayer carbide coated inserts for machining AISI 304 austenitic steel with high speed to determine the thermal electromotive force (E.M.F.) generated signal from the hot junction to develop a relationship between generated E.M.F. and corresponding temperature. They found their

regression model reliable and could use it effectively to predict the interface temperature. Jianxin et al. 2012 (Jianxin et al., 2012) deposited different nitride coatings, CrN, TiN, CrAlN, and TiAlN, by cathodic arc evaporation (CAE) and performed erosion wear tests by dry blasting machine tools. They found that the addition of Al to the coating provided higher erosion wear resistance. The TiN and CrN coatings showed a brittle fracture, and the AlTiN and CrAlN coatings showed micro and cycle fatigue fracture.

Based on the reviews of cermet, the authors proposed the cermet as a cutting tool to machine the stainless steel over the coated cemented carbide tools. It is reported in the literature and our previous study (U. S. Patel et al., 2020) that a common wear mechanism in cermet tools is chipping, cracking, and notching. The literature found that it is difficult to find a coating specifically designed for cermet to perform under dry high-speed cutting for stainless steel materials. Therefore, the current research is particularly focused on the use of the cermet tools for machining stainless steel under dry high-speed conditions. The challenges involved in this research are the limited work on the study of wear mechanisms, performance, development of the coating, and addressing issues involved during the machining process. To develop a coating for a specific application, it is important to understand the wear behaviour and the causes for the failure of the coating. The purpose of this present study is to examine the wear mechanisms of conventional coatings (TiN) and the current commercial coatings under challenging machining conditions (dry-high speed), coating composition and mechanical properties. This research work thoroughly investigates the performance of various commercial and in-house Ti-based coatings with various compositions and micro-mechanical properties. It will contribute to and enrich the

development of CERMET as a promising cutting tool for machining the challenging material 304 stainless steel in high-speed dry conditions. Overall, it will contribute by providing an alternative efficient PVD coated CERMET tool that can increase productivity and meet the growing demand from the manufacturing sector, be environmentally friendly, and reduce production expenses.

4.2   Experimental Procedure

4.2.1   Machining Studies

Dry high-speed machining tests were performed on a CNC OKUMA crown L1060 lathe. The workpiece material was AISI 304 steel with a hardness of 125 BHN. The workpiece mechanical and chemical compositions are given in Table 4.1. The detailed composition and microstructure of each of the CERMET tools have been described previously by Patel et al. (U. Patel et al., 2020).   The related commercially coated tool from the same manufacturer was used in this study and compared with identical uncoated tools with in-house coatings. The commercially coated and in-house coated tools are listed in Table 4.2 with tool nomenclators. The machining tests were performed at a feed rate of 0.15mm/rev, depth of cut of 0.4mm, and cutting speed of 240m/min.

Tool wear changes were characterized by volume wear measurements taken by an Alicona Infinite Focus G5 3D surface measurement system (Alicona Manufacturing Inc., Bartlett, IL, USA). A JEOL 6610LV Scanning Electron Microscope (SEM) was used to capture the tool wear and edge geometry at different magnifications to observe the wear behaviour at

fixed machining intervals and to examine the cermet structure. Energy-dispersive X-ray spectroscopy (EDS) was used for compositional analysis.

Table 4.1 *Chemical composition and mechanical properties of AISI 304 stainless steel*

Chemical composition (%)								
C	Si	Mn	P	S	Cr	Ni	N	Balance
0.08	0.75	2.0$_{max}$	0.045$_{max}$	0.03$_{max}$	18-20	8-10.5	0.1$_{max}$	Fe(iron)
Mechanical properties								
Yield Strength	Tensile Strength	Elongation	Modulus of Elasticity	Shear Modulus		Hardness	Poisson's Ratio	
215 MPa	505 MPa	70%	193-200 GPa	86 GPa		123 HB	0.29	

Table 4.2 *Tool coating nomenclator and composition*

Uncoated Tool (CNMG 120408/CNMG 432)	Coating		Coating Composition (wt%)				Coated Tool Nomenclator
			Ti	Al	Cr	N	
Tool A	TiAlCrN	Commercial	28	18	7	42	Tool A$_c$
Tool C	TiN	Commercial	62			38	Tool C$_c$
Tool D	TiAlN	Commercial	39	27		34	Tool D$_c$
	TiAlN 2773	In house	24	34		42	Tool D$_{TAN2773}$
	TiAlN 5050	In house	41	20		39	Tool D$_{TAN5050}$

Tool life tests were conducted following the ISO 3685:1993 standard. Flank wear and notch wear were measured at fixed cutting length intervals using a Mitutoyo digital micrometer

and a KEYENCE-VHX 5000 digital microscope. A tool life criterion limit of 0.3mm was fixed based on the ISO 3685:1993 standard (Standardization, 2006). The hardness of different inserts was measured using a Vickers indenter. The structure of different cermet tools was studied by X-ray diffraction (XRD) (D8 Discover DAVINCI.DESIGN diffractometer, with Parallel Focus Goebel Mirror and Vantec 500 area detector) using a cobalt sealed tube source (λavg = 1.79026 Å). Samples were scanned in six steps within the 22-112ºC temperature range with an exposure time of 480s for each step. The chemical compositions of workpiece materials and uncoated tools' geometry, designation, and hardness were reported in previous work (U. S. Patel et al., 2020). The formation and chemical composition of the formed tribofilms were analysed using X-Ray Photoelectron Spectroscopy (XPS) (PHI Quantera II Scanning XPS Microprobe). The X-ray beam condition was 50u12.5W15KV. The samples were sputtered for gentle cleaning to remove any contamination from the surface. The survey spectra were collected at 224eV with the step size 0.8eV and a high-resolution spectrum was collected at 26eV with the step size 0.1eV at the 45˚ take-off angle.

4.2.2 Coating Deposition (In-house) and Characterization:

In-house coatings were deposited on the polished coupons and commercial uncoated inserts. The cathodic arc ion deposition technique (Kobelco AIP-S20) was used for the deposition of the in-house coatings. Two different titanium and aluminium based solid metal targets with different compositions TiAlN2773 (27%Ti, 73%Al) and TiAlN5050 (50%Ti, 50%Al) with 99.98% purity, were used to deposit TiAlN coatings. The coatings

were deposited by rotating the sample table at 4RPM. Nitrogen was used as a process gas to keep the deposition pressure at 3.75Pa, the bias voltage was -60V, the cathode arc current was 150A, and the substrate temperature was maintained at 525°C for 55 minutes.

A calo test instrument (BC-2 Ball Crater Device) with a 30mm diameter ball (AISI 52100m Grade 25 Chromium steel) was used to measure coating thickness using 1µm diamond paste. The measured thicknesses were confirmed with optical measurements of the crater. The micromechanical properties of the coatings (both commercial and in-house) were evaluated using Anton Paar NHT[3] Nanoindentation Tester at room temperature using a diamond Berkovich indenter following the ISO14577–4 standard. The load was adjusted to keep the indentation contact depth within 1/10 of the coating's thickness to minimize the effect of the substrate and to ensure that only coating properties were measured. There were around 41 indentation measurements performed on each sample. The topography and morphology of the coated tools were measured by Anton Paar Tosca[TM] 400 atomic force microscope (AFM) (Graz, Austria). Scanning was performed using a silicon probe at a scan rate of 0.3 lines/sec with tapping mode. The scan size was 30X30 µm and a resolution of 400X400 for all coating scans.

The scratch tests were performed using an Anton Paar-RST[3] Revetest® Scratch Tester (Switzerland) on the flat part of the commercially coated inserts and the flat polished coupons of in-house coated samples. A standard Rockwell diamond indenter with a 200µm tip radius was used to perform the progressive load scratch tests. The scratch length was 1.5mm and around 3 scratches were made on each sample. Each scratch test was done

following a 3-scan procedure where at first a pre topography scan was performed at 0.5N load and then a progressive load scratch scan was performed where the load was steadily increased from 0.5 N to 60N, and finally, a post topography scan was performed at 0.5N load.

4.3   Results and Discussion

In this study, three uncoated cermet tools from the authors' previous study (U. S. Patel et al., 2020) were used (Table 4.2). The previous study showed that Tool A had the maximum tool life compared to Tool C and D. In this current investigation, similar studies were carried out to compare the performances of the same tools with coatings. Thus, three different commercial coatings on tools A, C, and D were studied to identify the effects of PVD coatings on wear mechanism and tool life during high-speed dry finish turning of 304 stainless steel. The other major objective of this research work was to take the worst-performing tool (Tool D) from the previous investigation, as it is easily available and economical, and deposit in-house coatings on it to improve its performance and provide a more economical solution.

4.3.1   Tool Performance Analysis

Cutting tests based on ISO 3685 standard were carried out with the tool failure criteria of dominant wear (notch wear and flank wear) of 300µm.

4.3.1.1 Tool Life Comparison of Uncoated Vs Commercially Coated tools

Tool performance based on the flank wear and notch wear is presented in Figure 4.1 (a) & (b). The uncoated Tool A shows a tool life of 2668m with flank and notch wear lengths of 88µm and 300µm (Figure 4.1 (a&b)). Tool A with the TiAlCrN commercial coating (Tool Ac) shows the longest tool life compared to the other coated, and uncoated tools studied, with a maximum tool life of 3733m with 110µm of flank wear and 320µm of notch length (Figure 4.1 (a) & (b)), an increase of 1065m over uncoated Tool A. Tool C with commercial coating TiN (Tool C_c) shows a tool life of 1870m, which is comparable to the uncoated Tool C with a tool life of 2000m. The flank and notch wear observed is respectively 84µm and 300µm for Tool C and 113µm and 300µm for Tool C_c (Figure 4.1 (a) & (b)).
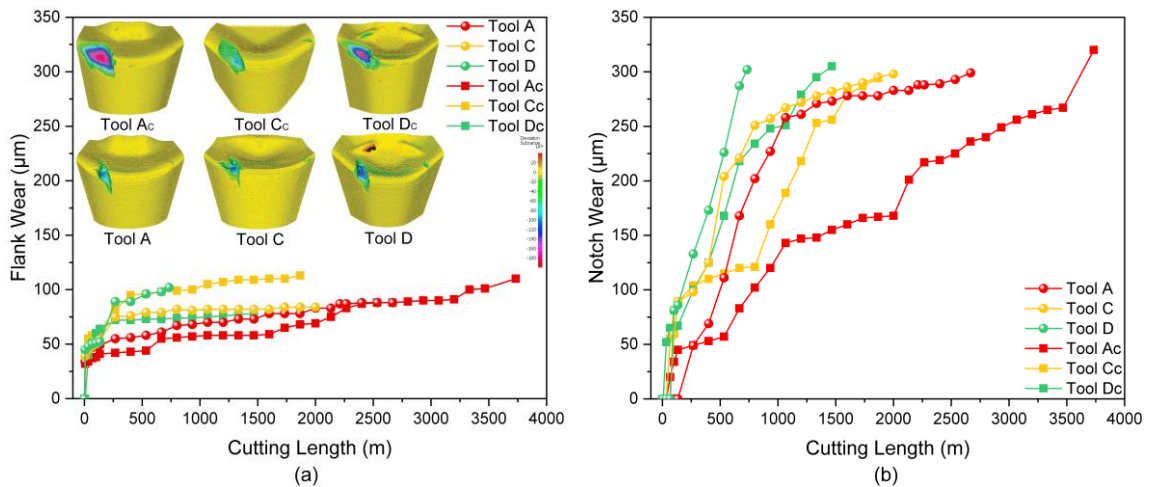
Figure 4.1 *Tool life comparison for uncoated and respected commercial coatings with respect to (a) flank wear, (b) notch wear*

It can be concluded that TiN coating does not provide any significant improvement in tool performance. Uncoated Tool D shows a tool life of 733m with flank wear of 102µm and notch wear of 300µm. Tool D with commercial coating TiAlN (Tool Dc) shows longer tool

life of 1470m with 78µm of flank wear and 305µm of notch wear (Figure 4.1 (a) & (b)), an increase of 737m.

4.3.1.2   Tool Life Comparison of Commercially Vs In-House Coated tools

Tool performances based on the flank wear and notch wear for commercial coating and in-house coatings on Tool D are represented in Figure 4.2 (a) & (b). Tool $D_{TAN5050}$ shows the longest tool life compared to Tool D_c and Tool $D_{TAN2773}$. Tool $D_{TAN5050}$ shows tool life of 2800m with flank wear of 93µm and notch wear of 304µm, which is an increase of 1334m over Tool Dc (Figure 4.2 (a) & (b)) and 2799m more than the uncoated Tool D.
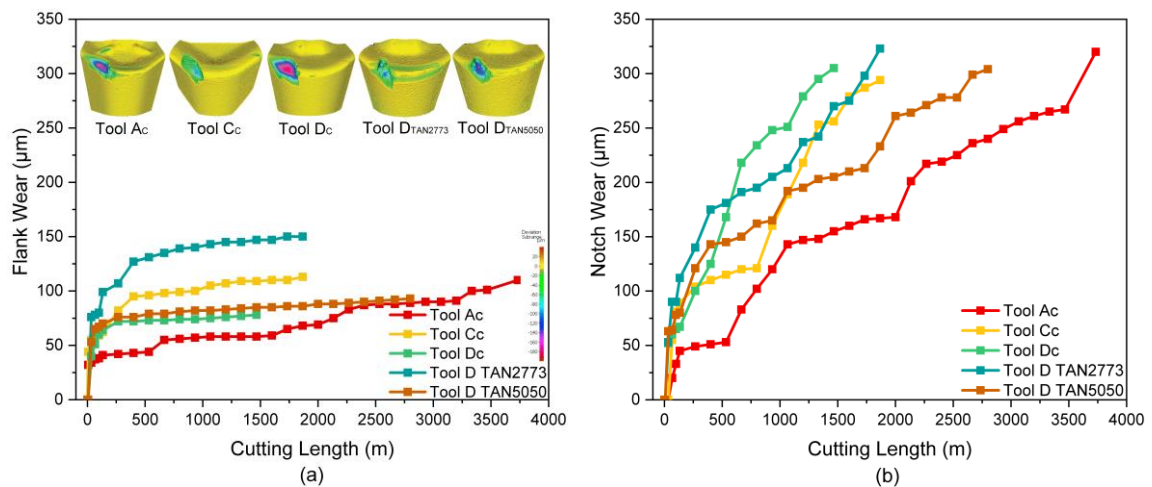
Figure 4.2 *Tool life comparison for commercial and in-house coatings with respect to*

(a) flank wear, (b) notch wear

Tool $D_{TAN2773}$ shows improved performance over Tool D_c. It shows 400m more tool life with flank wear of 150µm and notch wear of 323µm compared to Tool D_c and 1133m compared to uncoated Tool D_c. Among the coated Tool D group, Tool $D_{TAN2773}$ shows the greatest flank wear of 150µm (Figure 4.2 (a) & (b)), which is also evident from the SEM

images (Figure 4.3), while Tool $D_{TAN5050}$ shows the least flank wear at 93µm. Tool D_c shows the shortest tool life of the coated tools by 1470m. However, Tool D_c flank wear trend is similar to that of Tool $D_{TAN5050}$, while Tool $D_{TAN2773}$ shows highest flank wear of all coated tools in the "Tool D" group. These results show that variation in the concentration of various elements in a coating can have a significant effect on the performance.

Tool C_c does not show significantly improved performance over uncoated Tool C. Tool C_c shows the same tool life as Tool $D_{TAN2773}$. Overall, comparing all coated tools, Tool A_c shows the highest tool life of 3733m (with the improvement of 1066m compared to uncoated Tool A) and second highest performance is by in-house coating Tool $D_{TAN5050}$ with tool life of 2800m (with the improvement of 2066m compared to uncoated Tool D).

4.3.2 Wear Mechanism

The progressive wear study was conducted at fixed cutting lengths of 7m, 34m, 133m, and 666m to understand why a particular coating is performing best or worst, and its wear mechanism.

4.3.2.1   Wear Mechanism at 7m Cutting Length

Figure 4.3 shows SEM images of the wear progressions of commercially coated tools Tool A_c, C_c, D_c and in-house coated Tool $D_{TAN2773}$ and Tool $D_{TAN5050}$. Tool A_c developed flacking of the coating at the edge. It was also observed that all tools had workpiece material adhering to the edge on the flank side of the tool. However, no microchipping was observed for Tool A_c in the first pass of cutting of 7m. Tool C_c showed the greatest adhesion, mostly

on the. Tool C_c showed microchipping from its first pass or initial stage of the cutting process after a machining length of 7m. This micro-chipping forms due to continuous rubbing of the work-hardened burr which is generated at the chip edge during machining.
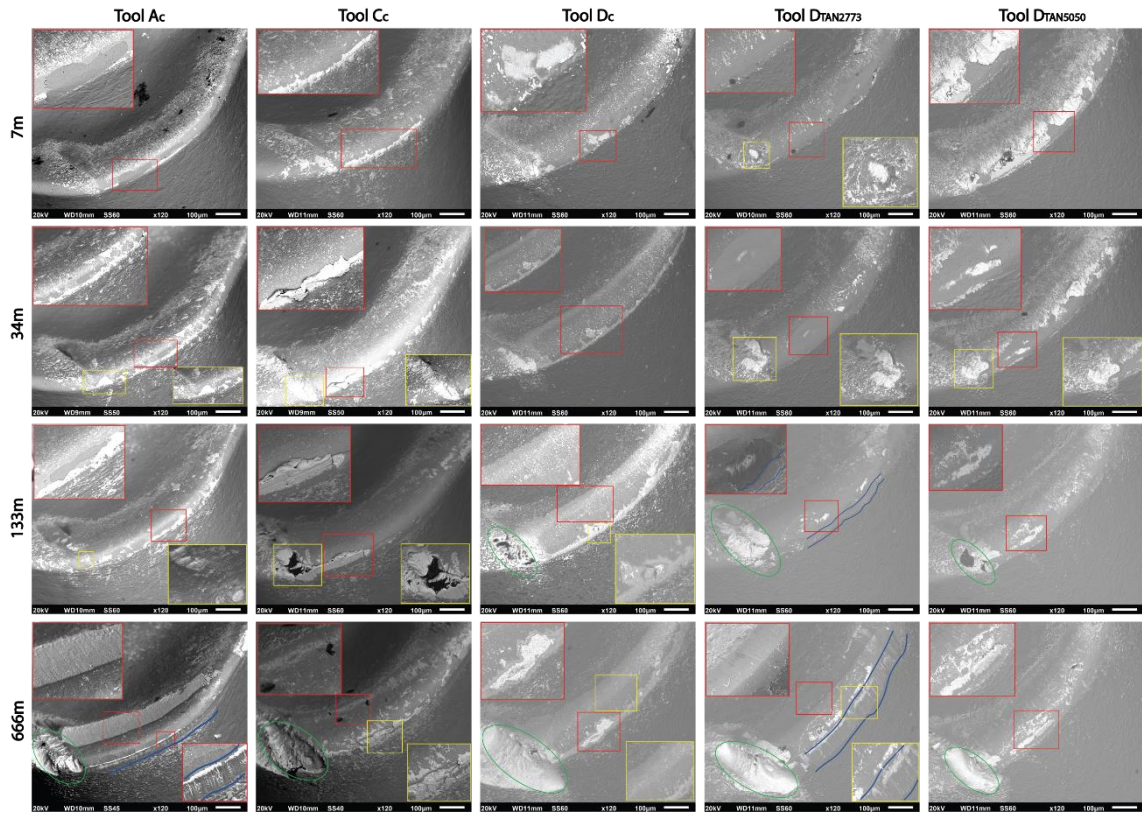
Figure 4.3 *Progressive wear mechanism study at a specific interval of cutting at 7m, 34m, 133m, and 666m with the help of SEM images of all coated tools (Tool A_C, Tool C_C, Tool D_C, Tool $D_{TAN2773}$, Tool $D_{TAN5050}$)*

This micro-chipping increased with cutting length. It was observed that some workpiece material adhered along the cutting edge. For Tool D_c, microchipping at a depth of the cut notch area was observed at the first cutting pass of 7m. Flacking of the coating was observed on the cutting edge, which mainly occurred due to work piece material sticking at the tool edge (BUE - Built-Up Edge) and being removed during (Breaking of BUE) the

108

cutting process. Tool $D_{TAN2773}$ showed micro chipping at the DOC notch, and it clearly showed substrate exposure. Tool $D_{TAN2773}$ coating also showed flacking or signs of removed coating from the edge of the tool. Tool $D_{TAN2773}$ had lower adhesion compared to other tools. This may be due to the coating material resisting adhesion or be that adhesion is weak enough that BUE is quickly removed during machining. Tool$_{DTAN5050}$ shows a very small amount of micro chipping as compared to Tool C_c and Tool $D_{TAN2773}$ after 7m of cutting. However, coated Tool $D_{TAN5050}$ had the greatest adhesion along the tool edge, as seen in Figure 4.3 marked red.

Since the workpiece material in this experiment is very sticky, another reason for microchipping may be the combined effect of adhesion and diffusion wear. During the sticking phase, diffusion of the coating and tools occurs. As a result, the tool coating and the binder of the tool become weak. During the machining process, when work-hard chips pass through the surface of the tool, they can break the tool segment and progressively remove smaller pieces of the tool, resulting in microchipping and notching.

4.3.2.2   Wear Mechanism at 34m Cutting Length

After 34m of machining, Tool A_c workpiece material sticking was observed along the cutting edge, as illustrated in Figure 4.3. At this point, coated Tool A_c still resisted the micro chipping and exposure of the tool substrate. At the same machining length Tool C_c showed significant chipping at DOC notch and started forming a notch groove that was clearly visible (Figure 4.3). This rapid notch formation is also a consequence low percentage of W and the lack of (TiW)C phases in the tool substrate, which are known to provide good

binding power and increase wear resistance (U. S. Patel et al., 2020). A large BUE was also observed for Tool C_c. In Tool D_c, microchipping increased, and after a machining length of 34m the tool formed a larger chip at the DOC notch edge. The tool substrate was now clearly visible at the notch where the coating was eliminated, and tool material was removed. This indicates that the coating on the cutting edge of the tool was deteriorating. Tool D_c did not show much sticking of material but began to show signs of wear on the rake face. Tool $D_{TAN2773}$ showed a low amount of sticking. However, Tool $D_{TAN2773}$ lost coating material, as seen in Figure 4.3. Tool $D_{TAN2773}$ shows coating chipping and exposure of the tool substrate near the tool edge and rake face (marked red in Figure 4.3). At this point, Tool $D_{TAN2773}$ was showing an excess amount of chipping on the notch. Tool $D_{TAN5050}$ exhibited increased micro-chipping in the DOC notch area. It was also observed that the Tool $D_{TAN5050}$ had begun to lose the coating on the edge of the tool (marked red in Figure 4.3), which is not due to tool wear, but due to the removal of BUE on the tool cutting edge. The material glued to the tool/coating, or BUE, is removed from the tool during the machining process, taking away part of it and reducing the coating performance by reducing the thickness of the protective PVD coating.

4.3.2.3   Wear Mechanism at 133m Cutting Length

After 133 m of machining, micro-chipping of the coating and tool at DOC notch area began for Tool A_c, while the other coated tools showed the same effect from the start of the machining test. This shows that Tool A_c was performing comparatively better in the initial stage of machining. There is also evidence of BUE, as shown in Figure 4.3. The notch observed for Tool C_c observed had grown as material continued to stick and push into the

valley of the notch. The glued material will peel off the coating on the tool, and the material begins to etch the tool as is clear from Figure 4.3 for the Tool C_c (marked yellow) at 133m. Tool C_c coating performs poorly; there is no significant improvement in tool protection against wear compared to uncoated Tool C

At the same cutting length of 133 m, Tool D_c showed an increase in microchipping, and a larger notch in the DOC region (marked in green) began to appear. Substrate exposure at the cutting edge (marked yellow) was also observed as a result of material sticking and descending. The tool had lost more coating along the edge, and more substrate was revealed along the edge. Additionally, Tool D_c exhibited rake wear or diffusion wear (marked red), which could be caused by wear of the coating due to slipping of chips along the rake face. In addition, this area is subjected to high cutting temperatures, which can lead to rake wear due to diffusion of the coating material. Tool $D_{TAN2773}$ at the same stage shows a significant increase in DOC chipping and notch formed over Tool D_c, and some evidence of material sticking that is found near the valley of the notch. Tool $D_{TAN2773}$ lost a greater amount of coating with less sticking. As in Figure 4.3, marked red, the coating was flaking off with a chunk of material near the cutting edge, resulting in substrate exposure at certain locations. There was also an indication of flank wear at this machining stage (marked with blue lines). The Tool $D_{TAN5050}$ showed an increase in microchipping and notch (marked green) beginning to take shape. Tool $D_{TAN5050}$ also showed substrate exposure near the cutting edge (marked red) due to sticking and removal of material. Tool $D_{TAN5050}$ showed good wear resistance compared to Tool D_c and Tool $D_{TAN2773}$ after machining of 133m.

4.3.2.4   Wear Mechanism at 666m Cutting Length

At 666m cutting length, Tool A_c has increased microchipping and takes the shape of a large

notch (marked green) in the DOC, and diffusion wear was fully visible in the BSE SEM

image (marked red) Figure 4.3. A sign of worn coating was seen near the cutting edge and

flank side (marked blue line). Tool A_c showed comparatively delayed microchipping and

delayed notch formation; However, Tool A_c showed more diffusion wear than other tools.

At the same cutting length, Tool C_c was showing diffusion wear (marked red). The notch

of the tool had increased and formed a large canyon on the DOC. The process of BUE

formation and removal had continued in Tool C_c to the point where the entire coating from

edge to rake was removed, exposing the tool (yellow mark) with severe adhesion of the

material, as seen in Figure 4.3. At this point, the Tool D_c had developed a large notch in the

DOC region (denoted in green). Peeling of the coating continued, and the substrate near the

cutting edge began to reveal a large substrate area. Tool D_c showed increased diffusion

wear, but the tool substrate was not exposed on the tool's rake face (denoted in yellow).

Tool $D_{TAN2773}$ had greater flank wear (marked blue in the yellow box) and greater substrate

exposure compared to all coated tools near the entire cutting edge. Tool $D_{TAN2773}$ also had

more diffusion wear than the previous stage (marked red). The tool coating has lost more

material by flank wear, diffusion wear. Tool $D_{TAN2773}$ also had a large notch on the DOC

(marked green). Tool $D_{TAN5050}$ showed an increase in the notch (marked green), and a large

canyon had formed on the DOC. A small amount of substrate exposure could be detected

in Tool $D_{TAN5050}$ near the tool cutting edge and some signs of material sticking, causing the

coating to peel off and substrate exposure (marked red in Figure 4.3). Overall, after 666m

of machining, the Tool $D_{TAN5050}$ shows relatively good performance in terms of wear resistance, based on low flank wear and low diffusion wear, compared to other Tool D coating variants.

4.3.2.5   Wear Mechanism Based on Tribological Analysis

The effect of the tool structure or composition is combined with the study of progressive wear in order to understand, evaluate and compare the commercial and in-house coatings. During the cutting process, along with the high cutting force, the rake face is exposed to high temperature, caused by a combination of primary and secondary shear deformation of the workpiece material during the machining. This process generates a tribofilm from various elements present in the coating and the surrounding air (oxygen). Depending on the type of tool coating element (Ti, Al, Cr), the corresponding tribofilm is formed, as shown in Figure 4.4. XPS analysis of tribofilms provides an explanation for the wear mechanism of the coating and the device performance. XPS data is collected on the rake face of the tool where crater wear or diffusion wear occurs. The properties of the coatings depend on a small range of crystalline structures and the chemical state of the components.

Figure 4.4 (a) shows that TiO_2 is formed during the machining process as Ti has a valence state that establishes vacancies and forms TiO_2. TiO_2 has high friction characteristics. Therefore, Tool C_c (all stages in Figure 4.3) shows more material sticking along the cutting edge than the rest of the coated tools, as Tool C_c has 62% of Ti content, which is highest compared to all coatings (Table 4.2). The formed oxides shear easily from the interface, and this may be the cause of the rapid wear of the TiN coating for Tool C_c.

113
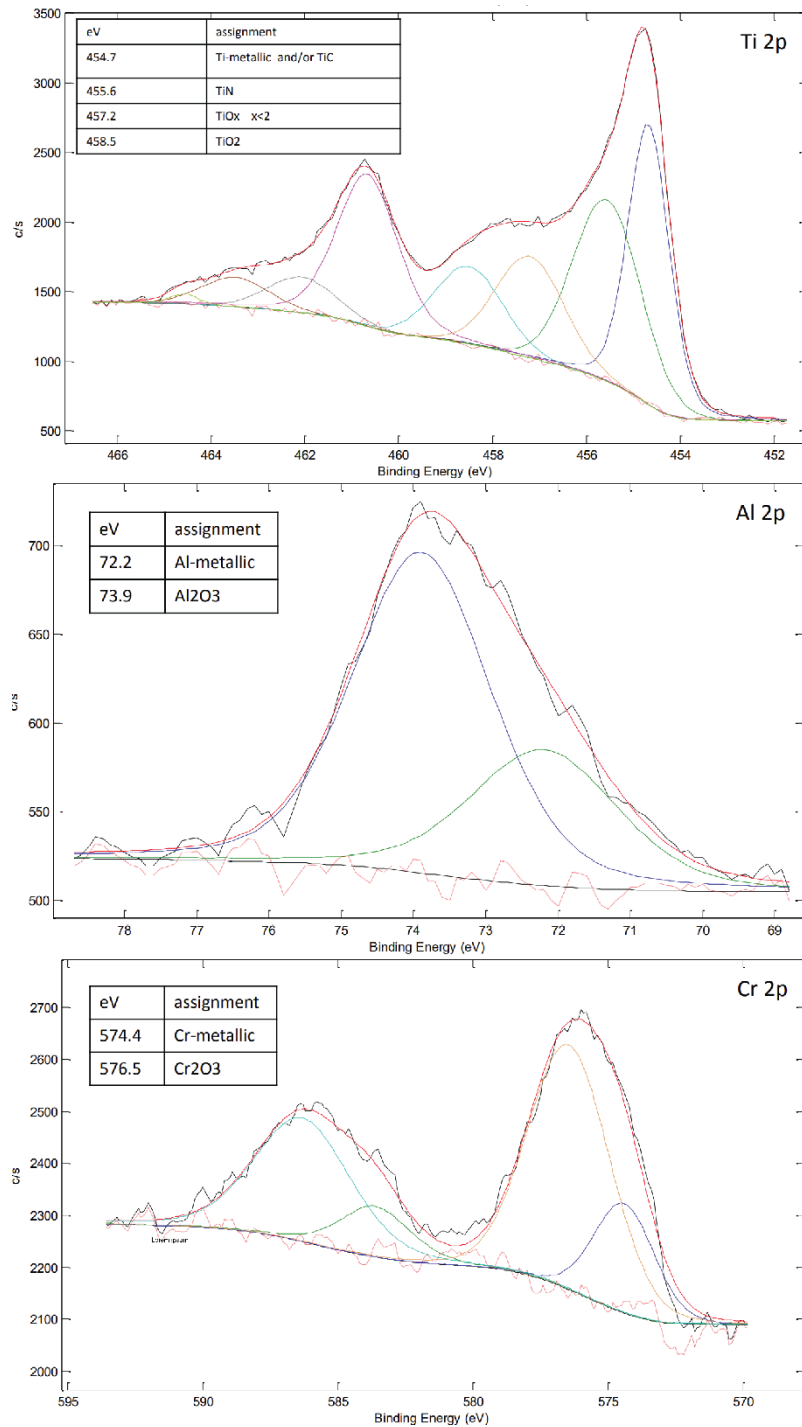
Figure 4.4 High-resolution XPS spectrum data of Ti, Al, and Cr tribo films, collected

from rake face of the used tested coated cutting tools.

It is clear from Figure 4.4 that, during the machining process, the Al present in the coating is forming Al_2O_3 (Aluminum oxide). The oxides of aluminum are brittle in nature and can fail during machining. Tool $D_{TAN2773}$ contains the highest amount of aluminum in the coating, 34% of all the coated tools (Table 4.2), and higher amounts of aluminum oxides will be formed during the machining process. This leads to rapid failure or wears off the coating, which is consistent with the evidence for the Tool $D_{TAN2773}$ wear mechanism in Figure 4.3, which shows that Tool $D_{TAN2773}$ has the greatest amount of flank wear and volume loss of the coating compared to the other tools. Therefore, it can be said that excessive amounts of aluminum can cause rapid wear of the coating due to the formation of Al_2O_3 (Aluminum oxide).

Figure 4.4 (c) shows that during the machining process, Tool A_c coating forms a steady-state of Cr_2O_3 tribofilms from the Cr present in TiAlCrN. In many cases, it also forms (Al, Cr)$_2$O$_3$ mixed oxides due to the Al element in the coating. These dense oxide films help protect the tool from oxidizing wear. Oxidation occurs mainly in the DOC region of the tool, where the tool is more exposed to atmospheric oxygen with higher cutting temperatures, which leads or notch wear to the tool. From Figure 4.3, it is clear that the Tool A_c resists notch wear up to a machining length of 133 m, while the other coated tools show notch wears from the beginning of the machining. Tool protection is most important in the initial stage of machining and helps the cutting tools to perform for a longer period. Due to the greater protection of the coating in the initial stage of coating, Tool A_c has a longer performance than the rest of the coated tools.

4.3.3 Coating Characterization

Table 4.3 Micro-mechanical properties and other relevant characteristics of the coatings

Coating	Thickness	Hardness GPa, H	Elastic modulus GPa, E	H/E	H^3/E^2	Plasticity Index	Ra (nm)
Tool A_c	3.90±0.45	28.01±3.94	428.07±106.82	0.0654	0.1200	0.4638	37.10±7.43
Tool C_c	3.05±0.44	25.62±1.77	428.37±64.68	0.0598	0.0916	0.5789	41.78±5.91
Tool D_c	1.38±0.26	25.93±1.82	466.55±76.33	0.0556	0.0801	0.5434	44.98±10.94
Tool $D_{TAN2773}$	4.64±0.09	23.04±2.19	256.15±36.20	0.0900	0.1865	0.4293	29.34±5.02
Tool $D_{TAN5050}$	3.54±0.11	33.95±2.01	489.29±65.01	0.0694	0.1634	0.5051	35.66±5.28

Table 4.3 presents the thicknesses, micro-mechanical properties, and other relevant characteristics of all the coatings investigated in this study.

The H/E and H^3/E^2 ratios were calculated from each coating's hardness (H) and elastic modulus (E). Research suggests that a higher H/E ratio, which is related to the elastic strain, usually results in a reduction in wear (Leyland and Matthews, 2000). The H^3/E^2 ratio can be used as a measure of resistance to plastic deformation and as a way to correlate the mechanical properties to wear resistance of hard coatings (Tsui et al., 1995). A higher H^3/E^2 ratio means a higher ability of a coating to dissipate energy due to plastic deformation during loading. In this regard, the higher H/E and H^3/E^2 values of Tool A_c and Tool $D_{TAN5050}$ indicate better performance, which is also confirmed by machining studies, where these two coated tools have performed better than other tools (Figure 4.2). However, it has been seen that an optimized rather than maximized combination of H and E sometimes works better depending on the application (Chowdhury et al., 2017); Tool A_c indicates better performance, although it has slightly lower values compared to Tool $D_{TAN5050}$. The highest

H/E and H^3/E^2 values for Tool $D_{TAN2773}$ are because of its considerably low elastic modulus compared to the other coatings, which is actually not desirable. Researchers (Spurr and Newcombe, 1957; Lancaster, 1963) have found that wear resistance increases with elastic modulus. Such a low E value indicates that the coating will start deforming much earlier than the other coatings (Leyland and Matthews, 2000; Beake and Fox-Rabinovich, 2014). The machining results (Figure 4.2) & SEM results (Figure 4.3) confirm this. The inferior performance of Tool C_c and Tool D_c can be attributed to a lower H/E ratio, which can actually be used as a measure of brittleness, and a higher plasticity index, which is the ratio between the plastic work done during indentation and the total plastic and elastic work done during indentation (Beake et al., 2009).

The lower H, H/E ratio and higher plasticity index indicates that the coatings are softer and prone to early plastic deformation compared to Tools A_c and Tool $D_{TAN5050}$, which can be useful in many other cutting conditions (Chowdhury et al., 2021), but for the specific application studied in this current investigation, coatings with comparatively higher hardness, H/E ratio and lower plasticity index are showing better performances.

Figure 4.5 presents AFM images of the surface morphologies of the coatings showing the tops of the typical columnar grains. Although Table 4.2 shows that Tool D_c and Tool $D_{TAN5050}$ had similar compositions, both machining and micro-mechanical studies (Figure 4.2 and Table 4.3) show that they are quite different. This difference can be attributed to differences in the coating structure seen in Figure 4.5. Tool D_c has a comparatively larger column size than Tool $D_{TAN5050}$, which has finer and denser columnar structure. Research

has shown that, despite having similar compositions, column size, distribution and inter-column spacings can have a huge impact on coating properties and performances (Luo et al., 2004, 2011; Fan et al., 2015; Ganvir et al., 2018; Qiu et al., 2021)
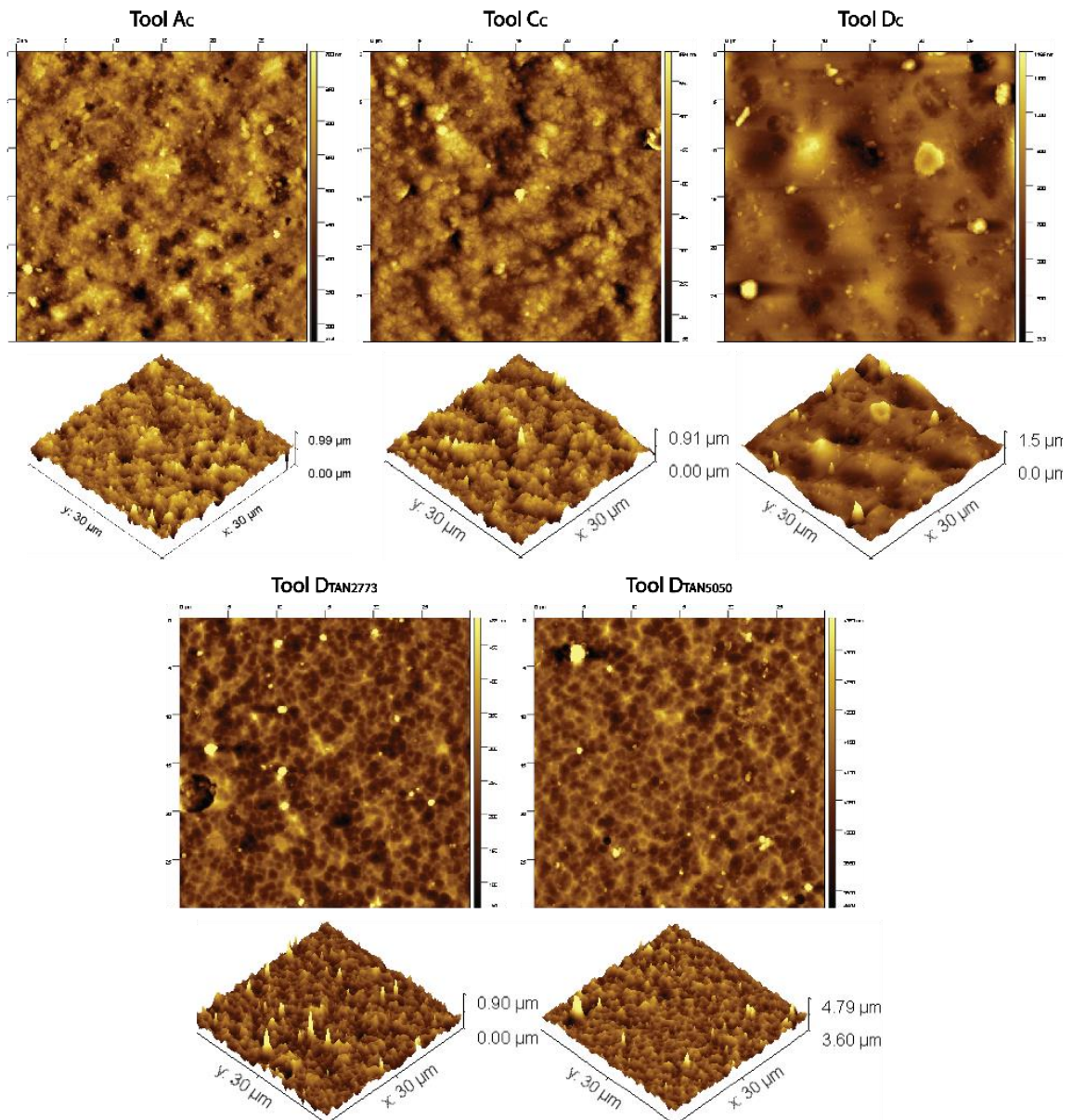
Figure 4.5 *AFM images that are showing coating surface topography and structure in 2D and 3D view of commercial and in-house coatings.*

Table 4.4 *Tool coating nomenclator and composition*

Tool	L_{c1} (N)	L_{c2} (N)
Tool A$_c$	38.5	51.01
Tool C$_c$	0.76	41.20
Tool D$_c$	11.75	47.56
Tool D$_{TAN2773}$	0.61	41.45
Tool D$_{TAN5050}$	42.28	47.7

Figure 4.6 shows the scratch test results for all coatings, and Table 4.4 shows the critical load for failure data. L_{c1} represents the first visible failure or cohesive failure, and L_{c2} represents the ultimate failure or substrate exposure due to adhesive failure. Failure is early in the case of Tool C$_c$ with lower H/E and H^3/E^2 values and Tool D$_{TAN2773}$ with unusually low E value. Although L_{c2} is comparable to Tool D$_{TAN5050}$, Tool D$_c$ starts to show signs of deformation quite early (L_{c1}). Higher plasticity index and bigger column sizes (Figure 4.5) of Tool D$_c$ indicate its softer nature and tendency to deform plastically, and a lower H/E ratio indicates lower wear resistance, leading to poor performance during the machining studies.

The initial failures were observed for Tool A$_c$ and Tool D$_{TAN5050}$ at loads 38.5N and 42.28N, respectively, which are higher than all other coatings. Tool A$_c$ and Tool D$_{TAN5050}$ also show high ultimate failure loads, L_{c2}, meaning that both coated tools can withstand higher loads before the failure occurs. This is also evident from the SEM progressive wear (Figure 4.3), which shows delayed wear and less notching compared to all coated tools. Thus, a combination of higher H/E and H^3/E^2 values (Table 4.3), which indicate higher wear

resistance, and better load-bearing capabilities, and higher L_{c1} and L_{c2} values, which indicate delayed failure, of Tool A_c and Tool $D_{TAN5050}$ help explain why Tool A_c and Tool $D_{TAN5050}$ outperform the other coated tools during actual machining studies (Figure 4.1 & Figure 4.2).
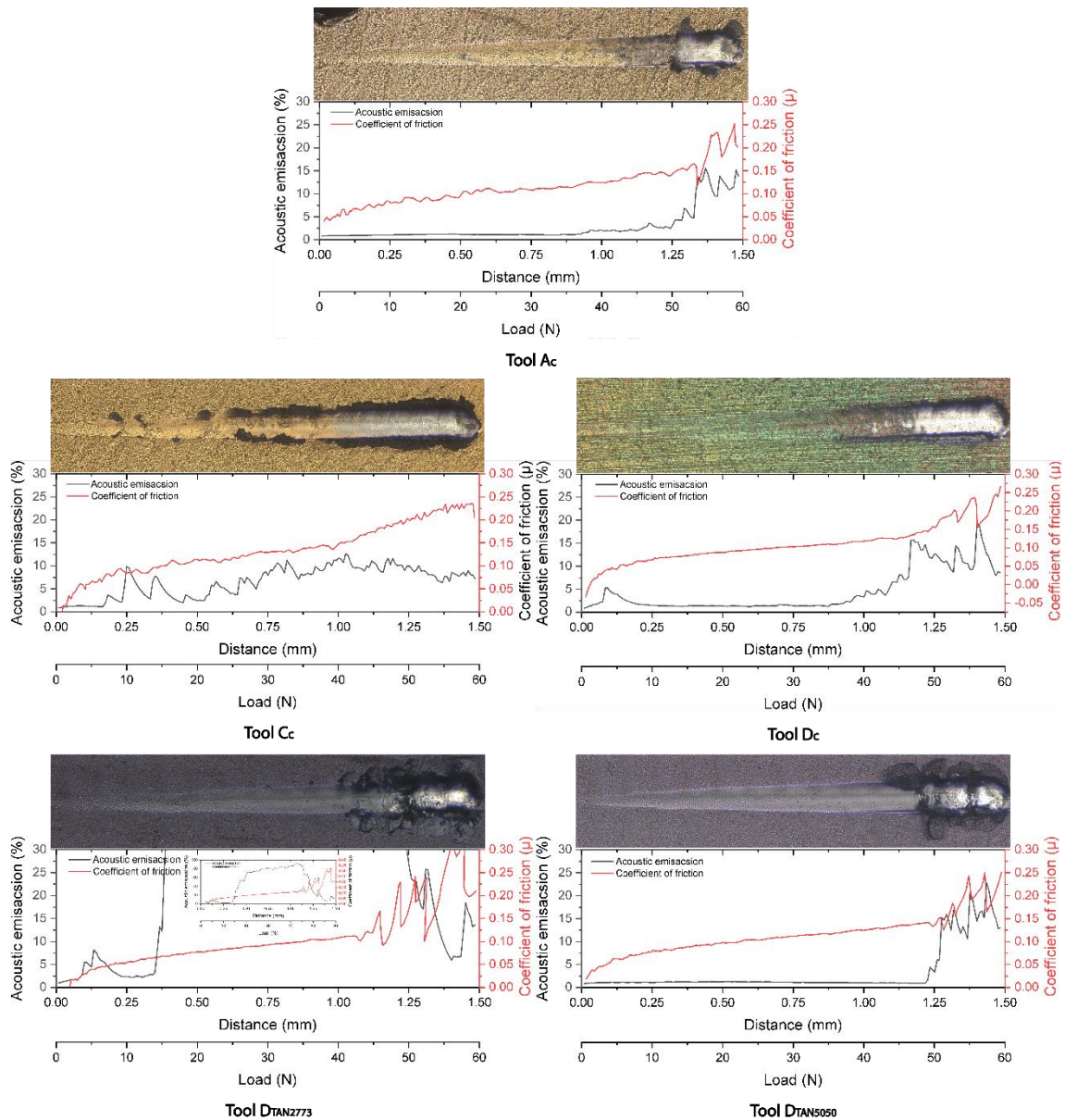
Figure 4.6 *Scratch test images of coatings with acoustic emission and coefficient of friction in relation to scratch length and load.*

120

4.4 Conclusions

The performance of coated CERMET tools during dry high-speed machining of stainless steel 304 is assessed. Designing a coating that can perform under such challenging machining conditions requires comparative and progressively in-depth studies to understand the impact of wear mechanisms and behaviour of a coating and its elements on cutting tool performance. Among all the commercial and in-house coatings, Tool A_c had the longest tool life, and Tool $_{DTAN5050}$ was found to have the best performing coating of the Tool D group.

Tool C_c shows no improvement in terms of wear resistance over the uncoated Tool C. Tool D_c shows a slight improvement in terms of tool life over uncoated Tool D, which shows early wearing from the DOC notch, which develops into a large valley. Tool $D_{TAN2773}$ reduces notch wear compared to Tool D_c, and Tool $D_{TAN5050}$ improves this further by delaying wear in the DOC notch valley by 666m. In the Tool D group, the Tool $D_{TAN5050}$ performed best.

All of the coatings studied form tribofilms based on their composition (TiO_2, Al_2O_3, Cr_2O_3). The TiO_2 tribofilms have high friction characteristics and shears easily from the interface. This may be a reason for the rapid wear of the TiN coating (Tool C_c). The addition of Al is beneficial to the coating by improving thermal stability and wear performance. However, a slight decrease in performance was found with excessive amounts of aluminum. The aluminum oxide formed is brittle in nature and can cause coating failure. Friction wear, oxidation, adhesive wear and brittle failure were the main wear mechanisms of

121

TiAlN/AlTiN (Tool $D_{TAN5050}$). It can be said that the optimized Al material can improve the wear resistance. Coating TiAlCrN (Tool A_c) shows superior oxidation resistance of the coating at the initial stage of machining due to the formation of stable Cr_2O_3 and/or dense $(Al, Cr)_2O_3$ mixed oxide tribofilms, which provides thermal barrier properties at high cutting temperature. This improved wear resistance significantly increased the life of the tool in the initial stages.

The micro-mechanical testing and AFM studies showed that relatively higher H/E and H^3/E^2 values along with finer and denser column structure of the coatings contribute to better wear resistance of the coatings. Also, test results suggested that coatings with a lower plasticity index performed better for this application. Scratch tests also indicated that deformation is delayed in such coatings, resulting in improved tool life with enhanced wear protection.

It was observed that the micro-mechanical properties of the coatings changes with coating composition and deposition parameters. Further studies can be performed by replacing or adding various elements to the existing coating composition and by optimizing the PVD coating deposition parameters to enhance wear performance and extend tool life.

4.5   Acknowledgments

4.6 References

Beake, B. D. et al. (2009) 'Coating optimisation for high speed machining with advanced nanomechanical test methods', Surface and Coatings Technology, 203(13), pp. 1919–1925. doi: 10.1016/j.surfcoat.2009.01.025.

Beake, B. D. and Fox-Rabinovich, G. S. (2014) 'Progress in high temperature nanomechanical testing of coatings for optimising their performance in high speed machining', Surface and Coatings Technology, 255, pp. 102–111. doi: 10.1016/j.surfcoat.2014.02.062.

Breidenstein, B. and Denkena, B. (2013) 'Significance of residual stress in PVD-coated carbide cutting tools', CIRP Annals - Manufacturing Technology, 62(1), pp. 67–70. doi: 10.1016/j.cirp.2013.03.101.

Chen, X., Xu, J. and Xiao, Q. (2015) 'Cutting performance and wear characteristics of Ti(C,N)-based cermet tool in machining hardened steel', International Journal of Refractory Metals and Hard Materials, 52, pp. 143–150. doi: 10.1016/j.ijrmhm.2015.06.006.

Chowdhury, M. S. I. et al. (2017) 'Wear behaviour of coated carbide tools during machining of Ti6Al4V aerospace alloy associated with strong built up edge formation', Surface and Coatings Technology, 313, pp. 319–327. doi: 10.1016/j.surfcoat.2017.01.115.

Chowdhury, M. S. I. et al. (2021) 'Investigation of the Wear Performance of TiB2 Coated Cutting Tools during the Machining of Ti6Al4V Alloy', Materials, 14(11), p. 2799. doi: 10.3390/ma14112799.

D'Errico, G. ., Calzavarini, R. and Vicenzi, B. (1998) 'Influences of PVD coatings on cermet tool life in continuous and interrupted turning', Journal of Materials Processing Technology, 78(1–3), pp. 53–58. doi: 10.1016/S0924-0136(97)00463-9.

Dobrzański, L. A. and Gołombek, K. (2005) 'Structure and properties of the cutting tools made from cemented carbides and cermets with the TiN + mono-, gradient- or multi(Ti, Al, Si)N + TiN nanocrystalline coatings', Journal of Materials Processing Technology, 164–165, pp. 805–815. doi: 10.1016/j.jmatprotec.2005.02.072.

Dolinšek, S. and Soković, M. (1998) 'Influence of TiN (PVD) coating on the tool on the identification parameters in turning', Journal of Materials Processing Technology, 78(1–3), pp. 67–74. doi: 10.1016/S0924-0136(97)00465-2.

Fan, Z. et al. (2015) 'Influence of columnar grain microstructure on thermal shock resistance of laser re-melted ZrO2-7wt.% Y2O3 coatings and their failure mechanism', Surface and Coatings Technology, 277, pp. 188–196. doi: 10.1016/j.surfcoat.2015.07.036.

Ganvir, A. et al. (2018) 'Tailoring columnar microstructure of axial suspension plasma sprayed TBCs for superior thermal shock performance', Materials and Design, 144, pp. 192–208. doi: 10.1016/j.matdes.2018.02.011.

Ghani, J. A., Choudhury, I. A. and Masjuki, H. H. (2004) 'Wear mechanism of TiN coated carbide and uncoated cermets tools at high cutting speed applications', Journal of Materials Processing Technology, 153–154(1–3), pp. 1067–1073. doi: 10.1016/j.jmatprotec.2004.04.352.

Jianxin, D. et al. (2012) 'Erosion wear of CrN , TiN , CrAlN , and TiAlN PVD nitride coatings', Int. Journal of Refractory Metals and Hard Materials, 35, pp. 10–16. doi: 10.1016/j.ijrmhm.2012.03.002.

Kaladhar, M. (2019) 'Evaluation of hard coating materials performance on machinability issues and material removal rate during turning operations', Measurement: Journal of the International Measurement Confederation, 135, pp. 493–502. doi: 10.1016/j.measurement.2018.11.066.

Kalss, W. et al. (2006) 'Modern coatings in high performance cutting applications', International Journal of Refractory Metals & Hard Materials, 24, pp. 399–404. doi: 10.1016/j.ijrmhm.2005.11.005.

Kulkarni, A., Sargade, V. and More, C. (2018) 'Machinability Investigation of AISI 304 Austenitic Stainless Steels using Multilayer AlTiN/TiAlN Coated Carbide Inserts', Procedia Manufacturing, 20, pp. 548–553. doi: 10.1016/j.promfg.2018.02.082.

Lancaster, J. K. (1963) 'The relationship between the wear of carbon brush materials and their elastic moduli', British Journal of Applied Physics, 14(8), pp. 497–505. doi: 10.1088/0508-3443/14/8/311.

Leyland, A. and Matthews, A. (2000) 'On the significance of the H/E ratio in wear control: A nanocomposite coating approach to optimised tribological behaviour', Wear, 246(1–2), pp. 1–11. doi: 10.1016/S0043-1648(00)00488-9.

Li, T. et al. (2017) 'Structures and properties of TiAlCrN coatings deposited on Ti(C,N)-based cermets with various WC contents', International Journal of Refractory Metals and Hard Materials, 69(April), pp. 247–253. doi: 10.1016/j.ijrmhm.2017.08.020.

Luo, Q. et al. (2004) 'Transmission electron microscopy and x-ray diffraction investigation of the microstructure of nanoscale multilayer TiAlN/VN grown by unbalanced magnetron deposition', Journal of Materials Research, 19(4), pp. 1093–1104. doi: 10.1557/JMR.2004.0143.

Luo, Q. et al. (2011) 'Structure characterization and tribological study of magnetron sputtered nanocomposite nc-TiAlV(N,C)/a-C coatings', Journal of Materials Chemistry, 21(26), pp. 9746–9756. doi: 10.1039/c1jm10707k.

Noordin, M. Y. et al. (2001) 'Performance evaluation of cemented carbide tools in turning AISI 1010 steel', Journal of Materials Processing Technology, 116(1), pp. 16–21. doi: 10.1016/S0924-0136(01)00838-X.

Noordin, M. Y., Venkatesh, V. C. and Sharif, S. (2007) 'Dry turning of tempered martensitic stainless tool steel using coated cermet and coated carbide tools', Journal of Materials Processing Technology, 185(1–3), pp. 83–90. doi: 10.1016/j.jmatprotec.2006.03.137.

Ortner, H. M., Ettmayer, P. and Kolaska, H. (2014) 'The history of the technological progress of hardmetals', International Journal of Refractory Metals and Hard Materials, 44, pp. 148–159. doi: 10.1016/j.ijrmhm.2013.07.014.

Patel, U. et al. (2020) 'Dataset and methodology on identification and correlation of secondary carbides with microstructure, wear mechanism, and tool performance for different CERMET grades during high-speed dry finish turning of AISI 304 stainless steel', Data in Brief, p. 105753. doi: https://doi.org/10.1016/j.dib.2020.105753.

Patel, U. S. et al. (2016) 'Investigation of Various Properties for Zirconium Oxide Films Synthesized by Sputtering', Procedia Technology, 23, pp. 336–343. doi: 10.1016/j.protcy.2016.03.035.

Patel, U. S. et al. (2020) 'Influence of secondary carbides on microstructure, wear mechanism, and tool performance for different cermet grades during high-speed dry finish turning of AISI 304 stainless steel', Wear, 452–453, p. 203285. doi: 10.1016/j.wear.2020.203285.

Peng, Y., Miao, H. and Peng, Z. (2013) 'Development of TiCN-based cermets: Mechanical properties and wear mechanism', International Journal of Refractory Metals and Hard Materials, 39, pp. 78–89. doi: 10.1016/j.ijrmhm.2012.07.001.

Qiu, S. Y. et al. (2021) 'Microstructure Dependence of Effective Thermal Conductivity of EB-PVD TBCs', Materials, 14(8), pp. 1–17. doi: 10.3390/ma14081838.

Sarjana, S. S. et al. (2020a) 'Study on cutting performance of cermet tool in turning of hardened alloy steel', International Journal of Refractory Metals and Hard Materials, 91(January), pp. 5–8. doi: 10.1016/j.ijrmhm.2020.105255.

Sarjana, S. S. et al. (2020b) 'Study on cutting performance of cermet tool in turning of hardened alloy steel', International Journal of Refractory Metals and Hard Materials, 91(January), p. 105255. doi: 10.1016/j.ijrmhm.2020.105255.

Soković, M. and Bahor, M. (1998) 'On the inter-relationships of some machinability parameters in finish machining with cermet TiN (PVD) coated tools', Journal of Materials Processing Technology, 78(1–3), pp. 163–170. doi: 10.1016/S0924-0136(97)00479-2.

Spurr, R. and Newcombe, T. (1957) 'The friction and wear of various materials sliding against unlubricated surfaces of different types and degrees of roughness, in: Proceedings of the Conference on Lubrication and Wear Institution of Mechanical Engineers', in. London, UK: Inst. Mech. Eng., p. 269.

Standardization, F. O. R. (2006) 'IS0 3685:Tool-life testing with single-point turning tools'.

Stanford, M. et al. (2009) 'Investigation into the use of gaseous and liquid nitrogen as a cutting fluid when turning BS 970-80A15 (En32b) plain carbon steel using WC-Co uncoated tooling', Journal of Materials Processing Technology, 209(2), pp. 961–972. doi: 10.1016/j.jmatprotec.2008.03.003.

Suresh, R., Basavarajappa, S. and Gaitonde, V. N. (2015) 'Experimental studies on the performance of multilayer coated carbide tool in hard turning of high strength low alloy steel', Journal of Materials Research, 30(20), pp. 3056–3064. doi: 10.1557/jmr.2015.236.

Tiwari, P. K. et al. (2020) 'Performance evaluation of coated cermet insert in hard turning', Materials Today: Proceedings, (xxxx). doi: 10.1016/j.matpr.2020.02.424.

Tsui, T. Y. et al. (1995) 'Nanoindentation and nanoscratching of hard carbon coatings for magnetic disks', in Materials Research Society Symposium - Proceedings. MRS Proc, pp. 447–452. doi: 10.1557/proc-383-447.

Vandierendonck, K. and Van Stappen, M. (1997) 'Study of the performance of PVD and PCVD coated cermets for different cutting applications', Surface and Coatings Technology, 97(1–3), pp. 218–223. doi: 10.1016/S0257-8972(97)00552-5.

Wolfe, G. J., Petrosky, C. J. and Quinto, D. T. (1986) 'The role of hard coatings in carbide milling tools', Journal of Vacuum Science & Technology A, 2747(April 1986), pp. 2747–2754. doi: 10.1116/1.573673.

Yamamoto, K. et al. (2003) 'Properties of (Ti , Cr , Al) N coatings with high Al content deposited by new plasma enhanced arc-cathode', 175, pp. 620–626. doi: 10.1016/S0257-8972.

Zhang, Y. et al. (2017) 'Experimental study on cutting performance of microwave sintered Ti(C, N)/Al2O3 cermet tool in the dry machining of hardened steel', International Journal

of Advanced Manufacturing Technology, 91(9–12), pp. 3933–3941. doi: 10.1007/s00170-017-0062-2.

Zou, B. et al. (2014) 'Study of a hot-pressed sintering preparation of Ti(C7N3)-based composite cermets materials and their performance as cutting tools', Journal of Alloys and Compounds, 611, pp. 363–371. doi: 10.1016/j.jallcom.2014.05.150.

Zou, B. et al. (2015) 'Tool damage and machined-surface quality using hot-pressed sintering Ti(C7N3)/WC/TaC cermet cutting inserts for high-speed turning stainless steels', International Journal of Advanced Manufacturing Technology, 79(1–4), pp. 197–210. doi: 10.1007/s00170-015-6823-x.

Chapter 5 : In-house Coating Development and Comparison of Performance

Complete citation:

U. Patel, B Bose, S. Rawal, A.F.M. Arif, S. Veldhuis, Development of various advanced PVD coatings to enhance the machining performance of CERMET tools for high-speed dry finish turning of AISI 304 stainless steel, Submitted to the "International Journal of Refractory Metals and Hard Materials" journal, September 2021.

Copyright:

Author's Contributions:

Uttkarsh Patel	Conceptualization, Investigation, Formal analysis, Validation, Visualization, Methodology, Data Curation, Writing - Original Draft
Bipasha Bose	Methodology, Validation, Writing - Review & Editing
Sushant Rawal	Conceptualization, Methodology, Validation, Supervision, Writing - Review & Editing
Abul Fazal M Arif	Conceptualization, Methodology, Project administration, Writing - Review & Editing
Stephen Veldhuis	Resources, Project administration, Funding acquisition, Supervision

Abstract

This research aims to evaluate various in-house developed PVD coatings for cermet tools, specifically for high-speed dry turning of austenitic stainless steel (AISI 304). In the present study, various combinations of coating elements such as Ti, Al, Cr, Si, Y, and Ta were selected, deposited and developed as a PVD coating on cermet cutting tools, and evaluated based on tool life by turning test. The study of tool and coating wear mechanism is progressively done by Scanning Electron Microscope (SEM). The micro-mechanical properties of the coatings were accessed with the help of nano indentations, and adhesion was assessed using scratch testing. The coating surface topography and morphology were examined using Atomic Force Microscopy (AFM) and high-resolution SEM imaging. This research indicates that the coating with the Ti element is performing better than the one without Ti. The optimized composition of Ti, Al, and Cr elements works best and better than other compositions of Ti, Al, and Ta coatings. The addition of excessive amounts of Cr and Si, Y degrades the performance. A detailed description of the coating performance based on micro-mechanical, structure, and other characterization tests is discussed in detail in this research work.

Keywords: PVD; Coating; Cermet; 304 stainless steel; tool wear; dry machining; high-speed machining

5.1 Introduction

Stainless steel is widely used as a steel material that consumes 70% of all other steel. Due to greater durability, sustainability, and higher corrosion resistance, it is widely used in many commercial applications such as machinery, pharmaceutical, food manufacturing, aerospace, chemical, and many more (Trent and Wright, 2000). In all industries, the machining of stainless steel is directly or indirectly involved. AISI 304 steel is considered under the difficult-to-cut material category. The material's properties of high work hardening, low thermal conductivity, and high toughness make it difficult to cut. Due to high adhesion, diffusion, abrasive wear, and high cutting temperatures requiring coolant, it hinders tool performance, which adds to the higher machining costs (Nayak et al., 2014; Sharma, Tiwari and Dixit, 2016).

Currently, the machining industry demands and is moving towards dry and high-speed machining as it is cost-effective, causes less pollution, and less risk to the operators' health (Sreejith and Ngoi, 2000). Machining the tool at high speed adds more heat output to the chip contact area, and the dry machining process adds more material to the adhesive on the tool and adds more heat generation during the machining process. (Bapat et al., 2015). Therefore, conventional tools are not able to withstand high attrition wear and cutting temperatures. To meet the high hot hardness and toughness of the tool for such applications, cermet [Ceramic (TiC as core grain) and metal (Cobalt (Co) and Nickel (Ni) as a binder)] as a cutting tool are reported previously for such challenging dry high-speed machining conditions (U. S. Patel et al., 2020). However, substituting the cutting tool material is not

the only solution. It is still necessary to extend the tool life by adding a layer of protection with the help of coating.

The first coated cutting tools were developed in the 1960s-70s by Chemical Vapour Deposition (CVD) technology. The tools were placed in the reactor at a high temperature (1000°C), changing the property of the cutting tool and reducing the machining performance. CVD also produces high surface roughness on the coated surface and is poor at depositing on sharp edges such as the cutting edge. Therefore, CVD is less popular than Physical Vapour Deposition (PVD) coating for cutting tool applications. The PVD coating was developed in the 1980s and deposited on carbide cutting tools (Wolfe, Petrosky and Quinto, 1986). The PVD coating can be deposited at a low temperature of 500°C. The PVD coating also provides good coverage for a coating with state-of-the-art and high compressive residual stress. Therefore, PVD coatings are more popular for depositing coatings for cutting tools in the machining industries.

Titanium (Ti)-based on the first and second generation of PVD coatings are restricted to special cutting conditions (limited cutting speed). The researcher developed more coatings with binary ternary and more complex Ti-based PVD coating to enhance performance by combining different properties of different coatings and elements, i.e. TiAlCN, TiAlNbN, TiAlCrN, TiN/CrN, TiN/TiAlN, and many others. Arndt M et al. 2003 developed an AlTiN coating which showed that coating with Al content could provide better wear protection than coating without aluminium due to its low thermal conductivity and oxidation resistance at elevated cutting temperatures (Arndt and Kacsich, 2003). Sert H et al. conducted a study in 2005 on the wear of TiAlN PVD coating and TiN CVD coating and

cermet tool during machining of AISI 5140 steel (Sert et al., 2005). The results show that

the coated cermet cutting tool was not promising. The best cutting speed observed with

TiAlN coating was 200m/min. With PVD coating technology, Andrino et al. (2006)

developed various ternary and complex coatings (AlCrN, AlCrNbN; fg-AlTiN and nc-

AlTiN) on carbide end mills for machining stainless steel 316L. nc-AlTiN coated cutting

tool shows better performance than other coatings (Endrino, Fox-Rabinovich and Gey,

2006). Fox GS et al. 2009 shows that Al-rich TiAlN and CrAlN series coatings showed

favourable results for cutting hard materials (Fox-Rabinovich et al., 2009). Kladhar et al.

2012 reported that TiAlN-TiN coated carbide cutting tools showed superior performance

and improved surface roughness after TiCN-TiN coating while machining stainless steel.

Limited work is also reported for high-speed machining of stainless steel (Kaladhar,

Venkata Subbaiah and Srinivasa Rao, 2012). Poomari A et al. 2012 conducted a machining

study with AISI 4340 steel using cermet coated TiAlN with cryogenic treatment. The result

shows that the cryogenically treated TiAlN coated cermet tool outperforms the uncoated

and untreated coated cermet cutting tool (Poomari et al., 2012). Li T. et al. 2017 studied the

structure and properties of TiAlCrN coating on the cermet tool with various WC contents

(Li et al., 2017). The grain size of the coating decreases with increasing the WC, and the

coated tool worsens when WC crosses more than 10 wt%. Yanga W et al. 2017 studied

PVD-coated TiAlN and TiAlN/CrAlN cermet tools (Yang et al., 2017). The structure of

the coating was columnar and blocked grain. The test was performed on 9CrSi2Mn steel

with turning operation. The TiAlN/CrAlN coating results show high flank wear, and TiAlN

coating shows high oxidation wear with low abrasive wear. Tiwari P.K. and others in 2020

investigated the performance of multi-layer coated TiN/TiCN/TiN cermet tool under machining of AISI 4340 steel and found surface finish within 1.6µm (Tiwari et al., 2020). TiAlN coating is the most widely used PVD coating for machining application due to its high hardness (33GPa) and low friction. The coating also shows good oxidation resistance at 800°C and abrasion resistance at elevated cutting temperatures (Bouzakis et al., 2013; Du et al., 2014). The researchers are also adding Cr to TiAlN coating to increase the solubility range of AlN in complex nitrides to develop more Al-Cr bonds, to increase the coating ability to provide high hot hardness and oxidation resistance property demanded in machining (Santana et al., 2004; Fox-Rabinovich et al., 2009).

Some research shows good performance of certain coatings for applications with specific conditions (Noordin, Venkatesh and Sharif, 2007; Das et al., 2016; Touggui et al., 2021). However, the results are not comparable because not all coatings have been studied simultaneously under the same conditions from coating development to final application, such as the same machining conditions. The objective of this research work is to develop various in-house PVD coating for cermet tools under the same specification with a different elemental composition specifically for high-speed dry turning of austenitic stainless steel (AISI 304). The PVD coated cermet tools were tested, and the durability of the coatings was evaluated based on the tool life, wear mechanism, and micro-mechanical properties of the PVD coatings.

5.2   Experimental Procedure

5.2.1   Coating Design and Deposition

The in-house coating development was conducted based on the findings of the uncoated study and the desired requirement for the current application. It was reported that Titanium (Ti) is widely used as PVD coating for machining application due to its high chemical inertness, excellent adhesion, wear resistance at elevated temperature and hard coating surface to reduce wear (Zhang and Zhu, 1993). It was also found that a cermet tool that contained tantalum (Ta) gives a low amount of wear (Yu, Huang and Xu, 2015; U. S. Patel et al., 2020). Therefore, the integration of Ta into the coating should help improve the coating performance. It is reported that the addition of aluminum (Al) will substitute Ti atoms with smaller Al atoms, reducing the lattice parameter of the coating structure, leading to the betterment of the coatings (Inspektor and Salvador, 2014). The adhesion of the coating to the cermet tool is one of the important factors. The addition of chromium (Cr) to the coating may reduce stress and improve adhesion, resulting in improved tribological properties (Willmann et al., 2007). Cr and Al form oxides at high temperatures that increase thermal stability, oxidation resistance, and mechanical strength, making the coating self-adaptive (Warcholinski and Gilewicz, 2011). Silicon (Si) and yttrium (Y) can be added to coatings to improve their grain refinement and prevent grain coarsening (Fox-Rabinovich et al., 2010). These scientific findings reported in the literature and recent work published by the authors were the main criteria to design and develop various combinations of in-

house coatings with Ti, Al, Cr, Ta, Si, and Y as the main elements. The performance was investigated further in detail for the current machining application.

5.2.2 Machining Studies

Machining studies were performed with the metal cutting of AISI 304 steel (125 BHN hardness) using the turning process on a CNC OKUMA Crown L1060 lathe. Machining tests were performed at a feed rate of 0.15 mm/rev, a cut depth of 0.4 mm, and a 240 m/min cutting speed. The mechanical and chemical composition of the workpiece material is given in Table 5.1. The microstructure, geometry, designation, and hardness of the uncoated cermet tool have been previously investigated and described by Patel et al (U. Patel et al., 2020; U. S. Patel et al., 2020).

Table 5.1 *Chemical composition and mechanical properties of AISI 304 stainless steel*

Chemical composition (%)								
C	Si	Mn	P	S	Cr	Ni	N	Balance
0.08	0.75	2.0_{max}	0.045_{max}	0.03_{max}	18-20	8-10.5	0.10_{max}	Fe(iron)
Mechanical properties								
Yield Strength	Tensile Strength	Elongation	Modulus of Elasticity		Shear Modulus	Hardness		Poisson's Ratio
215 MPa	505 MPa	70%	193-200 GPa		86 GPa	123 HB		0.29
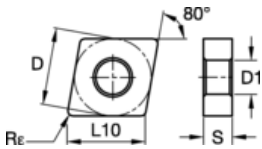
The composition of the cermet tool is presented in Table 5.2. The various PVD coating composition combinations were developed and deposited on cermet cutting tools (inserts) and compared with each other in terms of machining performance and wear resistance. The

coated tools are listed in Table 5.3, along with the equipment nomenclature and coating composition concentration.

Table 5.2 Elemental concentration (wt.%) of uncoated cermet tools By EDS (U. S. Patel et al., 2020).

	Ti	W	Co	Ni	Nb	V	C	N	Mo	Ta	Others
Tool D	38.2	20.1	7.3	7.0	5.1		14.8	3.7			Balance

Table 5.3 Type and geometry of cutting tools, and coatings nomenclature and composition

Uncoated Tool	Coating Target	Coating Composition (wt%) after deposition (EDS)							Coated Tool Nomenclator	Measured edge radius of coated cutting tool (µm)	Tool geometry of the inserts CNMG 120408 / CNMG 432
		Ti	Al	Cr	Ta	Si	Y	N			
Tool D	$Al_{70}Cr_{30}$		38	36				26	Tool D_{AlCrN}	53.35±0.58	
	$Ti_{25}Al_{65}Cr_{10}$	27	34	12				26	Tool $D_{TiAlCrN}$	57.27±1.32	
	$Ti_{20}Al_{55}Cr_{20}Si_3Y_2$	20	27	22		1	4	26	Tool $D_{TiAlCrSiYN}$	55.78±2.19	
	$Ti_{35}Al_{57}Ta_8$	34	26		15			24	Tool $D_{TiAlTaN}$	57.96±1.61	
	Cr_{100} & $Ti_{35}Al_{57}Ta_8$	17	13	43	7			22	Tool $D_{(Cr-TiAlTa)N}$	53.39±1.02	

D= 12.70mm
L10= 12.90mm
Rε=0.8mm
D1=5.16mm
S=4.76mm

The cutting tool wears changes (wear volume) were recorded and tracked with the help of a 3D surface measurement system (Alcona Infinite Focus G5, Alicona Manufacturing Inc., Bartlett, IL, USA). The 3D tool scanned model was also used to measure the change of the cutting-edge radius after the coating deposition, as shown in Figure 5.1.

1. Cross section plane selection

2. 2D profile generation for further measurement

Rake angle measurement

Cutting edge radius measuremnt

3. Cutting tool geometry measurement
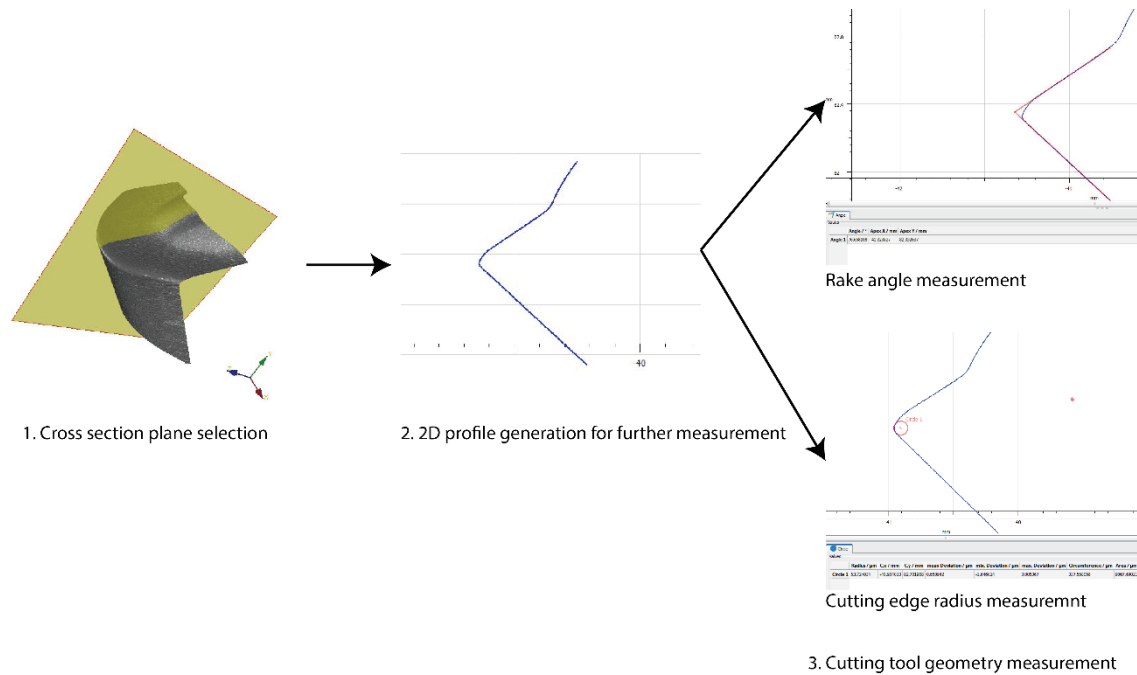
Figure 5.1 *Cutting tool geometry measurement (measurement process steps)*

The cutting force data were collected with a dynamometer (Kistler Type 9129AA), which was mounted on turret with the help of a Type 9129AD1 adapter and the tools with Type 9129AE1 holder. Data were collected with a connecting cable: Kistler Type 1687BQ02, Amplifier: Kistler Type 5167A41 using software named Kistler DynoWare Type 2825A-03, version 3.1.0.0, with sample rates of 10000 Hz. A scanning electron microscope (SEM) [JEOL 6610LV] was used to capture high magnification and resolution images to examine wear changes at fixed cutting intervals to study progressive wear. Energy-Dispersive X-ray Spectroscopy (EDS) was also performed on JEOL 6610LV to analyse and measure the composition concentration of the coating after deposition. EDS was conducted on coating deposited on flat polished cermet tool substrate to increase data accuracy at 10-12 mm working distance. Coated cutting tool life was performed according to ISO 3685:1993 standard with flank and notch wear as the measuring criterion. Flank and notch wear was

140

measured with the help of an optical microscope with XY table operated from Mitutoyo digital micrometre and KEYENCE-VHX 5000 digital microscope.

Since the dominant tool wear is the notch wear, the notch wear criterion was considered to be 300µm for the present research study, according to ISO 3685:1993 (Standardization, 2006). The formed tribofilms were characterized using X-ray photoelectron spectroscopy (XPS) (PHI Quantera II Scanning XPS Microprobe) and X-ray beam 50u12.5W15KV. The sample surface is gently cleaned to remove any contamination with the help of sputtering, and quality data is collected from tribofilms. First, with a step size of 0.8eV, the survey spectra were collected at 224eV and then, with a step size of 0.1eV, a high-resolution spectrum was collected at 26eV for the specific peak.

5.2.3 Coating Deposition (In-house) and Characterization:

All in-house coatings were deposited on CNMG 120408/CNMG 432 uncoated insert (for machining study) and SNMN 120408/SNMN 432 (for characterization) flat polished uncoated insert. All coatings except (Cr-TiAlTa)N were deposited with 99.98% purity with the help of single solid metal targets with different compositions and concentrations, as listed in Table 5.3. The coating (Cr-TiAlTa)N was deposited with two different targets of Cr and TiAlTa. The uncoated insert was mounted on the rotating table after ultrasound cleaning at a rotation speed of 4rpm. The coatings were deposited to keep the deposition pressure constant at 3.75Pa, the cathode current at 150A, and a bias voltage of -60V, while the cutting tool substrate temperature was 525°C. The deposition time was 55 min for all coatings except (Cr-TiAlTa)N, where deposition time was cut short to 28 min to achieve

comparable coating thickness. The deposition rate was kept constant to maintain a constant coating thickness.

The coating thickness was measured using a calo test instrument (BC-2 Ball Crater Device) with a 30mm diameter ball (AISI 52100m Grade 25 Chromium steel). The calo test was performed with a 1μm diamond paste to accelerate the calo crater wear rate. The crater was measured using a KEYENCE-VHX 5000 digital microscope. The thickness of all coated equipment is listed in Table 5.3. The microscopic mechanical properties of the coating were characterized with the help of Anton Paar NHT[3] nanoindenter (Anton Paar, Switzerland). The test was performed at room temperature using a diamond Berkovich indenter following the ISO14577–4 standard. The indentation contact section was kept within 1/10th of the thickness of the coating in order to avoid the substrate effect on the results. Scratch tests were performed on the flat polished coated inserts with the help of Anton Paar-RST3 Revetest® Scratch Tester (Anton Paar, Switzerland). A 100μm tip radius Rockwell diamond indenter was used to conduct the progressive load scratch test. The length of the scratch test was 3mm, with 3 scratches on each sample. The test was performed in 3 phases. The first phase runs at a very low load of 0.5N to measure the topography scan. The second phase does actual progressive load scratch starting with 0.5N until 60N over a 3 mm scratch length. The final scan was performed as a post topography scan with a 0.5N load. It helps to see the elastic recovery of the coating after the scratch test, actual penetration depth, and residual penetration depth. AFM was used to measure the surface topography and morphology of the coatings with an Anton Paar Tosca™ 400 atomic force microscope

(AFM) (Graz, Austria) using silicon probe-tapping mode. The scan was performed at a size of 30X30 μm and a resolution of 400X400 with a 0.3 line/sec rate.

5.3 Results and Discussion

In the present study, five different coatings compositions (AlCrN, TiAlCrN, TiAlCrSiYN, TiAlTaN, Cr-TiAlTaN) were used to deposit on the uncoated cermet Tool D (U. S. Patel et al., 2020). A previous study performed by the authors showed that in-house coatings performed better than commercial coatings with similar coating compositions. Hence, moving forward to develop a better performing coating, various combinations of coatings were studied. All coatings were compared for tool life performance and progressive wear mechanism. The coatings were also compared for their microstructure and micro-mechanical properties.

5.3.1 Tool Performance Analysis

Cutting tests based on the ISO 3685 standard were performed with a tool failure criterion of dominant wear (notch wear) of 300μm. Tool performance based on flank wear and notch wear for all in-house developed coatings AlCrN (Tool D_{AlCrN}), TiAlCrN (Tool $D_{TiAlCrN}$), TiAlCrSiYN (Tool $D_{TiAlCrSiYN}$), TiAlTaN (Tool $D_{TiAlTaN}$), Cr-TiAlTaN (Tool $D_{Cr-TiAlTaN}$) on Tool Ds are showed in Figure 5.2 (a) and (b).

Tool $D_{TiAlCrN}$ shows the best performance among all coated tools, followed by Tool D_{TiAlTa}. The maximum tool life of Tool $D_{TiAlCrN}$ is 3066m, and the flank and notch wear are 191μm and 306μm, respectively. Tool D_{TiAlTa} then shows a maximum tool life of 2666m with flank and notch wear of 169μm and 302μm, respectively. Tool D_{AlCrN}, Tool $D_{TiAlCrSiYN}$, Tool D_{Cr-}

TiAlTa, shows modest performance with tool life of 1333m, 1333m, 1200m, respectively. Tool D$_{TiAlCrN}$ improved tool life by approximately 318% compared to the uncoated tool (733m (U. S. Patel et al., 2020)) and 218% compared to commercially coated TiAlN tool (Tool Dc 1466m), according to the authors' previous study which is currently under review for publication. Tool D$_{TiAlTa}$ improved tool life by 264% compared to the uncoated tool and 164% compared to Tool Dc. Tool D$_{TiAlCrN}$ and Tool D$_{TiAlTa}$ show delayed tool wear in the initial machining phase in all coated tools. It is imperative to protect the cutting tool at the initial stage of machining. Better wear-resistant performance, in the beginning, can lead to higher tool life. This is proven here by a tool life test comparison of all coated tools. Coatings on Tool D$_{TiAlCrN}$ and Tool D$_{TiAlTa}$ were found to be protective against microchipping at a depth of cut (DOC).

(a)   (b)
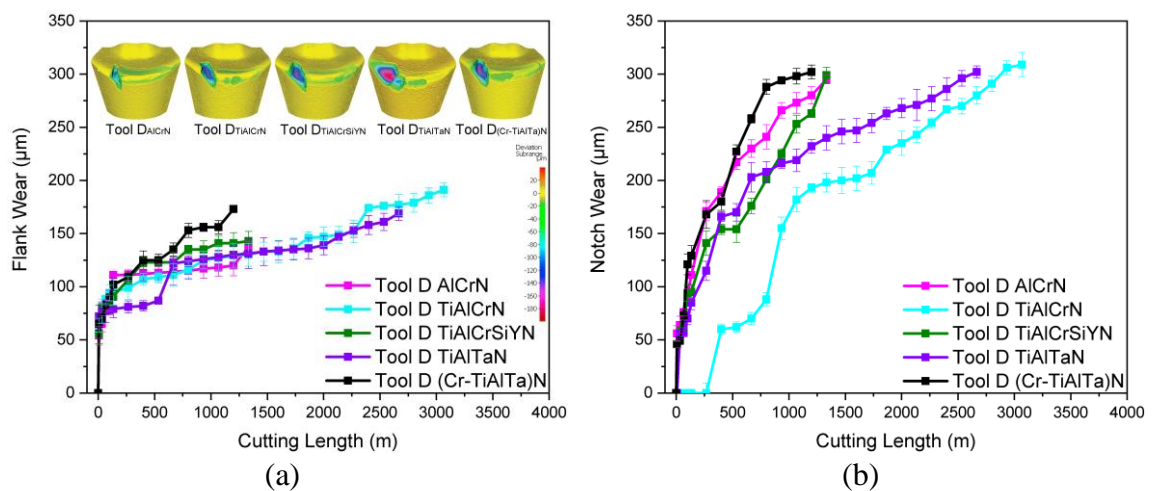
Figure 5.2 *Tool life comparison of various in-house coatings with respect to (a) flank*

wear, (b) notch wear

The coatings again protected the tools from microchipping and notching (Figure 5.2 & Figure 5.3), which were believed to have been introduced in the first pass of machining

(around 7m) for all other coated and uncoated tools, allowing machining of coating Tool D_{TiAlTa} up to 133m and machining of coating Tool $D_{TiAlCrN}$ up to 267m. The coated Tool $D_{TiAlCrN}$ and Tool D_{TiAlTa} were also observed to have less flank wear, abrasive wear, and diffusion than all the coated tools at the same stage. The rest of the coated tool performed modestly. These results indicate that variations in concentration and elements in a coating significantly affect performance and wear mechanisms.
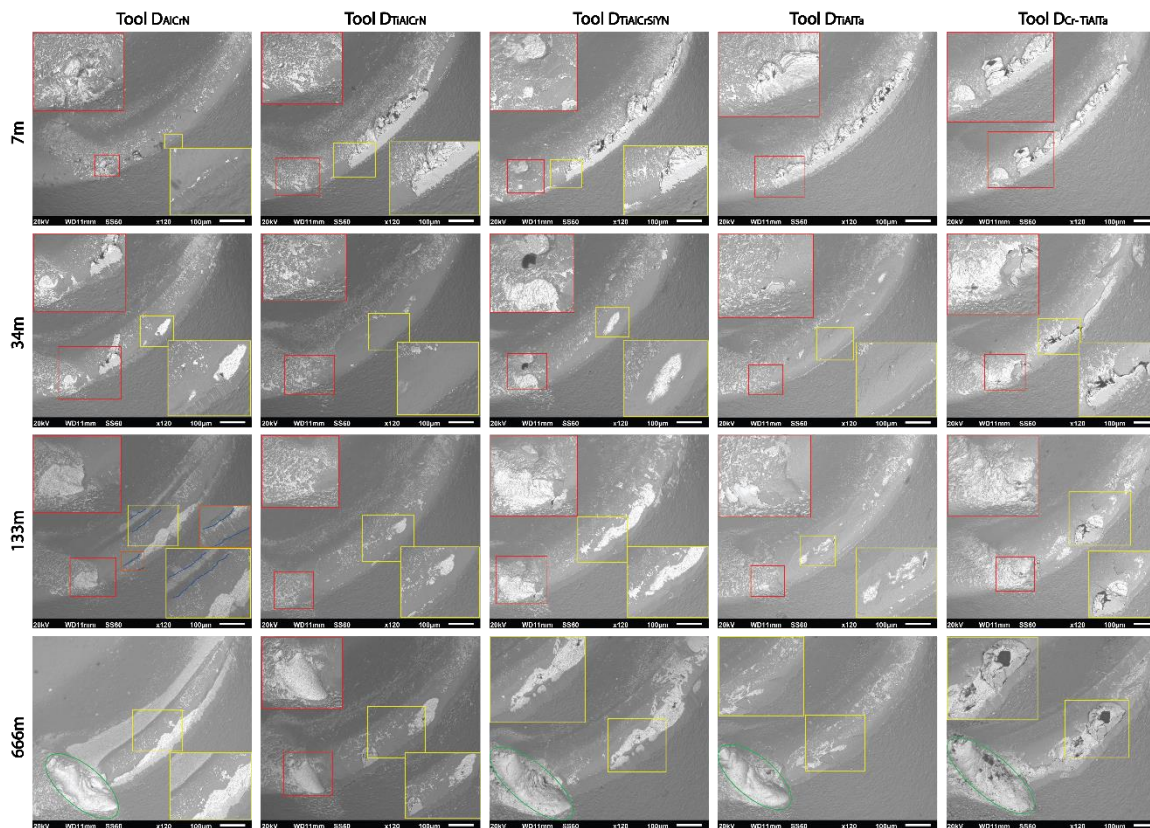
Figure 5.3 *Progressive wear mechanism study at a specific interval of cutting at 7m,*

34m, 133m, and 666m with the help of SEM images of all coated tools (Tool D_{AlCrN},

Tool $D_{TiAlCrN}$, Tool $D_{TiAlCrSiYN}$, Tool $D_{TiAlTaN}$, Tool $D_{Cr-TiAlTaN}$)

5.3.2 Wear Mechanism

Figure 5.3 shows a progressive wear study of all coated tools. Tool wear was observed for two reasons, the first by micro-chipping in the DOC region, which subsequently creates a large notch. The second reason is by adhesion to the workpiece material, which is sticking to the cutting edge (Built-up-edge, BUE) and taking off a portion of the coating away from the surface of the tool during machining, causing coating delamination and substrate exposure. Tool wear was mainly observed on the cutting edge near the DOC area. Adhesive wear was observed for all coating except Tool $D_{TiAlCrN}$ and Tool D_{TiAlTa}. A combination of diffusion and adhesive wear of the Tool D_{AlCrN} was observed. It is important to understand the mechanism of wear in order to compare the performance of the coated tools. Therefore, progressive wear was studied at fixed intervals of 7m, 34m, 133m, and 666m.

5.3.2.1 Progressive Wear Mechanism Study

At cutting length = 7m: Figure 5.3 represents the SEM images of the cutting edge of coated tools: Tool D_{AlCrN}, Tool $D_{TiAlCrN}$, Tool $D_{TiAlCrSiYN}$, Tool $D_{TiAlTaN}$, and Tool $D_{Cr-TiAlTaN}$. The Tool D_{AlCrN} shows microchipping (marked red) initiated in the DOC region while the rest of the cutting edge shows no adhesion. However, the flank wear (marked yellow) can be observed in the SEM images at the very early stage, higher than that of all other coated tools. Tool $D_{TiAlCrN}$ shows adhesion (BUE) in the middle of the cutting edge (marked yellow). There is also an indication of small adhesion in DOC. However, it does not show any chipping on the DOC or the cutting edge. The coating shows adhesion (BUE) (marked yellow) with the cutting edge of the Tool $D_{TiAlCrSiYN}$. The tool started showing microchipping and peeling off the coating on the DOC area (marked red). Tool $D_{TiAlTaN}$

shows workpiece material glued with the cutting edge (marked red). Tool $D_{TiAlTaN}$ shows no signs of microchipping in the DOC region compared to other coated cutting tools. Tool $D_{Cr-TiAlTaN}$ shows BUE on the cutting tool, microchipping was also observed in the DOC region as the material was significantly chipped in the DOC region.

At cutting length = 34m: Tool D_{AlCrN} shows the clear microchip region with the substrate clearly visible (marked red). It was also observed that a small area near the cutting-edge is peeled off by coating, and the substrate is clearly visible (marked yellow). The Tool D_{AlCrN} shows few signs of diffusion wear or rake wear, which is seen at the earliest stage compared to all coated cutting tools. It shows the removal of adhesion (BUE) from the middle of the cutting edge (marked in yellow) and the removal of the coating layer or signs of flaking. There is no sign of any chipping on the DOC or with the cutting edge. Overall, the tool is performing well as compared to the rest of the coatings. The Tool $D_{TiAlCrSiYN}$ also shows the removal of adhesion (BUE) (marked in yellow) along the cutting edge of the coating. When the glued material is removed from the coated tool, it also takes away a part of the coating and therefore causes substrate exposure (marked yellow). Tool $D_{TiAlCrSiYN}$ coating was observed to have a rapid increase in microchipping, and a large portion of the coating peeled off at the DOC region (marked red), much faster than all coatings. On the cutting edge of the Tool $D_{TiAlTaN}$ (marked red), the stuck workpiece material is now off the edge during machining. The removed glued material caused coating to peel near the cutting edge. Tool $D_{TiAlTaN}$ shows no signs of microchipping in the DOC region and performed similarly to Tool $D_{TiAlCrN}$. The Tool $D_{Cr-TiAlTaN}$ continues to show BUE on the cutting tool, with signs of chipped material removal and layer by layer coating removal in some places.

Microchipping in the DOC field is enormous and increasing in size as compared to all coated cutting tools.

At cutting length = 133m: After machining of 133m, the condition of Tool D$_{AlCrN}$ is extremely poor. The coating is removed from the entire cutting edge as a large portion of the material (marked in yellow). Microchipping (marked red) is getting bigger with loaded workpiece material inside the notch. In addition, diffusion wear is now clearly visible (marked with blue lines in yellow), which is much quicker than in all coated tools. In addition, the flank wear also increases significantly, as can be seen from the blue marked in the red box in Figure 5.3. Tool D$_{TiAlCrN}$ performs much better than all coating. The machining up to 133m Tool D$_{TiAlCrN}$ shows no microchipping at the DOC. However, it shows the first evidence of substrate exposure near the cutting edge (marked in yellow), mostly due to adhesive wear of the coating near the cutting edge. The Tool D$_{TiAlCrSiYN}$ shows the rapid growth and deepening of the microchipping at the DOC (marked red). It also begins to show substrate exposure at the cutting edge, which extends along the cutting edge (marked in yellow), which is considered poor because the tool edge is the critical part of the cutting tool for performing metal cutting. Tool D$_{TiAlTaN}$ shows substrate exposure at multiple locations on the tool's rake face (marked in yellow) due to coating flaking due to adhesion wear. It shows minor coating removal or chipping on the DOC (marked red). However, it is still not intense and does not show substrate exposure. Ultimately, the coating is still performing just as well as the Tool D$_{TiAlCrN}$. The Tool D$_{Cr-TiAlTaN}$ shows an increase in microchipping and forming of the big notch shape. The sticking and filling in this area (marked red) with the workpiece material is also observed. The remaining cutting

edge shows large spots of substrate exposure along the edge with the workpiece material on the tool edge (marked in yellow).

At cutting length = 666m: Tool D_{AlCrN} becomes completely coating-free after the machining of 666m. The coating wears off from the leading area of the cutting tool along the cutting edge. The entire cutting edge shows no coating, and the substrate is exposed. The tool also wore out the coating on the rake face of the cutting tool due to diffusion wear (marked in yellow). The microchipping of the Tool D_{AlCrN} is greatly increased, and the shape of the notch (marked green) is formed. Considering the wear of all these areas, the coated tool is now completely worn or wiped from the cutting tool in the area of cutting activity. Therefore, the Tool D_{AlCrN} is not expected to perform well because the coating is completely removed, and the tool is no longer protected. Figure 5.2 shows the evidence for the poor performance of Tool $D_{TiAlCrN}$. It shows the first evidence of chipping at the DOC (marked red) after machining 666m, while the rest of the coating tool shows signs at the beginning of the machining. Tool D_{AlCrN} performs well compared to all tools because it shows one spot of substrate exposure (marked in yellow) while the others are exposed at the entire cutting edge. Tool $D_{TiAlCrSiYN}$ observed more substrate exposure and high flank wear, followed by Tool D_{AlCrN}. The Tool $D_{TiAlCrSiYN}$ formed a large notch (marked green). Tool $D_{TiAlCrSiYN}$ is also seen to have diffusion wear as seen in the yellow mark and has worn off the coating on the rake face of the tool. Due to the high flank wear and coating peel off, the Tool $D_{TiAlCrSiYN}$ may not perform well, as is evident from Figure 5.2. Tool $D_{TiAlTaN}$ is a well-performing coated tool followed by Tool $D_{TiAlCrN}$. After machining 666m, the Tool $D_{TiAlTaN}$ shows a notch at the DOC (marked green). Furthermore, the Tool $D_{TiAlTaN}$ is still

performing well because the coated tool has very few spots with coating peel-off or substrate exposure. This is also evident from Figure 5.2 that Tool $D_{TiAlTaN}$ is a well-performed tool followed by Tool $D_{TiAlCrN}$. The condition of the Tool $D_{Cr-TiAlTaN}$ is deteriorating. As can be seen in Figure 5.3, the Tool $D_{Cr-TiAlTaN}$ forms a large notch. Tool $D_{TiAlCrSiYN}$ saw a significant amount of substrate exposure along the edge of the material sticking to the tool's edge (marked in yellow). Tool $D_{TiAlCrSiYN}$ was also observed to have higher flank wear followed by Tool D_{AlCrN}. Overall, the condition of the coated tool is deteriorating, like Tool $D_{TiAlCrSiYN}$, resulting in poor performance (Figure 5.2).

5.3.2.2 Discussion

Figure 5.4 represents the cutting force data for all the coated tools. A significant cutting force difference was observed for coatings with and without titanium (Ti) content. Tool D_{AlCrN} shows the lowest cutting force in all directions. Table 5.4 shows that the chip shear angle for this tool is also the highest among all other coated tools. Based on the Merchant circle diagram, the shear force vector decreases when the shear angle increases, meaning less force is needed to shear the workpiece material to form a chip. However, Tool D_{AlCrN} was not performing well during machining. Therefore, the role of the coating elements and the tribological response during the machining process needs more explanation, as discussed below.

The role of titanium (Ti) in coating development for coated cutting tools is important. M. Danek et al. found that Ti ions rapidly diffuse over the surface of the coating and forms an oxide layer (Figure 5.5) at high temperatures (Danek et al., 2017). This provides greater protection and time for other oxides (aluminium and chromium) to form, reduces wear of

the oxide layers, and protects tools by prolonging the life of the oxide tribo films. Therefore, coating tools without Ti, such as Tool D$_{AlCrN}$ are less likely to perform well for the current application.

Table 5.4 *Cutting force and related derived data concerning the tribological performance.*

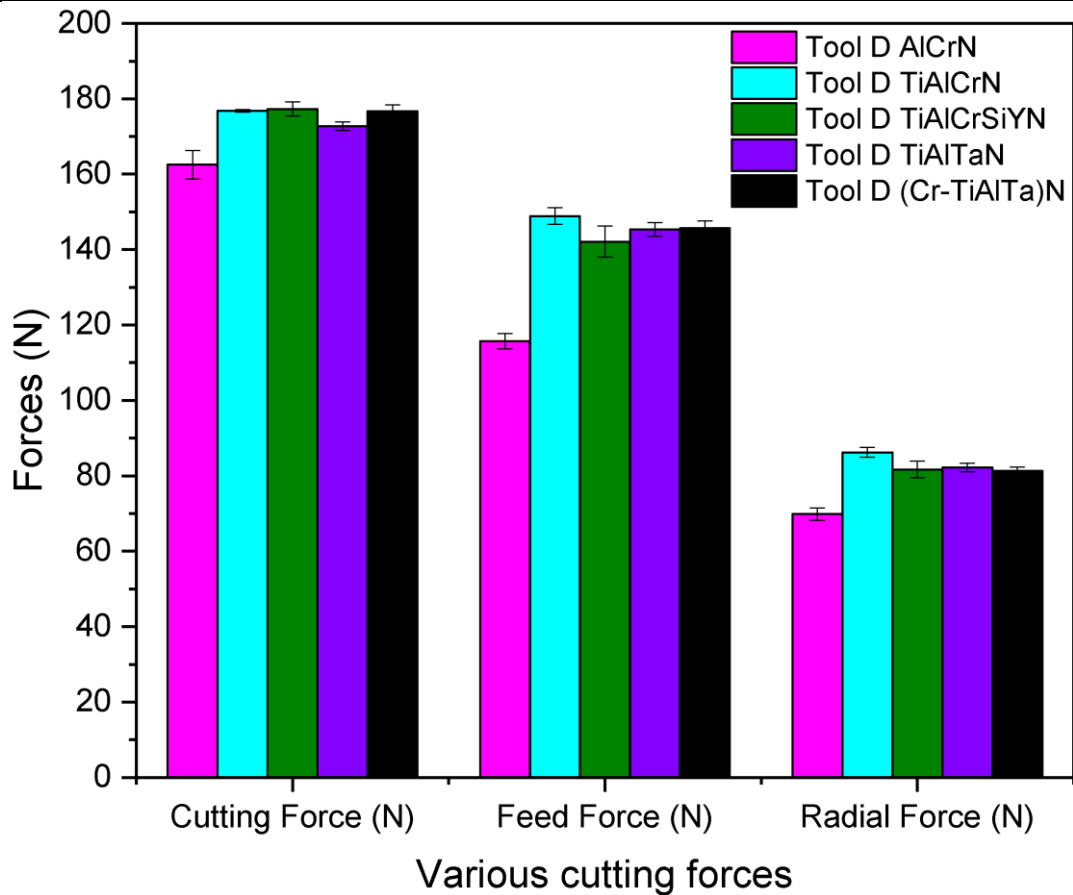| Coated tool	Edge radius (µm)	Rake Angle (α) °	Cutting force (Fp) N	Shear Angle (Φ) °	Chip velocity (V$_c$)
Tool D$_{AlCrN}$	53.34±0.58	13.13±0.15	162.47	25.12	104.18
Tool D$_{TiAlCrN}$	57.27±1.32	14.24±0.06	176.77	22.89	94.43
Tool D$_{TiAlCrSiYN}$	55.78±2.19	13.60±0.11	177.25	23.62	97.65
Tool D$_{TiAlTaN}$	57.96±1.61	13.04±0.05	172.75	22.98	95.16
Tool D$_{Cr-TiAlTaN}$	53.38±1.02	12.92±0.17	176.72	23.32	96.60

Figure 5.4 *Comparison of all cutting forces for all coated tools.*

In addition, Tool D_{AlCrN} contains a high amount of aluminium (Al) and is observed to form

an aluminium oxide tribo film (Figure 5.5) during the machining process.
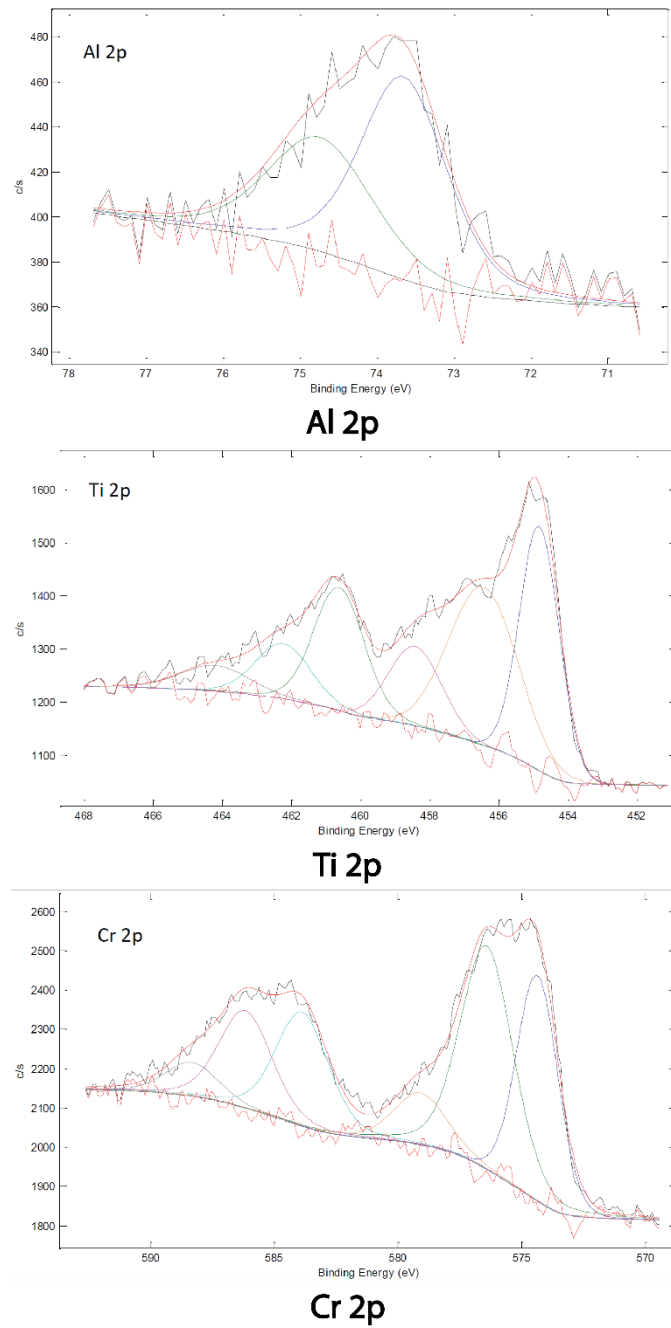

Al 2p

Ti 2p

Cr 2p

Figure 5.5 XPS data (spectra) of tribofilms from worn rake face of coated cutting tools.

The oxides of aluminium are brittle in nature and can easily fail during machining (U. S. Patel et al., 2020). So, aluminium oxides can easily break along with the chip during the chip sliding process. On the contrary, Tool $D_{TiAlCrN}$ coating contains relatively less Al than Tool D_{AlCrN} and less chromium (Cr) than all coatings. In addition, during the machining process, chromium (Cr) forms stable and dense Cr_2O_3 (Figure 5.5) which is a hard oxide tribo films. These formed oxide films protect the tools and coating from wear and oxidation, resulting in enhanced tribological properties.

Tool $D_{TiAlCrSiY}$ was found to perform poorly for current machining applications. The Tool $D_{TiAlCrSiYN}$ was observed to have high coating peeling during the machining process (Figure 5.3). Tool $D_{TiAlCrSiYN}$ contains high amounts of Cr and Si (Table 5.3). In the chip sticking stage, the Cr and Si elements inter-diffuse with the workpiece material (a sign of diffusion observed at 666m Figure 5.3) and weaken the coating. Literature shows that at a high cutting temperature, the tantalum presents in the coating forms tribo films of Ta_2O_5 and Ta_4O, and these oxides act as lubricants during the machining process (Yu, Huang and Xu, 2015; U. S. Patel et al., 2020). It explains the better machining performance of Tool $D_{TiAlTaN}$.

5.3.3 Coating Characterization

Figure 5.6 shows high-resolution SEM images of the structural characteristics of the coatings and indicates that all the coatings have columnar structures. Although the structures look somewhat similar, some differences can be noticed after more careful observation. Both Tool $D_{TiAlTaN}$ and Tool $D_{TiAlCrSiYN}$ show densely packed columnar

structures compared to the other coatings. Research has shown that highly dense column boundaries or lower inter-column spacings result in higher hardness values (Luo et al., 2004).
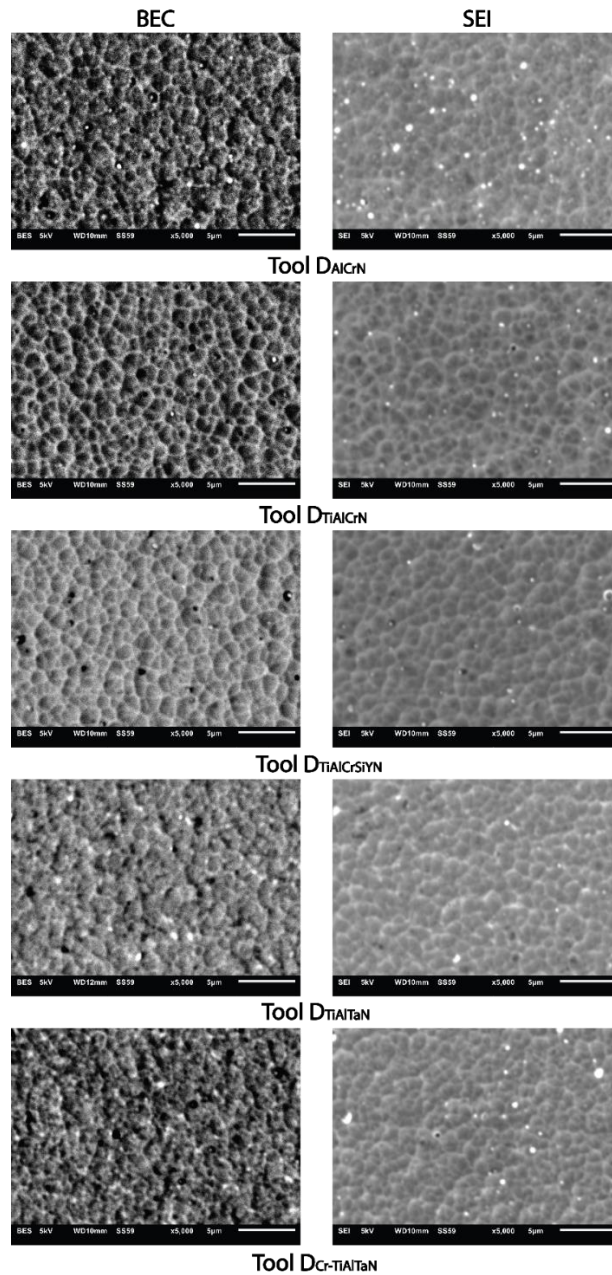
Figure 5.6 *SEM images of coating surface topography and structure with Backscattered electron image (BEC) and secondary electron images (SEI).*

So, the high hardness values (Table 5.5) of these coatings can be related to their comparatively more densely packed structures. Figure 5.7 shows AFM scans of the surface of the coatings. Although Table 5.5 shows that Tool $D_{TiAlCrN}$ has the lowest roughness, the roughness values of all the coatings are too low to affect machining performances significantly.

Figure 5.7 *AFM images of coating surface topography in 2D and 3D view of commercial and in-house coatings.*

Table 5.5 *Micro-mechanical properties and other relevant characteristics of the coatings*

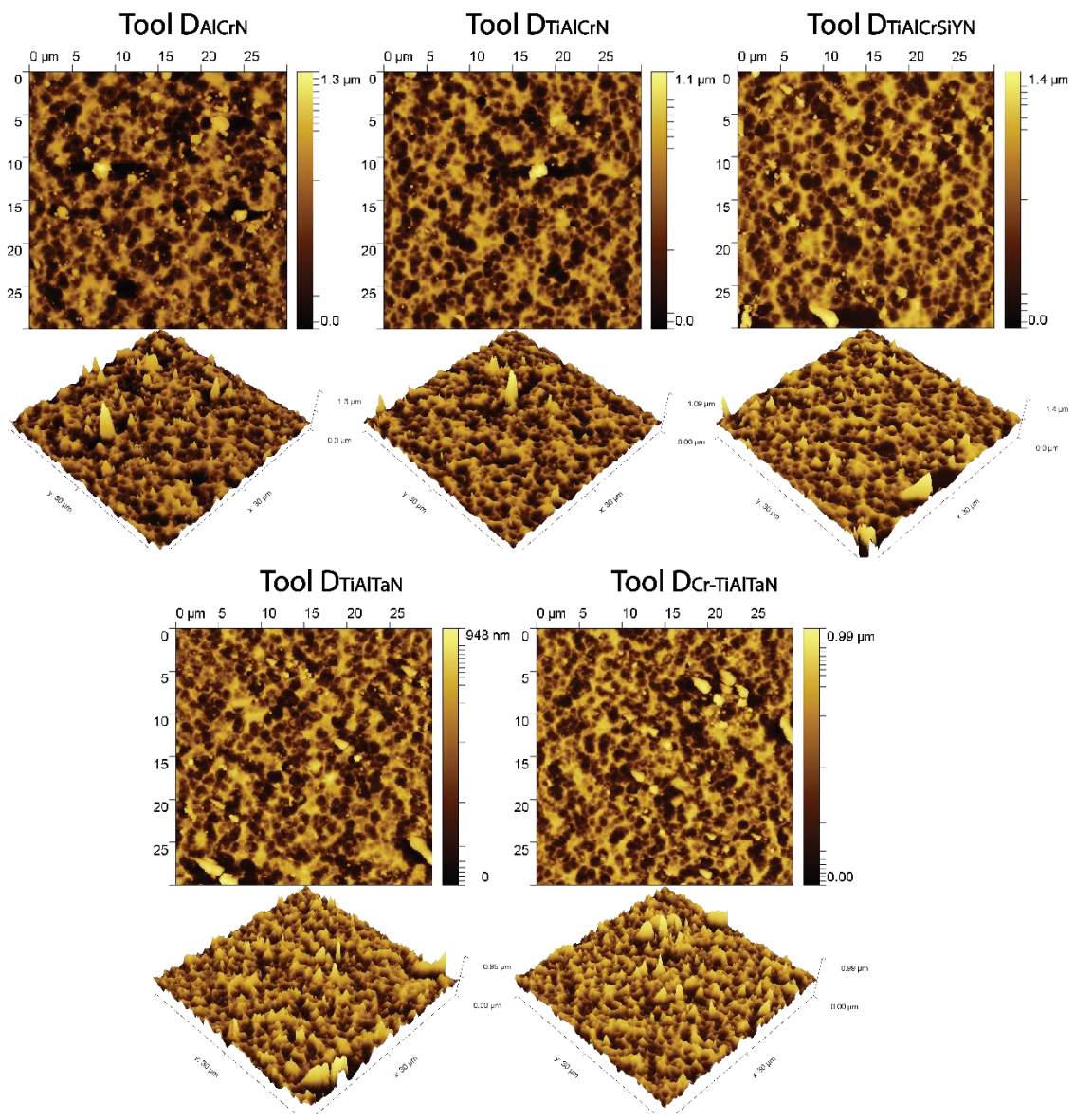| Nomenclator	Thickness	Hardness (H), GPa	Elastic modulus (E), GPa	H/E	H^3/E^2	Plasticity Index	Ra (nm)
Tool D$_{AlCrN}$	3.90±0.02	35.45±2.24	500.88±81.44	0.0708	0.1775	0.4458	36.36±3.99
Tool D$_{TiAlCrN}$	3.24±0.15	33.73±2.96	396.06±65.43	0.0852	0.2446	0.4276	28.14±5.86
Tool D$_{TiAlCrSiYN}$	3.58±0.08	42.36±2.79	462.90±40.17	0.0915	0.3546	0.3967	37±5.84
Tool D$_{TiAlTaN}$	4.07±0.15	47.80±5.55	599.02±69.41	0.0798	0.3043	0.4056	40.44±9.06
Tool D$_{Cr-TiAlTaN}$	3.59±0.07	35.67±4.48	509.54±74.44	0.0700	0.1748	0.4499	41.48±6.17

The thickness and micro-mechanical properties of the coatings are presented in Table 5.5. The H/E and H^3/E^2 ratios were calculated from coating's hardness (H) and elastic modulus (E), which were determined from nanoindentation tests. The H/E ratio signifies the elastic strain to failure characteristics and can be used to measure the wear resistance property of the coatings (Leyland and Matthews, 2000; Beake and Fox-Rabinovich, 2014). It can also be considered a measure of coating brittleness or the ability of the surface to dissipate the energy of deformation during the cutting process. The H^3/E^2 ratio refers to a coating's ability to resist plastic deformation or its load support (Tsui et al., 1995). The plasticity index represents the ratio of the plastic work done and the total work done (elastic and plastic work) during the nanoindentation test. It can be depicted as a measure of toughness.

As discussed earlier, both Tool D$_{TiAlTaN}$ and Tool D$_{TiAlCrSiYN}$ show higher hardness values. However, the Tool D$_{TiAlTaN}$ performs better during machining studies (Figure 5.2). This can be due to the fact that Tool D$_{TiAlCrSiYN}$ is more brittle due to high H/E ratio, which can be used as a measure of brittleness (Leyland and Matthews, 2000). Tool D$_{TiAlCrSiYN}$ shows a higher H/E value but a lower plasticity index, which indicates that the coating is more brittle and prone to break rather drastically. Although higher H/E can be associated with better

wear-resistant, research (Chowdhury et al., 2017) has shown that an optimized value rather than a maximized value is more desirable. It is interesting to see that from the two best performing tools, Tool $D_{TiAlCrN}$, which is the best performing tool, has the lowest H and E values, and Tool $D_{TiAlTaN}$, the second-best tool has the highest H and E values. This proves that more than the high or low values of H and E, the optimum combination of H and E is what really matters. Although a slightly lower H^3/E^2 values of coating Tool $D_{TiAlCrN}$ indicate a slightly lower ability to resist plastic deformation and higher plasticity index indicate that the coating may yield earlier than Tool $D_{TiAlTaN}$. It has been seen that early yielding followed by gradual plastic deformation may work better than delayed but drastic brittle failure (Chowdhury et al., 2021). The remaining two tools, Tool D_{AlCrN} and Tool $D_{Cr-TiAlTaN}$, have lower H/E and H^3/E^2 values, especially very low H^3/E^2 values indicating very low load-bearing capabilities. The coatings also have higher plasticity index values. Such combinations of H, E and plasticity index are not usually good for high-speed machining applications, which is also reflected in their performances during machining test.

Table 5.6 Scratch test data

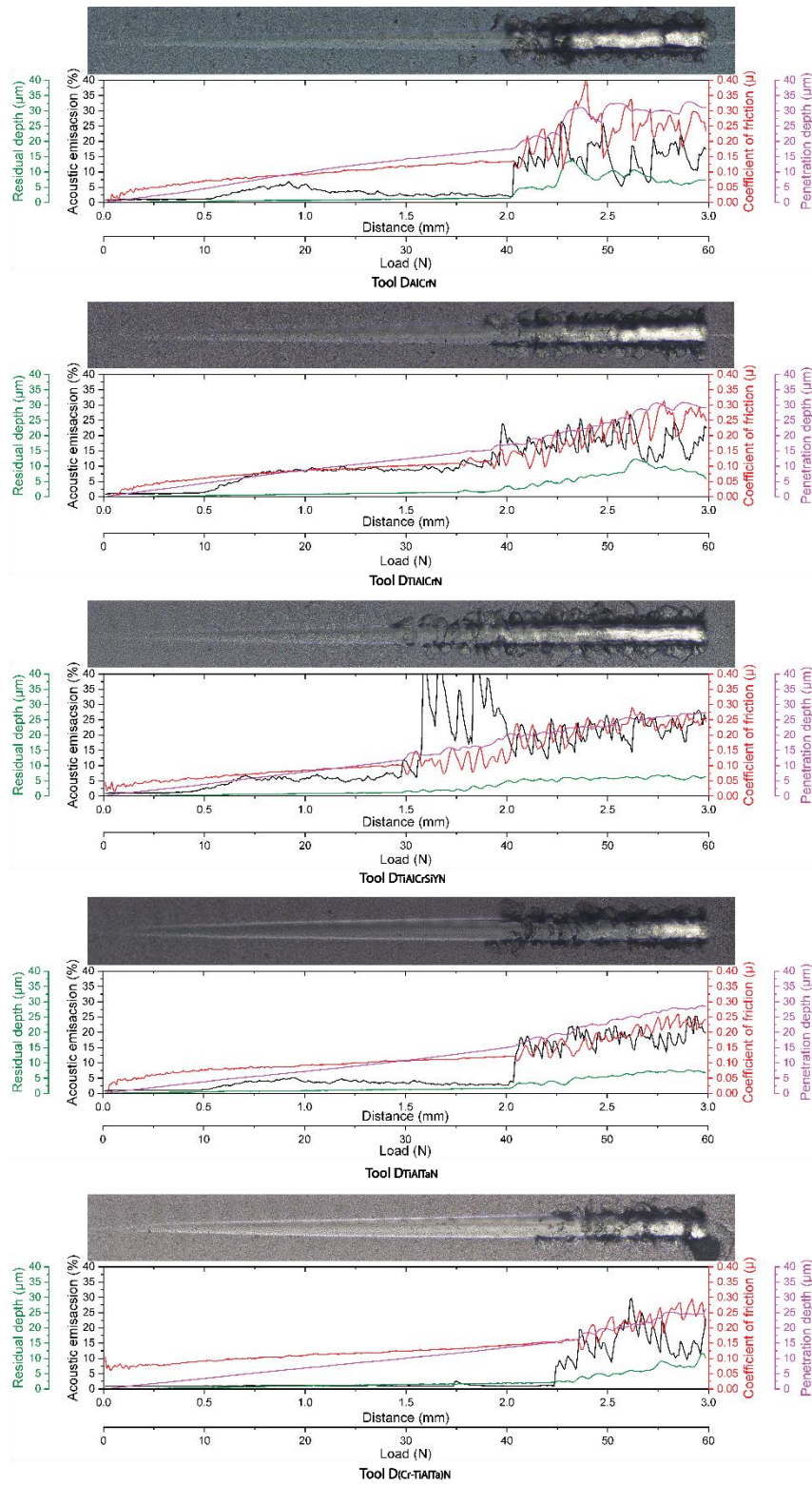| Tool	Lc_1 (N)	Lc_2 (N)
Tool D_{AlCrN}	20.40	40.63
Tool $D_{TiAlCrN}$	29.44	39.43
Tool $D_{TiAlCrSiYN}$	Not observed	30.12
Tool $D_{TiAlTaN}$	Not observed	41.04
Tool $D_{Cr-TiAlTaN}$	Not observed	44.85

Figure 5.8 *Scratch test images of coatings with acoustic emission, coefficient of friction, residual depth and penetration depth in relation tso scratch length and load.*

Figure 5.8represents scratch test results and scratch wear track images for all coatings. Table 5.6 shows the L_{c1} and L_{c2} data, representing the critical load for the first visible failure resulting from cohesive failure (L_{c1}) and the ultimate failure, mostly from substrate exposure due to adhesive failure (L_{c2}). As discussed earlier, the scratch track and the scratch test data also show drastic brittle deformation in Tool $D_{Cr-TiAlTaN}$. It also fails earlier, at a much lower load of 30.12N, than all other coatings during the scratch test. Figure 5.3 also shows early coating failure during machining, which shortens the Tool $D_{Cr-TiAlTaN}$'s life (Figure 5.2). Now, if we consider the two best performing tools, as discussed earlier, TiAlCrN coating yields early (L_{c1}), where the scratch track began to show signs of initial deformation or the start of cohesive failure at a lower critical load (L_{c1}) but underwent plastic deformation without significant cracking until L_{c2}. The adhesive failure L_{c2} values of Tool $D_{TiAlCrN}$ and Tool $D_{TiAlTaN}$ coatings are very comparable. However, here we have to consider the higher thickness of Tool $D_{TiAlTaN}$ coating (Table 5.5), which can affect the L_{c2} values of the scratch test by delaying final failure or substrate exposure resulting in higher L_{c2} values compared to thinner coating. Thus, considering the coating thickness, TiAlCrN coating has better adhesion than TiAlTaN coating.

Considering that TiAlCrN is the thinnest among all coatings, it is expected that the final failure will be somewhat delayed for the thicker coatings. The scratch results of Tool D_{AlCrN} show that the coating starts to fail early with cohesive failure (L_{c1}) (crack formation) at a low load of 20.4N compared to other coatings and despite having similar L_{c2} values, which is also due to higher thickness, substrate exposure is much earlier compared to others except Tool $D_{TiAlCrSiYN}$. Also, it was seen before that the coating has a low H/E ratio which makes

it less wear-resistant making the coating vulnerable under heavy load, and it fails early due to cracking or peeling of the layers, also observed in Figure 5.3, resulting in easier and faster wear of the coating, hindering the life of the cutting tool. Tool $D_{Cr-TiAlTaN}$ scratch test results show the highest ultimate failure load (L_{c2} – 44.85N) with no visual evidence of the first cohesive failure (L_{c1}). The coating has low H/E and H^3/E^2 ratios and high plasticity index, a combination which makes the coating less wear-resistant and too soft, which resulted in high material sticking, making the coating weaker under the extreme cutting conditions and ultimately failing easily and rapidly, as seen in SEM wear morphology (Figure 5.3).

5.4   TiAlCrN Coating Performance With a Different Cermet Tool.

The previous study shows that different cermet tools had similar wear mechanisms with variations in tool life (U. S. Patel et al., 2020). The TiAlCrN coating was deposited on a previous study Tool A. Tool A has high hardness with finer and denser microstructure, the optimum amount of binder, hard (TiW)C phase, which gives tool good performance with high wear resistance (U. S. Patel et al., 2020). Table 5.7 and Figure 5.9 show tool life improvement with in-house coating compared to uncoated and commercial coatings with newly developed advanced in-house coating TiAlCrN for Tool A and Tool D. The inhouse coating TiAlCrN coating shows promising results with uncoated Tool A and Tool D with a consistent improvement of 2266m and 2333m, respectively. Therefore, results show that TiAlCrN was able to successfully delay wear for different compositions of cermet tools.

Table 5.7 *Tool life comparisons of Tool A and Tool D*

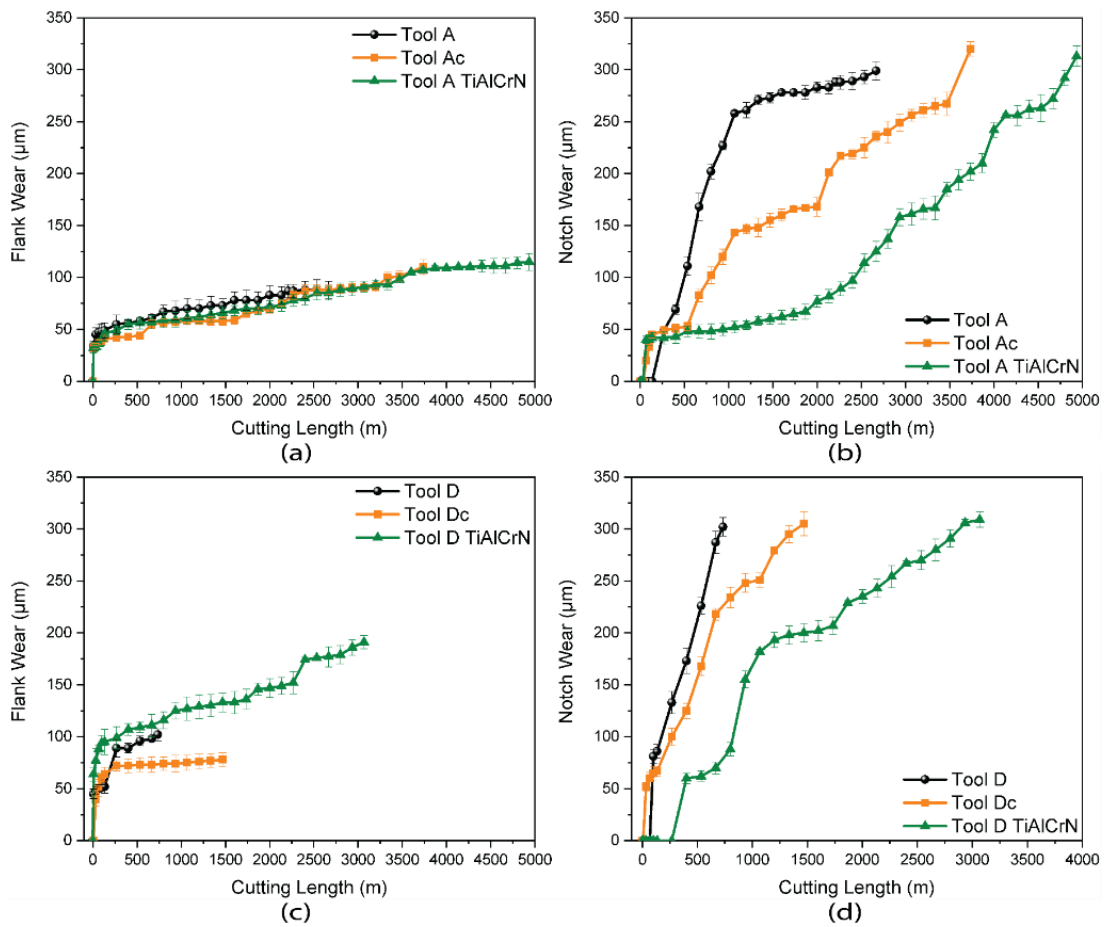| Tools	Tool A	Tool D
Uncoated	2667	733
Commercial coating	3733 (TiAlCrN)	1466 (TiAlN)
In-house new coating (TiAlCrN)	4933	3066

***Figure* 5.9** *Tool life comparison of uncoated, commercial coated, and in-house coated (TiAlCrN) Tool A and Tool D with respect to flank wear (a) & (c), notch wear (b) & (d).*

5.5　Conclusions

The machining of stainless steel 304 in the high-speed dry turning process causes two major wears of the cutting tool. One, as large notches resulting from microchipping, and second, the adhesion wear causing BUE and coating peeling followed by substrate exposure. The developed coating must delay microchipping and protect itself from adhesion wear to achieve good cutting performance.

Different coating compositions and concentrations significantly alter the micro-mechanical properties of the coating resulting in wear performance and machining performance, specifically addressing microchipping. Various combinations of coating elements were developed considering micromechanical properties and tribological behaviour. The best performing coating was Tool $D_{TiAlCrN}$, followed by Tool $D_{TiAlTaN}$. The Tool $D_{TiAlCrN}$ and Tool $D_{TiAlTaN}$ coatings show the optimized value of H/E and H^3/E^2, leading to better micro-mechanical properties and wear resistance. Generated tribo films are oxidation-resistant and lubricious. The TiAlCrN and TiAlTaN coatings delayed the microchipping wear and reduced the sticking of material on the surface, which led to the enhancement of the tool life by 318%. The addition of Si and Y to coating Tool $D_{TiAlCrSiYN}$ showed the fine and refined grain structure that resulted in high H/E and H^3/E^2. Exceeding the desired value of H/E and H^3/E^2 resulted in early brittle failure and reduced the coating's ability to perform well under high loads. The optimized amount of Cr gave the best performance instead of the excessively added Cr, which deteriorated the performance for Tool $D_{Cr-TiAlTaN}$ coatings due to lower H/E resulting in lower wear resistance of the coating.

The coating TiAlCrN shows consistent improvement in terms of tool life with the newly developed in-house coating with various uncoated cermet tools.

5.6 Acknowledgments

5.7 References

Arndt, M. and Kacsich, T. (2003) 'Performance of new AlTiN coatings in dry and high speed cutting', Surface and Coatings Technology, 163(164), pp. 674–680. doi: 10.1016/S0257-8972(02)00694-1.

Bapat, P. S. et al. (2015) 'A Numerical Model to Obtain Temperature Distribution During Hard Turning of AISI 52100 Steel', Materials Today: Proceedings, 2(4–5), pp. 1907–1914. doi: 10.1016/j.matpr.2015.07.150.

Beake, B. D. and Fox-Rabinovich, G. S. (2014) 'Progress in high temperature nanomechanical testing of coatings for optimising their performance in high speed machining', Surface and Coatings Technology, 255, pp. 102–111. doi: 10.1016/j.surfcoat.2014.02.062.

Bouzakis, K. D. et al. (2013) 'Effect of silicon content on PVD film mechanical properties and cutting performance of coated cemented carbide inserts', Surface and Coatings Technology, 237, pp. 379–389. doi: 10.1016/j.surfcoat.2013.06.044.

Chowdhury, M. S. I. et al. (2017) 'Wear behaviour of coated carbide tools during machining of Ti6Al4V aerospace alloy associated with strong built up edge formation', Surface and Coatings Technology, 313, pp. 319–327. doi: 10.1016/j.surfcoat.2017.01.115.

Chowdhury, M. S. I. et al. (2021) 'Investigation of the wear performance of tib2 coated cutting tools during the machining of ti6al4v alloy', Materials, 14(11). doi: 10.3390/ma14112799.

Danek, M. et al. (2017) 'Influence of Cr additions on the structure and oxidation resistance of multilayered TiAlCrN films', Surface and Coatings Technology, 313, pp. 158–167. doi: 10.1016/j.surfcoat.2017.01.053.

Das, A. et al. (2016) 'Comparative Assessment on Machinability Aspects of AISI 4340 Alloy Steel Using Uncoated Carbide and Coated Cermet Inserts During Hard Turning', Arabian Journal for Science and Engineering, 41(11), pp. 4531–4552. doi: 10.1007/s13369-016-2160-0.

Du, H. et al. (2014) 'Effect of Ar/N2 flow ratio on oxidation resistance and properties of TiAl(La)N coatings', International Journal of Refractory Metals and Hard Materials, 46, pp. 173–180. doi: 10.1016/J.IJRMHM.2014.06.012.

Endrino, J. L., Fox-Rabinovich, G. S. and Gey, C. (2006) 'Hard AlTiN, AlCrN PVD coatings for machining of austenitic stainless steel', Surface and Coatings Technology, 200(24), pp. 6840–6845. doi: 10.1016/j.surfcoat.2005.10.030.

Fox-Rabinovich, G. S. et al. (2009) 'Design and performance of AlTiN and TiAlCrN PVD coatings for machining of hard to cut materials', Surface and Coatings Technology, 204(4), pp. 489–496. doi: 10.1016/j.surfcoat.2009.08.021.

Fox-Rabinovich, G. S. et al. (2010) 'Structure, properties and wear performance of nano-multilayered TiAlCrSiYN/TiAlCrN coatings during machining of Ni-based aerospace superalloys', Surface and Coatings Technology, 204(21–22), pp. 3698–3706. doi: 10.1016/j.surfcoat.2010.04.050.

Inspektor, A. and Salvador, P. A. (2014) 'Architecture of PVD coatings for metalcutting applications: A review', Surface and Coatings Technology, 257, pp. 138–153. doi: 10.1016/j.surfcoat.2014.08.068.

Kaladhar, M., Venkata Subbaiah, K. and Srinivasa Rao, C. H. (2012) 'Machining of austenitic stainless steels - A review', International Journal of Machining and Machinability of Materials, 12(1–2), pp. 178–192. doi: 10.1504/IJMMM.2012.048564.

Leyland, A. and Matthews, A. (2000) 'On the significance of the H/E ratio in wear control: A nanocomposite coating approach to optimised tribological behaviour', Wear, 246(1–2), pp. 1–11. doi: 10.1016/S0043-1648(00)00488-9.

Li, T. et al. (2017) 'Structures and properties of TiAlCrN coatings deposited on Ti(C,N)-based cermets with various WC contents', International Journal of Refractory Metals and Hard Materials, 69(April), pp. 247–253. doi: 10.1016/j.ijrmhm.2017.08.020.

Luo, Q. et al. (2004) 'Transmission electron microscopy and x-ray diffraction investigation of the microstructure of nanoscale multilayer TiAlN/VN grown by unbalanced magnetron deposition', Journal of Materials Research, 19(4), pp. 1093–1104. doi: 10.1557/JMR.2004.0143.

Nayak, S. K. et al. (2014) 'Multi-objective Optimization of Machining Parameters During Dry Turning of AISI 304 Austenitic Stainless Steel Using Grey Relational Analysis', Procedia Materials Science, 6(Icmpc), pp. 701–708. doi: 10.1016/j.mspro.2014.07.086.

Noordin, M. Y., Venkatesh, V. C. and Sharif, S. (2007) 'Dry turning of tempered martensitic stainless tool steel using coated cermet and coated carbide tools', Journal of Materials Processing Technology, 185(1–3), pp. 83–90. doi: 10.1016/j.jmatprotec.2006.03.137.

Patel, U. et al. (2020) 'Dataset and methodology on identification and correlation of secondary carbides with microstructure, wear mechanism, and tool performance for different CERMET grades during high-speed dry finish turning of AISI 304 stainless steel', Data in Brief, p. 105753. doi: https://doi.org/10.1016/j.dib.2020.105753.

Patel, U. S. et al. (2020) 'Influence of secondary carbides on microstructure, wear mechanism, and tool performance for different cermet grades during high-speed dry finish

turning of AISI 304 stainless steel', Wear, 452–453, p. 203285. doi: 10.1016/j.wear.2020.203285.

Poomari, A. et al. (2012) 'Wear Performance of Ti-Al-N Coated and Cryogenically Treated Cermet Tools While Machining Aisi 4340 Steel', Advanced Materials Research, 622–623, pp. 404–408. doi: 10.4028/www.scientific.net/AMR.622-623.404.

Santana, A. E. et al. (2004) 'Microstructure and mechanical behavior of TiAlCrN multilayer thin films', Surface and Coatings Technology, 177–178, pp. 334–340. doi: 10.1016/j.surfcoat.2003.09.023.

Sert, H. et al. (2005) 'Wear behavior of PVD TiAlN, CVD TiN coated and Cermet cutting tools', Tribology in Industry, 27(3–4), pp. 3–9.

Sharma, A. K., Tiwari, A. K. and Dixit, A. R. (2016) 'Effects of Minimum Quantity Lubrication (MQL) in machining processes using conventional and nanofluid based cutting fluids: A comprehensive review', Journal of Cleaner Production, 127, pp. 1–18. doi: 10.1016/j.jclepro.2016.03.146.

Sreejith, P. S. and Ngoi, B. K. A. (2000) 'Dry machining: Machining of the future', Journal of Materials Processing Technology, 101(January 1999), pp. 287–291. doi: 10.1016/S0924-0136(00)00445-3.

Standardization, F. O. R. (2006) 'IS0 3685:Tool-life testing with single-point turning tools'.

Tiwari, P. K. et al. (2020) 'Performance evaluation of coated cermet insert in hard turning', Materials Today: Proceedings, (xxxx). doi: 10.1016/j.matpr.2020.02.424.

Touggui, Y. et al. (2021) 'A comparative study on performance of cermet and coated carbide inserts in straight turning AISI 316L austenitic stainless steel', International Journal of Advanced Manufacturing Technology, 112(1–2), pp. 241–260. doi: 10.1007/s00170-020-06385-5.

Trent, E. M. and Wright, P. K. (2000) Metal Cutting, Vasa.

Tsui, T. Y. et al. (1995) 'Nanoindentation and nanoscratching of hard carbon coatings for magnetic disks', in Materials Research Society Symposium - Proceedings. MRS Proc, pp. 447–452. doi: 10.1557/proc-383-447.

Warcholinski, B. and Gilewicz, A. (2011) 'Mechanical properties of multilayer TiAlN/CrN coatings deposited by cathodic arc evaporation', Surface Engineering, 27(7), pp. 491–497. doi: 10.1179/026708410X12786785573355.

Willmann, H. et al. (2007) 'Thermal stability and age hardening of supersaturated AlCrN hard coatings', International Heat Treatment and Surface Engineering, 1(2), pp. 75–79. doi: 10.1179/174951507x193657.

Wolfe, G. J., Petrosky, C. J. and Quinto, D. T. (1986) 'The role of hard coatings in carbide milling tools', Journal of Vacuum Science & Technology A, 2747(April 1986), pp. 2747–2754. doi: 10.1116/1.573673.

Yang, W. et al. (2017) 'Structure and properties of PVD TiAlN and TiAlN/CrAlN coated Ti(C, N)-based cermets', Ceramics International, 43(2), pp. 1911–1915. doi: 10.1016/j.ceramint.2016.10.151.

Yu, L., Huang, T. and Xu, J. (2015) 'Effect of vanadium content on microstructure, mechanical and tribological properties of TaVCN composite films', Fenmo Yejin Cailiao Kexue yu Gongcheng/Materials Science and Engineering of Powder Metallurgy, 20(1).

Zhang, S. and Zhu, W. (1993) 'TiN coating of tool steels: a review', Journal of Materials Processing Tech., 39(1–2), pp. 165–177. doi: 10.1016/0924-0136(93)90016-Y.

Chapter 6 : Conclusions and Future Directions

6.1 General Conclusions

Stainless steel is one of the most widely used materials, covering three-quarters of the metal/alloy market. It is in high demand due to its excellent properties, such as high corrosion resistance, high mechanical strength, and low thermal conductivity for various applications in many industrial sectors, including aerospace and die/mold industries. There is a very high demand for high-speed machining in these industries. The cost-saving aspect and environmental impact are two major reasons for a recent high demand for dry machining. Stainless steel tends to stick, causing BUE and rapid tool wear due to adhesive wear. It is extremely challenging to perform machining of such material under dry high-speed machining conditions, as it often results in rapid performance and tool failure of various tool materials. Cermet tools have unique properties of high wear resistance and high fracture toughness and are thus the focus in recent research activities as a potential tool material.

This research investigates the wear mechanisms of various commercial uncoated and coated cermet tools for high-speed dry turning of stainless steel 304. The scientific insight is used to develop an in-house PVD coating for cermet tools that addresses the aforementioned conditions and enhances the tool capability and performance compared to commercial uncoated and coated cermet tools for dry machining of stainless steel.

This research discusses in-depth studies needed to understand the cermet tool and its wear mechanism to develop a PVD coating for specific applications involving dry machining of stainless steel. In this study, a reverse engineering approach is used to reveal the compositions and microstructure of commercial uncoated cermet tools and PVD-coated cermet tools. The study includes an in-depth study of uncoated cermet and coating with machining and characterization experiments including SEM, EDS, XRD, AFM, nanoindentation, scratch test, wear measurement with an optical 3D microscope, and force acquisition by a force dynamometer. This research approach facilitated finding the wear mechanism and failure mode of uncoated and PVD-coated cermet tools. This scientific insight was used to develop in-house PVD coatings for performance enhancement. It delayed wear of the cermet tools to extend tool capability and wear resistance to perform under dry high-speed machining conditions for stainless steel.

The important conclusions from this research work and outcomes of each research objective for this thesis are summarized as follows:

1. For uncoated cermet tools under high-speed dry machining conditions considered in this study, notch wear was observed to be the most dominant wear type for all cermet tools. The major wear initiation and changes occur from the first pass of machining with pitting wear, then microchipping and ultimately form notching at the end.

2. The different constituents of the cermet tools alter the microstructure of the tool, resulting in variation of the micromechanical properties of the cermet tools. This variation reflects the different wear intensities in different cermet tools. The tool

171

with a fine and rounded core and low porosity performed best during machining and showed delayed wear progression compared to the others. The presence of a small proportion of tungsten (W) helped form rims around the core that held the core well and increased wear and machining performance. Elements such as vanadium (V) and tantalum (Ta) formed lubricating films, which reduced the amount of tool wear. Finally, binder concentration is critically important, as excessive binders such as cobalt (Co) and nickel (Ni) rapidly degrade equipment performance by accelerating notch wear. Ultimately, major wear occurs in the initial machining stage. Hence all material and property effects need to be considered and addressed to delay wear and improve cermet tool performance.

3. It was observed that not all commercial coatings provide significant improvements in tool life. The commercial coatings with Ti, Al, and Cr as a major elemental content show higher performance than other commercial coated tools, delaying the wear during the first two passes, but later, high diffusion wear is observed for them.

4. The comparison of commercial coatings of Ti and Al as a major element and in-house coating shows that the latter performed well. The in-house coating has a superior columnar structure and performs well compared to similar elements contained in commercial coatings based on the in-depth coating characterization and investigation of micromechanical properties.

5. The coating with only Ti as a major element (TiN) shows poor performance because the titanium oxide film cannot protect the coating and shows no

improvement in machining performance. The addition of Al improves performance. However, excessive Al leads to the formation of aluminum oxide films that are brittle and fail easily, thereby limiting the performance of the coating. The main wear mechanisms for these Ti and Al-based coatings were abrasive wear, oxidation wear, adhesive wear, and brittle failure. Titanium (Ti), when present with other alloying elements, improves performance by forming respective tribofilms.

6. The addition of chromium (Cr) results in stable and dense chromium and aluminum-based composite oxide that protects tools and coating by resisting oxidation wear. The optimized amount of Cr reveals good performance rather than excessive Cr, which degrades performance by dispersing Cr into the workpiece. Tantalum (Ta) and its oxide tribofilms act as a lubricant and assist auxiliary materials in flowing smoothly across the surface, thereby reducing wear and prolonging tool life.

7. The micromechanical properties of the coating change with the composition and deposition parameters. In the current application, a low plasticity index value coating with higher H/E and H^3/E^2 and finer denser coating structure showed better wear resistance to a certain extent. The higher values of H/E and H^3/E^2 ratios do not lead to good performance. The in-house developed PVD TiAlCrN coating shows the best machining performance followed by TiAlTaN coating and prolongs the tools life of the cermet tools as compared to uncoated and coated commercial cermet tools by 318%.

6.2 Research Contributions

The major contributions of this thesis include identifying the wear mechanism and developing a coating for cermet tools to delay wear during high-speed dry machining of stainless steel. The contributions are summarized below:

1. A thorough, step-by-step study of the progressive wear mechanism was provided for the cermet tools having a different composition but the same geometry under the same machining condition. The detailed wear mechanism was fully explained scientifically in relation to the elemental composition and properties of a specific cermet tool. The important role of each element in the cermet tool was investigated and related to the structural aspect of the tools; variation in elemental composition significantly altered the mechanical properties and composition, which was an important factor in the wear mechanism and tool machining performance.

2. A detailed explanation of the coating failure mechanism was revealed with a step-by-step progressive wear study based on the composition of different coating elements. The influence of each coating element was methodically explained with respect to the micromechanical properties and tribo films formation. The performance of the coating element varied depending on the presence of other elements. Diffusion, adhesive, and notch wear were observed to be the dominant wear mechanisms; they were investigated in-depth and systematically explained.

3. The development of a new adaptive PVD coating specifically for cermet tools to machine stainless steel 304 under high-speed dry conditions was successfully accomplished. The in-house developed PVD coating for the cermet tool delayed major tool wear and extended tool life. A comprehensive explanation was provided outlining the performance improvements associated with the new coating under dry high-speed machining. Thus, the major achievement of this research work was the development of an in-house coating that outperformed commercially available coatings and which can be implemented by tool suppliers.

4. The in-house developed PVD coating was capable of increasing tool life by 318% compared to uncoated tools. The findings of this research work are expected to contribute to the aerospace and die/mold industries by reducing tool cost, coolant cost and production time, ultimately fulfilling the recent industry demands. In addition, it may play a major role in reducing environmental waste by reducing coolant waste and coolant pollutant gas from the machining process.

6.3 Recommendations for Future Research

This research work opens several avenues for future researchers and industrial practitioners to further improve the performance of cermet tools for various applications. Some of the suggestions to continue this research work further in the future are:

- Researchers can discover more about the cermet tool's performance by altering the elemental composition of the coating and develop an optimal combination to improve further the performance for the current application of machining stainless steel or other specific application.

- The in-house developed PVD coatings TiAlCrN and TiAlTaN have shown promising results. The optimization of these coating compositions may lead to more improvement of tool life and can be explored further.

- The effect of coating deposition parameters on the wear mechanism and micromechanical properties of the coating can be explored and optimized for improved performance.

- The adhesion of the coating can be further improved or explored with interlayer and multilayer coatings.

- Researchers can apply a similar approach to other applications such as drilling, milling, and other workpiece materials such as die steels, titanium, aluminium, etc. to develop novel high-performance coatings.